UNIVERSITA' VITA-SALUTE SAN RAFFAELE

CORSO DI DOTTORATO DI RICERCA INTERNAZIONALE IN MEDICINA MOLECOLARE

Curriculum in Basic and Applied Immunology and Oncology

EXPLOITING microRNA NETWORKS IN TUMOR-ASSOCIATED MACROPHAGES TO BOOST TUMOR IMMUNITY

DoS: Dr. Mario Leonardo Squadrito

Second Supervisor: Prof. Markus Stoffel

Tesi di DOTTORATO di RICERCA di Chiara Bresesti

matr. 017114

Ciclo di dottorato XXXVI

SSD MED/06; BIO/11; BIO/13

Anno Accademico 2022/2023

CONSULTAZIONE TESI DI DOTTORATO DI RICERCA

Il/la sottoscritto/*I* Chiara Bresesti

Matricola / *registration number* 017114

nata/ *born at* Alzano Lombardo (BG)

il/*on* 24/07/1996

autore della tesi di Dottorato di ricerca dal titolo / *author of the PhD Thesis titled*

Exploiting microRNA networks in tumor associated macrophages to boost tumor immunity

☐ AUTORIZZA la Consultazione della tesi / AUTHORIZES *the public release of the thesis*

☒ NON AUTORIZZA la Consultazione della tesi per 12 mesi /DOES NOT AUTHORIZE *the public release of the thesis for 12 months*

a partire dalla data di conseguimento del titolo e precisamente */ from the PhD thesis date, specifically*

Dal / *from* 15/01/24 Al / *to* 14/01/25

Poiché /*because*:

☒ l'intera ricerca o parti di essa sono potenzialmente soggette a brevettabilità/ *The whole project or part of it might be subject to patentability;*

☐ ci sono parti di tesi che sono già state sottoposte a un editore o sono in attesa di pubblicazione/ *Parts of the thesis have been or are being submitted to a publisher or are in press;*

☐ la tesi è finanziata da enti esterni che vantano dei diritti su di esse e sulla loro pubblicazione/ *the thesis project is financed by external bodies that have rights over it and on its publication.*

E' fatto divieto di riprodurre, in tutto o in parte, quanto in essa contenuto / *Copyright the contents of the thesis in whole or in part is forbidden*

Data /Date 11/12/2023 Firma /Signature Chiara Bresesti

DECLARATION

This thesis has been:

- composed by myself and has not been used in any previous application for a degree. Throughout the text I use both 'I' and 'We' interchangeably.
- has been written according to the editing guidelines approved by the University.

Permission to use images and other material covered by copyright has been sought and obtained.

All the results presented here were obtained by myself, except for:

1) MRI analysis were performed at the Ospedale San Raffaele Preclinical imaging Facility by Tamara Canu
2) Bioinformatical analysis of the scRNA-seq data (Results, chapter 3.1.2), polyA-enriched and small RNAseq data (Results, chapter 3.1.3) and RNAseq data (Results, chapter 3.4.2) was performed with the help of Stefano Beretta and Marco Monti (Gene transfer technology and new gene therapy strategies Unit, San Raffaele Telethon Institute for Gene and Cell Therapy)

All of the data presented in the Results section are unpublished, and do not appear in any previous paper featuring me as an author.

All sources of information are acknowledged by means of reference.

Abstract

Viral vectors are versatile and efficient tools for genetic engineering of eukaryotic cells. Among these, VSV-G-pseudotyped lentiviral vectors (LVs) have been extensively investigated for their broad tropism and capacity to stably transduce proliferating and non-proliferating cells. Upon intravenous injection in non-human primates and mice, LVs transduce numerous cell populations, especially in the spleen and the liver. Building on this observation, systemically delivered LVs can be exploited to enforce gene expression, knockout genes of interest and measure microRNA (miRNA) activity in LV-targeted phagocytic cells, thus allowing to investigate gene circuits active during physiological and pathological conditions (e.g. cancer).

We delivered GFP-encoding LVs to adult mice and used immunofluorescence confocal imaging and flow cytometry to identify transduced hepatic and splenic cell populations. We performed a scRNAseq on transduced splenic cells, and analyzed key populations in depth by poly-A enriched and small RNA sequencing. We injected mice with miRNA reporter LVs to infer miRNA activity *in vivo* in both homeostasis and in presence of liver metastasis. Finally, we exploited LVs to enforce selected miRNA expression in phagocytic cells *in vitro*, and *in vivo* in a colorectal cancer liver metastasis setting. We performed a transcriptomic analysis of transduced cells, and evaluated miRNA expression impact on tumor growth and immune phenotype in two murine liver metastasis models.

We identified different splenic cell populations transduced by LVs, including distinct subsets of macrophages, dendritic cells and B cells. We also found multiple differentially expressed miRNAs that seem to be either lineage or population specific, supporting their function in myeloid cell differentiation and function. Finally, we investigated the biological activity of selected miRNAs *in vitro* and *in vivo*, and found that enforcing miR-342 expression promoted immune activation of macrophages, leukocyte infiltration, and a general reprogramming of tumor microenvironment in liver metastasis leading to tumor growth delay.

Overall, our work describes the phagocytic cells efficiently transduced upon systemic delivery of LVs in mice, as well as miRNAs that enable silencing of transgene products in off-target cells. Taken together these findings may be of interest for designing off-the-shelf gene-based therapeutic interventions for cancer or genetic diseases. Furthermore, we identified an antitumoral miRNA, which may be exploited to enhance anti-tumor immunity in combination with current cancer immunotherapy.

Ackowledgements

This PhD-project would not have been possible without the support of the many people involved, that helped me from an experimental and personal point of view during these years.

I would like to thank my DoS dr Mario Squadrito for his supervision, and the head of Targeted cancer gene therapy unit prof Luigi Naldini and for giving me the opportunity to participate in this fascinating project.

I would also like to extend my gratitude to all the Naldini lab members that supported me in this project, and in particular to the Marco, Giovanna, Mirko, and former members Thomas and Eloise. It really was a team effort, and this work wouldn't have been possible without your help and your insights.

I am grateful to Prof. Stoffel for serving as my external supervisor and always being available for interesting scientific discussions.

Finally, I would like to thank the IRCCS San Raffaele Hospital Flow Cytometry facility (FRACTAL), the IRCCS San Raffaele Center for Omics Sciences (COSR), the IRCCS San Raffaele Hospital Advanced Light and Electron Microscopy BioImaging Center (ALEMBIC), the preclinical Imaging facility, and the Animal House, which graciously provided us access to their expertise and resources.

This work was funded by Fondazione Cariplo (grant 2019-1834), which we would like to acknowledge for its financial support.

Table of contents

Acronyms and abbreviations 1

List of figures and tables 4

1 Introduction 5

1.1 Colorectal cancer liver metastases: an unmet clinical need 5

1.1.1 Colorectal cancer epidemiology 5

1.1.2 Colorectal cancer management: available therapies and prevention strategies 6

1.1.3 Liver as a privileged site for colorectal cancer metastasis 7

1.1.4 Colorectal cancer liver metastasis: clinical challenges and future perspectives . 10

1.2 Kupffer cells in homeostasis and disease 12

1.2.1 General characteristics and origin 12

1.2.2 Liver macrophages subsets and Kupffer cells markers 13

1.2.3 Kupffer cells role in homeostasis 15

1.2.4 Kupffer cells role in disease: focus on cancer 17

1.3 microRNAs as regulators of gene expression 21

1.3.1 Biosynthesis 21

1.3.2 Mechanism of action 24

1.3.3 microRNA role in macrophage biology 25

1.3.4 microRNA, cancer, and TAMs 28

1.4 Gene therapy: a promising tool to tackle human disease 30

1.4.1 Gene therapy approaches and platforms 30

1.4.2 Regulatory elements in gene therapy 32

1.4.3 In vivo gene therapy: the liver example 33

1.4.4 Gene therapy approaches in oncology 35

2 Aim of the work 37

3 Results 38

3.1 Characterization of splenic and hepatic populations preferentially transduced upon VSV-G pseudotyped LVs systemic delivery 38
3.1.1 Biodistribution study of intravenously injected VSV-G pseudotyped LVs 38
3.1.2 scRNA-seq unravels heterogeneity of LV-targeted splenic populations 43
3.1.3 Characterization of active gene networks in preferentially transduced hepatic and splenic cell populations 46
3.2 Evaluation of miRNA activity in LV-targeted cell populations in different pathophysiological conditions 48
3.2.2 Bidirectional LVs allow for miRNA-activity tracking in healthy liver and spleen 48
3.2.3 miR-342-3p activity in KCs diminishes in close proximity to CRC liver metastases 53
3.3 Enforcing miRNA expression in LV-targeted cell populations 55
3.3.1 Development and validation of a miR-342-3p overexpression cassette 55
3.3.2 Overexpression of selected miRNAs in a model of CRC liver metastasis 57
3.3.3 Overexpression of miR-342-3p in a more relevant CRC liver metastasis model hints to an antitumoral activity 60
3.4 Evaluating miR-342-3p impact on KCs biology and antitumoral activity 62
3.4.1 Development and validation of a miR-342-specific control and of miR-342-3p sponge LVs 62
3.4.2 In vitro expression regulation of miR-342-3p in a bona fide KC model suggests its relevance in immune activation and macrophage biology 64
3.4.3 In vivo overexpression of miR-342-3p in a CRC liver metastasis model confirms its activity in TME remodeling 68
4 Discussion 71
5 Materials and methods 79
5.1 Molecular biology 79
5.1.1 Plasmid design cloning and amplification 79
5.1.2 Vector copy number determination 80
5.1.3 Gene expression assays 82

5.2 Cell culture 82
5.2.1 HEK293T and MC38 cells 82
5.2.2 AKTPF cells 82
5.2.3 Hepa-CSF100 cells and conditioned media production 83
5.2.4 Immortalized KCs (KC1 cells) 83
5.2.5 LV production and titration 84
5.3 Mouse procedures 84
5.3.1 Intravenous injection 85
5.3.2 MC38 tumor implant 85
5.3.3 AKTPF tumor implant 85
5.3.4 Blood collection and analysis 86
5.3.5 MRI analysis 86
5.3.6 Sacrifice and necropsy 86
5.4 Flow cytometry (FC) 87
5.4.1 Sample preparation 87
5.4.2 Sample staining 87
5.5 Immunofluorescent imaging (IF) 89
5.5.1 Sample preparation 89
5.5.2 Sample staining 89
5.6 Transcriptomic analysis 90
5.6.1 Bulk poly-A enriched RNA-seq 90
5.6.2 Bulk small RNA-seq 91
5.6.3 Single cell RNA-seq 91
6 References 93

Acronyms and abbreviations

ABBREVIATION	DEFINITION
AAV	Adeno-associated virus
Ads	Adenovirus
AGO	Argonaute protein
APC	Antigen presenting cell
BMDM	Bone marrow derived macrophages
CAR	Chimeric antigen receptor
CPM	Count per million
CRC	Colorectal cancer
CRLM	Colorectal cancer liver metastasis
DC	Dendritic cell
DNA	Deoxyribonucleic acid
DGE	Differential gene expression
ECM	Extracellular matrix
EGFR	Epidermal growth factor receptor
EMT	Epithelial-to-mesenchymal transition
FACS	Flow-cytometry activated cell sorting
FC	Flow cytometry; Fold change
FDA	Food and drug administration
GSEA	Gene set enrichment analysis
HCC	Hepatocellular carcinoma
HDI	Human development index
HDL	High density lipoprotein
HIV	Human immunodeficiency 1 virus
HSC	Hematopoietic stem cell
HSPC	Hematopoietic stem and progenitor cell
IF	Immunofluorescence

ITR	Inverted terminal repeat
KC	Kupffer cell
LAM	Lipid associated macrophage
LCM	Liver capsule macrophage
LDL	Low density lipoprotein
LPS	Lipopolysaccharide
LSEC	Liver sinusoid endothelial cell
LTR	Long terminal repeat
LV	Lentivirus
MDSC	Myeloid derived suppressor cell
MFI	Mean fluorescent intensity
miRNA	Micro RNA
miRT	miRNA target sequence
MMR	DNA mismatch repair
MOI	Multiplicity of infection
mRNA	Messenger RNA
NK	Natural killer cell
NRAS	Neuroblastoma ras vital oncogene homolog
pDC	Plasmacytoid dendritic cell
RISC	RNA induced silencing complex
RNA	Ribonucleic acid
RT	Retrotranscription (product)
scRNA-seq	Single-cell RNA-seq
snRNA	Small nuclear RNA
TAM	Tumor associated macrophage
TLR	Toll-like receptor
TME	Tumor microenvironment
TU	Transducing unit
UMI	Unique molecular index

UT	Untransduced
UTR	Untranslated region
VCN	Vector copy number
VLDL	Very low density lipoprotein
VSV-G	Vescicular stomatititc virus glycoprotein

List of figures and tables

Figure 1. Schematics of the characteristics of colorectal cancer for different disease stages..6

Figure 2. Schematics of macro and micro vasculature in the liver 9

Figure 3 (a) Classically activated M1 and alternatively activated M2 macrophages (b) TAMs functions in 19

Figure 4 Canonical miRNA processing pathway 22

Figure 5 Overview of miRNAs involved in macrophage development and function.....27

Figure 6 VSV-G pseudotyped LV biodistribution experiment 42

Figure 7 scRNA-seq analysis of LV transduced spleen. 44

Figure 8 In depth characterization of the transcriptional landscape of LV-targeted cell populations. 46

Figure 9 Flow cytometry analysis of miRNA reporter LVs assay. 48

Figure 10 Immunofluorescence analysis of miRNA reporter LVs assay 50

Figure 11 miR-342-3p activity detection in CRC liver metastasis model 53

Figure 12 miR-342-3p overexpression LV design and validation.....56

Figure 13 miRNA enforced expression in MC38 tumor model 58

Figure 14. miR-342-3p enforced expression in AKTPF tumor model: early injection.....60

Figure 15 miRNA overexpression control and miRNA sponge design and validation……..62

Figure 16 In vitro analysis of miR-342-3p impact on KC1. 65

Figure 17 miR-342-3p enforced expression in AKTPF tumor model: late injection.....69

Table 1 List of non-commercial primers and probes employed…….. 81

Table 2 List of commercial TaqMan assays employed…….. 81

Table 3 List of antibodies employed for FACS analysis……... 88

Table 4 List of antibodies employed for IF analysis…… 90

1 Introduction

1.1 Colorectal cancer liver metastases: an unmet clinical need

1.1.1 Colorectal cancer epidemiology

Colorectal cancer (CRC) is one of the most prevalent oncologic diseases worldwide, with a staggering 1.93 million new cases diagnosed and 940.000 fatalities in 2020. It ranks as the third most common cancer in terms of occurrence and the second leading cause of cancer-related deaths globally (Xi & Xu, 2021; Martin *et al*, 2020).

Although CRC affects both genders, it exhibits an increased frequency among males in several high-income countries. For instance, in the USA CRC age-standardized incidence rate in 2020 was 25% higher in men than in women, respectively with a frequency of 28.7 versus 22.9 cases per 100.000 individuals. An even stronger trend is observed in Italy, with an age-standardized incidence of 34.2 vs 25.2 cases per 100.000 individuals, corresponding to a 36% increase in frequency in males compared to females (Sung *et al*, 2021). Such sex disparity can be attributed to various factors, including endogenous carcinogenic factors, hormonal exposures, and a greater prevalence of established risk factors in males (Siegel *et al*, 2023).

The median age at diagnosis for CRC patients is 65 years, a value that rapidly declined in recent years due to a rise in cases among individuals aged 55 years and younger, which in 2019 constituted up to 20% of all new diagnoses. Notably, while CRC incidence in the general population has steadily declined since the 1990s, the incidence among individuals aged 20-49 years during the same period has increased by nearly 50% (Miller *et al*, 2022). The causes for this rise among young adults are yet to be defined, but may be related to poor diet, sedentary lifestyle, and the obesity epidemic. Nonetheless, older individuals (over 65 years of age) remain the most affected demographic, with a CRC incidence rate of 160.9 cases per 100.000 individuals in the USA between 2015 and 2019 (Miller *et al*, 2022; Siegel *et al*, 2023).

In addition to gender and age-dependent differences, CRC incidence varies by country and appears to be positively correlated with the human development index (HDI) (Xi & Xu, 2021). In countries with high HDI CRC incidence is four times higher than in those with a low HDI, and although CRC rates have stabilized in highly developed nations, they have been slowly rising in developing ones. The difference can be partly explained by HDI taking into account life expectancy, and thus high HDI would reflect an older population that is more prone to

CRC development. Furthermore, individuals in highly developed countries are generally more exposed to CRC risk factors, such as alcohol, cigarette smoke, a fiber-poor diet and sedentary lifestyle (Xi & Xu, 2021).

1.1.2 Colorectal cancer management: available therapies and prevention strategies

As previously mentioned, a trend towards reduced incidence and mortality rates among CRC patients emerged in the last two decades as a result of great efforts made for earlier diagnosis and by the advancements in both surgical and pharmacological therapies. Nevertheless, treatment options and survival rate of CRC patients remain closely dependent on the disease stage at diagnosis (Figure 1) (Xi & Xu, 2021; Miller *et al*, 2022).

Patients diagnosed with regional or localized disease (stage I and II) generally respond well to surgical resection alone, whereas the majority of patients with invasive disease (stage III) has to undergo adjuvant chemotherapy to lower the risk of recurrence. For metastatic cancer (stage IV) a surgical intervention is rarely feasible, and it's often combined with or replaced by radiotherapy, chemotherapy, immunotherapy, or targeted therapy (Miller *et al*, 2022).

The choice of the pharmacological regimen for patients who cannot rely on surgical resection depends on both the tumor molecular characteristics and the natural history of the

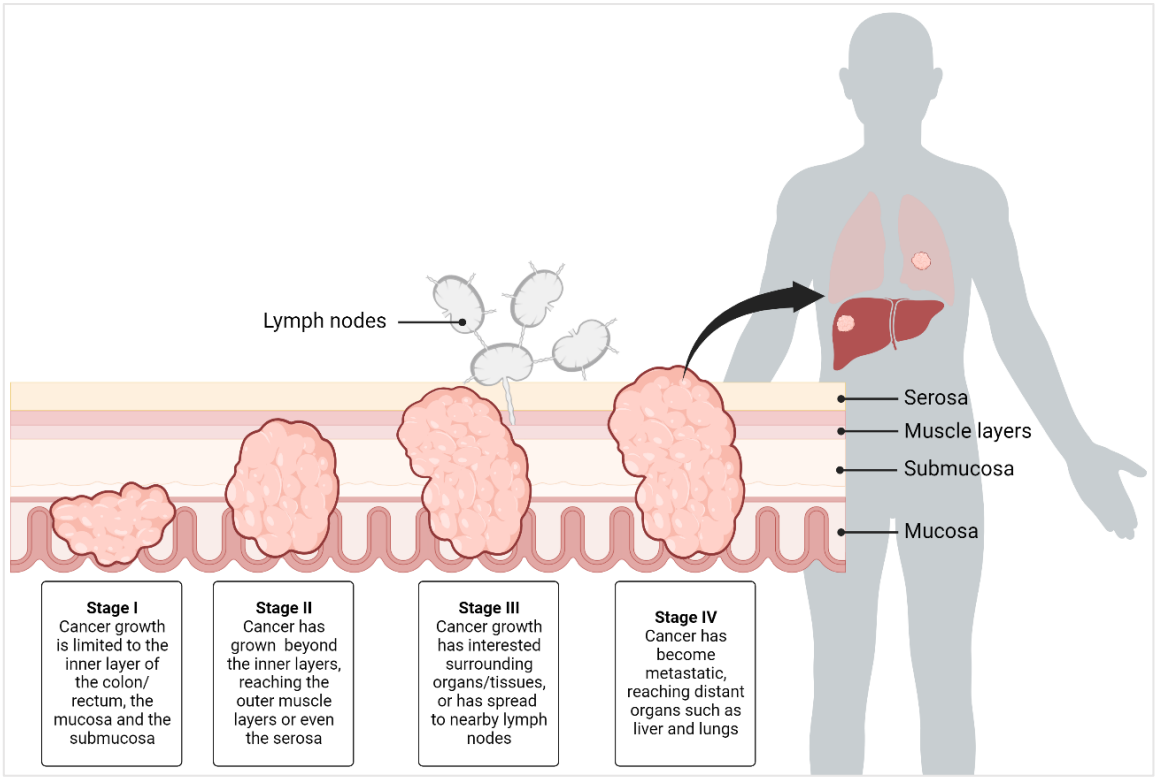


Figure 1. Schematics of the characteristics of colorectal cancer for different disease stages *Created with Biorender.com.*

disease. Fluoropyrimidines are conventionally employed as first-line chemotherapy for CRC due to their tolerability, making them suitable even for most frail patients. Alternatively, oxaliplatin or irinotecan-based regimens can be administered as monotherapy, or in combination with targeted therapies. Among the latter there are VEGF inhibitors, which are contraindicated in patients who have recently undergone surgery, and EGFR inhibitors, which are effective only in KRAS/NRAS wild-type tumors. Additionally, the immune checkpoint inhibitor pembrolizumab was FDA-approved for treating microsatellite instable//MMR-deficient CRC, which is more immunogenic, but not for microsatellite stable/MMR-proficient tumors, which are more common (Biller & Schrag, 2021; Martin *et al*, 2020).

Recently, multiple clinical trials have been testing second and third-line treatments for patients who relapse or progress after first-line treatments, or for those that are otherwise ineligible for traditional therapies (KRAS/NRAS mutant tumors). Among these treatments there are multi-kinase inhibitors, agents targeting different steps in EGFR signaling pathway, BRAF inhibitors, ERBB2-targeting agents, and anti-CTLA4 antibodies (Martin *et al*, 2020). Despite extensive efforts, the efficacy of these therapies remains modest, and surgical resection remains the gold standard for CRC treatment. This results in a significant disparity in 5-year survival rates by disease stage, with rates exceeding 90% for resectable stage I colon and rectal cancer, dropping to 11% and 15% respectively for inoperable stage IV disease (Siegel *et al*, 2023).

To shift CRC distribution towards early stages, many developed countries have focused their efforts on earlier diagnosis via population-based screening. As a matter of fact, CRC is generally asymptomatic, and when symptoms do appear, such as rectal bleeding, anemia, or abdominal pain, they are often associated to aggressive disease in advanced or metastatic stage. Therefore, the detection of precancerous lesions or early-stage CRC is only possible when screening pre-symptomatic individuals via stool-based tests (e.g., fecal occult blood test) or endoscopic methods (e.g., colonoscopy). In absence of highly effective treatments for late-stage metastatic disease, these prevention strategies are still considered among the most effective tools to alleviate the global impact of CRC (Xi & Xu, 2021; Siegel *et al*, 2023).

1.1.3 The liver as a privileged site for colorectal cancer metastasis

CRC is considered particularly prone to metastatization. Approximately 22% of CRC patients already display metastases at the time of diagnosis, and among those who don’t,

around 70% will eventually experience metastatic occurrence at later time-points (Wang *et al*, 2020). Despite minor variation in frequency depending on the molecular subtype and localization of the primary tumor, the most common sites for CRC metastasis are liver (~70%) and lung (~20%), followed by peritoneum, bone, and brain (Wang *et al*, 2020; Riihimäki *et al*, 2016). The liver represents a privileged site for CRC metastasis, most of the patients developing hepatic metastasis during the course of their disease (Martin *et al*, 2020). This can be attributed to peculiar anatomical, cellular, and immunological characteristics of the liver.

Firstly, blood flows directly from the colon to the liver through the portal vein, which drains both mesenteric veins (Figure 2). Physiologically, these blood vessels are meant to bring nutrients absorbed in the colon towards the liver, where most of their metabolic processing will take place. However, in presence of CRC these blood vessels also provide a privileged route for hematogenous dissemination of cancer cells from the primary tumor to the liver (Rhu *et al*, 2017). The liver is also particularly receptive to metastatic seeding due to the micro-anatomy of its blood vessels. Most of the hepatic vasculature consists of sinusoids, small blood vessels where the blood from the portal and the hepatic artery is collected and mix before draining towards the central vein (Figure 2). These vessels are characterized by a slow blood flow, a high density of pores and fenestrae, and by the absence of any physical barrier beneath the endothelium, making them particularly permissive to cell extravasation (Braet & Wisse, 2002).

Beyond hemodynamic considerations, the liver is also particularly susceptible to metastasis because of the cellular and molecular composition of the hepatic niche. In particular, liver sinusoid endothelial cells (LSECs) express several cell adhesion molecules responsible for the arrest and extravasation of circulating cancer cells, while hepatic stellate cells in the space underlying liver sinusoids respond to cancer cell seeding by forming a fibrotic niche that further enhances cancer cells engraftment (reviewed in Mielgo & Schmid, 2020).

Finally, the last factor making the liver particularly vulnerable to CRC metastasis is its immunologically tolerogenic environment, which may discourage the clearance of extravasating cancer cells by resident immune cells. Such immunosuppressed environment is required by liver physiological activity in tissue remodeling and metabolism, as well as its continuous exposure to dietary and microbial products, which poses the risk of excessive immune activation. To prevent chronic hepatic inflammation and tissue damage, the liver has

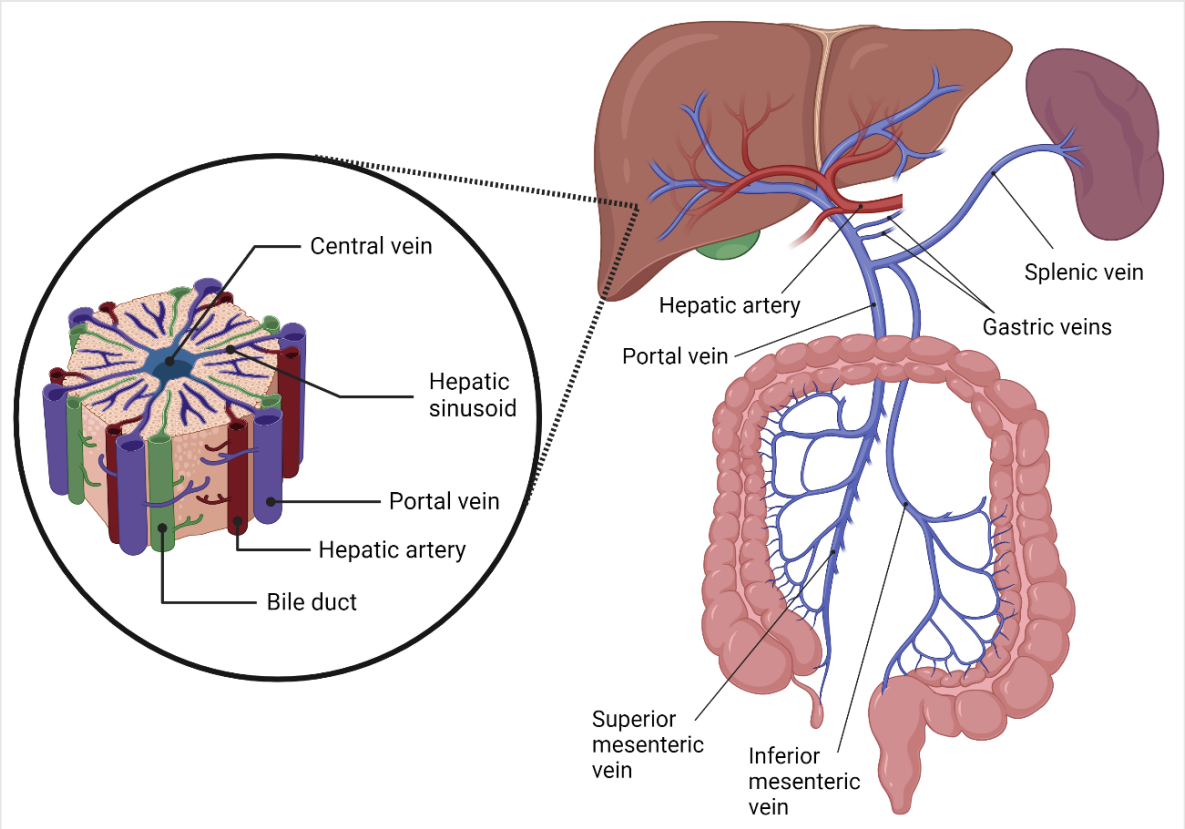


Figure 2. Schematics of macro and micro vasculature in the liver *The liver receives blood from the hepatic artery and the portal vein. The latter collects the circulation from the splenic vein, gastric veins, and mesenteric veins (on the right). At microscopic level, each hepatic lobule (in the circle on the left) is irrorated by both the portal vein and the hepatic artery, whose circulation mix in the hepatic sinusoids before reaching the central vein. The blood collected in the central vein drains towards the hepatic vein, which finally leads to the vena cava.*
Created with Biorender.com.

hence evolved a generally tolerogenic behavior towards immunostimulatory insults (Robinson *et al*, 2016). Examples of this immunosuppressive potential are evident in the field of organ transplantation, in which liver transplant performed alone or in combination with other organs significantly reduces the occurrence of graft rejection, and in some cases can even abrogate the need for immunosuppressive regiments (Londoño *et al*, 2013; Raichlin *et al*, 2009; Robinson *et al*, 2016).

The maintenance of hepatic tolerance is principally entrusted to liver resident myeloid cells, which contribute to its immunosuppressive micro-environment by producing immunoregulatory cytokines and by directing the adaptive immune response towards pro-tolerogenic responses.

For instance, Kupffer cells (KCs), liver resident macrophages, respond to gut-derived bacterial endotoxins by producing anti-inflammatory factors, notably IL10 and prostaglandins (Callery *et al*, 1991; Knoll *et al*, 1995). These mediators downregulate the expression of co-stimulatory molecules on antigen presenting cells (APCs), preventing the activation of CD4+ T cells and impairing the generation of an effective adaptive immune response (Groux *et al*, 1996; Knolle *et al*, 1998; You *et al*, 2008). KCs themselves, when presenting antigens for T cell priming, preferentially expands IL10 producing T regulatory cells, thus inducing antigen-specific tolerance (Heymann *et al*, 2015; You *et al*, 2008). A similar behavior is observed in hepatic dendritic cells (DCs), which are generally less proficient in activating T cells and produce significantly more IL10 compared with splenic DCs (Bamboat *et al*, 2009; De Creus *et al*, 2005).

Myeloid-derived suppressor cells (MDSCs) are another key player in maintaining liver tolerogenic environment. These cells are characterized by the ability to suppress T cell activation through the secretion of immunosuppressive cytokines IL10 and TGFβ, and the production of arginase and IDO, which deplete essential amino acids required for immune cell function (Gabrilovich & Nagaraj, 2009). MDSCs are normally present in the healthy liver, but can further expand by infiltration of circulating monocytes, which differentiate into MDSCs after transmigrating through LSECs (Zimmermann *et al*, 2016).

1.1.4 Colorectal cancer liver metastasis: clinical challenges and future perspectives

As previously discussed, colorectal cancer liver metastasis (CRLM) are not only frequent, but they also represent a major cause of concern for disease management, due to scarce therapeutic options.

Even though curative resection and chemotherapy remain the standard treatment for metastatic CRC, patients presenting with CRLM seldomly qualify for surgery. This ineligibility can be attributed to characteristics of the hepatic masses, such as their number, location, and size, or to the patient's clinical presentation, including the presence of extrahepatic masses or other comorbidities. Collectively, surgical resection is applicable only to 10-20% of CRLM patients (Biller & Schrag, 2021; Akgül *et al*, 2014).

Systemic antitumoral treatments are also generally impaired by the presence of CRLM, both because of factors associated to the metastatic process in general and to liver behavior in particular. For instance, tumor dissemination requires a certain phenotypic plasticity for

cancer cells to extravasate into the blood stream, infiltrate distant organs and colonize them. Such plasticity is often observed in highly aggressive end-stage metastatic cancers and is associated with resistance to standard therapies (Quintanal-Villalonga *et al*, 2020). Additionally, gene networks associated to epithelial-to-mesenchymal transition (EMT) partially overlap with those involved in cancer stemness, and they have been implicated not only in tumor progression and metastasis, but also in resistance to therapy (Zhao *et al*, 2022).

On the other hand, the immunosuppressive environment of the liver not only favors the establishment of liver metastasis, but also significantly impairs systemic antitumoral immune response, reducing immunotherapy efficacy. Preclinical models have shown that the presence of liver metastases, regardless of the primary tumor origin, leads to the apoptosis of tumor-specific CD8+ T cells, hampering the efficacy of anti-PDL1 treatment (Yu *et al*, 2021; Lee *et al*, 2020), These findings align with the systemic T cell loss observed in patients with liver metastasis, and may provide a mechanistic explanation for the reduced responsiveness to immunotherapy in such cases.

Up to date, all available therapies for CRC are affected by these resistance mechanisms, and they have proved ineffective in treating liver metastasis. Consequently, patients diagnosed with CRLM typically face poor prognosis. Understanding the mechanisms underlying CRC metastasis to the liver and developing novel strategies to mitigate it are crucial for improving the treatment outcomes and life expectancy of patients.

1.2 Kupffer cells in homeostasis and disease

1.2.1 General characteristics and origin

Liver resident macrophages, known as Kupffer cells (KCs) were first identified by Karl Wilhelm von Kupffer in 1876. They constitute a significant portion of the myeloid compartment, constituting 80-90% of all the tissue macrophages and 30-35% of non-parenchymal liver cells (Bilzer *et al*, 2006; Nguyen-Lefebvre & Horuzsko, 2015). As suggested by their prevalence, they have a crucial function, primarily in maintaining liver homeostasis, which is a critical regulator of the maintenance of the whole body.

KCs are located within the lumen of hepatic sinusoids, where they adhere to the endothelial cells lining these vessels and come into direct contact with the bloodstream. Owing to their anatomical location, KCs proficiently clear senescent or apoptotic cells from the blood, and they serve as first barrier against gut-derived bacteria and endotoxins. However, their function is not limited to scavenging cellular and microbial debris, but they also play a pivotal role in immune regulation and in various metabolic pathways, as it will be further discussed in chapter 1.2.2 (Nguyen-Lefebvre & Horuzsko, 2015; Krenkel & Tacke, 2017).

KCs constitute a population of self-sustaining, locally proliferating phagocytes separated from monocyte-derived, infiltrating macrophages. They originate from yolk sack-derived erythromyeloid progenitors that colonize the embryonic liver, proliferating and activating specific transcriptional programs that allow them to self-sustain throughout life (Soucie *et al*, 2016; Mass *et al*, 2016). In cases of extensive KC depletion during liver injury, they can be replenished by monocyte-derived macrophages, which acquire KC features following hepatic-niche colonization (Scott *et al*, 2016).

The extent to which colonizing monocytic cells resemble KCs is subject of debate, with some studies demonstrating a full correspondence (Scott *et al*, 2016) and other pointing out functional differences (Beattie *et al*, 2016). Nevertheless, it's clear that the liver microenvironment plays a pivotal role in directing KC differentiation, providing the decisive factors determining their phenotype (Lavin *et al*, 2014; Beattie *et al*, 2016). Therefore, the longer monocyte-derived macrophages reside in the liver, the more closely they resemble KCs in terms of phenotype and function, with an average "education" period of 30-60 days in mice (Blériot et al, 2020; David et al, 2016).

The lifespan of KCs has been scarcely investigated and remains controversial due to conflicting data. Initially, it was calculated to be 3.8 days (Bouwens *et al*, 1986), but more recent experimental evidence hints to a longer life span. KCs can be maintained for more than 40 days in monocytopenic mice (Naito & Takahashi, 1991), and following liver transplantation donor KCs are completely replaced within 15–30 days in rat, but can persist for up to 1 year in human (Takahashi, 1989). This suggests that the lifespan of KCs could extend to a few weeks in rodents to up to one year in humans.

1.2.2 Other subsets of liver macrophages and Kupffer cells markers

Hepatic macrophages exhibit remarkable heterogeneity in terms of origin, function, and localization (Blériot et al., 2020). In addition to KCs, which are the most abundant type of hepatic macrophages, other distinct populations of hepatic macrophages have been identified, such as liver capsule macrophages, bile duct-associated macrophages, and other macrophages temporarily infiltrating the liver, deriving from circulating monocytes or peritoneal macrophages (Guilliams *et al*, 2022).

KCs themselves exhibit some degree of heterogeneity, mainly dependent on their source of origin. As discussed in chapter 1.2.1, KCs almost entirely descend from yolk sac-derived erythromyeloid progenitors, but in particular circumstances they can also be repopulated from bone-marrow derived monocytes. These monocytic progenitors mature into the hepatic niche, hence the resulting macrophages display characteristics largely overlapping with those of erythromyeloid-derived KCs (Scott *et al*, 2016). For this reason, some authors refer indiscriminately to both as KCs, independently of their origin. However, some differences remain between the two populations, as shown by recent reports (Beattie *et al*, 2016; Guillot & Tacke, 2019), thus for the purpose of this thesis the term "KCs" will be used exclusively to refer to long-lived macrophages descending from erythromyeloid progenitors.

Most studies on macrophage ontogeny have been conducted in mice, identifying different surface antigens that allow to distinguish between murine KCs and macrophages of bone marrow origin. Despite a lack of unified markers, most authors agree that the latter express Ly6C protein on their surface, which is not present on KCs, and higher levels of CD11b (Zigmond *et al*, 2014; Movita *et al*, 2012). Moreover, the chemokine receptor CX3CR1 is expressed exclusively by cells of monocytic origins, including bone-marrow derived macrophages, in both rats and mice (Heymann *et al*, 2015).

Conversely, murine KCs express several markers useful to distinguish them from other resident macrophages, but not from hepatic monocytic macrophages, which tend to upregulate them as a result of their interaction with the hepatic niche. Among these markers, CLEC4F and TIMD4 are the paradigmatic markers defining KC molecular signature. CLEC4F is a C-type lectin responsible for the antigen presentation of glycolipid antigens, as well as partaking in the recognition and scavenging of desialylated platelets (Yang *et al*, 2013). TIMD4 is a phosphatidylserine-specific receptor involved in the elimination of apoptotic cells and in triggering Th2 cell differentiation (McGrath, 2018). Albeit not as liver-specific as CLEC4F, as it is also expressed by some subsets of splenic macrophages, TIMD4 can prove useful to distinguish monocyte-derived macrophages from KCs because its expression remains negligible for over one month after monocytic liver colonization (Scott *et al*, 2016). Other KC markers include VSIG4, MARCO and CD163, which are all involved in the recognition of bacteria and opsonized particles and the immune response against them (Novakowski *et al*, 2016; Beattie *et al*, 2016).

Apart from classifications based on their origin, KCs can also be divided into sub-populations following their bias towards specific biological functions. Recent reports have indeed identified two distinct functional subsets of KCs: immune-reactive KC1 and metabolically active KC2 (Blériot *et al*, 2021; De Simone *et al*, 2021). KC1 constitute the most abundant subset, accounting for 85% of total KCs. They are defined as a $CD206^{low}$ $ESAM^{-}$ and they are characterized by a strong immune signature. On the other hand, KC2 are $CD206^{high}$ $ESAM^{+}$, they express particularly high levels of fatty acid transporter CD36 and they are thus able to regulate both reactive oxygen species production and lipid peroxidation. KC2 have also been recently implicated in immune-regulatory functions, driving T cells priming in a model of viral hepatitis (De Simone *et al*, 2021). Interestingly, KC2 seem to express both typical KCs markers, like CLEC4F and TIMD4, and markers traditionally associated to endothelial cells, such as ESAM and CD31. This peculiar molecular signature has proven controversial, with new reports arguing how KC2 could derive from a contamination of isolated KCs with LSECs, and others supporting KC2 existence as a distinct cell population (Guilliams *et al*, 2022; Hume *et al*, 2022; Iannacone *et al*, 2022).

While monocyte-derived macrophages and KCs can share functions and characteristics, recent studies have identified two subsets of liver macrophages with markedly distinct features and localization. Liver capsule macrophages (LCMs) develop from bone marrow precursors

and express the macrophage markers F4/80, CSF-1R, CX3CR1 and CD14. Unlike KCs, LCMs display very long processes and are negative for TIMD4. It's speculated that LCMs play a role in defending the liver against microbial pathogens derived from the abdominal cavity, which have not entered the bloodstream and thus cannot be eliminated by KCs (David et al., 2016). Another recently identified population of liver macrophage is associated with bile ducts and expresses the GPNMB marker, defining them as lipid-associated macrophages (LAMs). LAMs also originate from bone marrow-derived precursors, but little is known about their function, which may be related to establishing tolerance against LPS (Remmerie *et al*, 2020).

1.2.3 Role of Kupffer cells in homeostasis

Along with DCs and LSECs, KCs constitute the reticulo-endothelial system, whose main function is clearing sinusoidal blood from senescent cells, antigens, pathogens, and toxins. KCs are particularly proficient at this task due to their localization in the sinusoidal lumen and to the expression of distinct complement receptors, Fc receptors, and scavenger receptors that allow them to efficiently phagocyte a number of different elements.

For instance, KCs can recognize complement C3-opsonized particles via classical complement receptors CR1, CR3 and CR4, but also through the nearly KC-exclusive CRIg (Helmy *et al*, 2006; Hinglais *et al*, 1989). KCs are also able to phagocyte antigens opsonized by both IgG and IgA, thanks to the presence of a wide variety of Fc receptors on their cell surface (Latvala *et al*, 2017; Vorsatz *et al*, 2021; van Egmond *et al*, 2000). Finally, KCs express scavenger receptors which allow the clearance of senescent or apoptotic cells, notably erythrocytes, as well as erythrocyte-derived vesicles and hemoglobin–haptoglobin complexes from the blood (McGrath, 2018; Willekens *et al*, 2005; Kristiansen *et al*, 2001; Novakowski *et al*, 2016).

The antigens thus internalized can be processed and exposed on the surface of KCs, to be presented to T cells, whereby KCs are considered professional antigen presenting cells (APCs). However, antigen presentation by KCs is not particularly potent, as they normally express low levels of MHC-II and co-stimulatory molecules (You *et al*, 2008). It's also important to remember that KCs play an essentially tolerogenic role in liver immunity, releasing immunosuppressive cytokines that inhibit DC-induced antigen presentation, suppress cytotoxic T cell function and in turn activate Tregs, as discussed in chapter 1.3.3.

Nevertheless, KCs can mount efficient immune responses when needed, for instance to trigger anti-inflammatory reactions and promote anti-microbial defense. KCs express toll-like receptors (TLR) recognizing bacterial LPS, and, under particular stress conditions, they produce (i) inflammatory mediators with a direct effect on microbial proliferation, and/or (ii) chemokines to recruit monocytes and neutrophils into the liver to control bacterial infection (Barsig *et al*, 1998; Su *et al*, 2000; Seki & Brenner, 2008).

KCs also play a fundamental role in iron recycling and bilirubin metabolism. As already mentioned, KCs are able to internalize hemoglobin directly, by hemoglobin-haptoglobin receptor CD163 or transferrin receptor TfR1, or indirectly, phagocyting senescent or imperfect erythrocytes and erythrocyte-derived vesicles (Gammella *et al*, 2014; Kristiansen *et al*, 2001). Following hemoglobin internalization, KCs employ the enzyme heme oxygenase 1 (HO-1) to release ferrous iron from the heme group, generating carbon monoxide and bile pigments as byproducts of the reaction (Nguyen-Lefebvre & Horuzsko, 2015; Gammella *et al*, 2014). Moreover, KCs participate in the homeostasis of iron by regulating hepcidin production and release from hepatocytes. This hormone inhibits gut iron absorption and iron release from splenic and hepatic macrophages, regulating its circulating levels. KCs negatively regulate hepcidin mRNA expression in hepatocytes, therefore increasing the levels of circulating iron (Theurl *et al*, 2008).

Similarly, KCs are able to modulate lipid homeostasis directly, regulating their trafficking, or indirectly, intervening on their metabolization by hepatocytes. For instance, KCs uptake low-density lipoproteins (LDLs), very low-density lipoproteins (VLDLs) and oxidized lipoproteins from the circulation via macropinocytosis, phagocytosis and scavenger receptor-mediated pathways, and degrade them to release free fatty acids and cholesterol (Tabas *et al*, 2016). On the other hand, KCs express transporters that regulate the efflux of cholesterol to apolipoproteins, promoting high-density lipoproteins (HDLs) formation (Hutchins & Heinecke, 2015). KCs are also the main source of cholesteryl ester transfer protein (CETP), a plasma protein mediating the exchange of lipids between HDL and VLDL (Wang *et al*, 2015). Additionally, KCs can secrete soluble factors that modulate oxidative metabolism in hepatocytes, increasing fatty acid breakdown or promoting their storage and accumulation (Odegaard *et al*, 2008; Diehl *et al*, 2020). Interestingly, macrophage polarization and lipid metabolism seem to be tightly intertwined, being driven by common transcription factors, epigenetic signatures and biochemical cues (Remmerie & Scott, 2018). In general, a reciprocal

relationship exists between pro-inflammatory M1 polarization and fatty acid synthesis, while pro-tolerogenic M2 polarization is associated to fatty acid oxidation.

1.2.4 Role of Kupffer cells in disease: focus on cancer

KCs are involved in several hepatic pathologies, including bacterial infections and viral hepatitis, as well as aseptic conditions such as liver fibrosis, alcoholic and non-alcoholic liver diseases, and cancer (Nguyen-Lefebvre & Horuzsko, 2015). Their impact on disease progression hinges on their activation state, which can vary depending on the stimuli to which they are exposed. Macrophages respond to environmental cues in an extremely plastic fashion, encompassing a spectrum of functional states ranging from classical activation (M1) to alternative activation (M2) phenotypes (Figure 3a). Importantly, these two states represent the extremes of the polarization process observed *in vitro*, and they are seldomly observed *in vivo*. Instead, macrophages in pathophysiological conditions tend to adopt intermediate phenotypes displaying mixed features of both M1 and M2 state.

M1 classical activation state is triggered by interferon gamma (IFN-γ) stimulation alone or combined with microbial products (LPS) and inflammatory cytokines (TNF) (Beljaars *et al*, 2014). M1 macrophages are characterized by high antigen presentation capacity, high expression of IL-1β, IL-12, IL-23 and interferon response genes, and by the production of nitric oxide (NO) and reactive oxygen species (ROS) (Beljaars *et al*, 2014; Mantovani *et al*, 2004; Hu & Ivashkiv, 2009). These macrophages are therefore considered antimicrobic and pro-inflammatory, and skew T cell responses towards Th1 (Mills *et al*, 2000).

Conversely, M2 alternative activation can be triggered by various stimuli, the prevalent being cytokines IL4, IL10, IL13, as well as IL33, TGF-β, G-CSF, and glucocorticoid hormones (Martinez *et al*, 2013). Different stimuli can activate different M2 phenotypes (M2a,b,c) with varying immune-modulating and wound healing capabilities (Martinez *et al*, 2013). In general, though, M2 macrophages downregulate IL12 and pro-inflammatory cytokines in favor of IL10 production, enhance antigen presentation to recruit Th2, and secrete extracellular matrix (ECM) components (Martinez *et al*, 2013; Beljaars *et al*, 2014; Anderson & Mosser, 2002; Edwards *et al*, 2006). Thus, M2 macrophages are generally considered pro-tolerogenic and involved in the process of tissue healing and resolution of inflammation.

Following this paradigm, M1-like KCs are more proficient at pathogen clearance and immunosurveillance but can inadvertently trigger excessive inflammation and chronic liver

damage. In contrast, M2-like KCs may facilitate the resolution of acute insults, but they might promote an immunosuppressive microenvironment that fosters tumor progression. This dual role of KCs in preventing or promoting pathological conditions is particularly evident in the field of cancer.

For instance, KCs role in hepatocellular carcinoma (HCC) is ambiguous, as they may both hinder and drive tumor development and progression. On the one hand, KCs are innate immune cells, and as such they actively contribute to tumor surveillance. They can be recruited by senescent hepatocytes through the CCL2-CCR2 axis to clear premalignant cells (Eggert *et al*, 2016). Furthermore, hepatic macrophages can prevent hepatocarcinogenesis by engaging CD4+ T cells and triggering adaptive antitumoral responses (Ma *et al*, 2016). On the other hand, chronic inflammation promoted by KCs is pro-tumorigenic, and can drive neoplastic transformation and HCC formation. For instance, following activation by prolonged exposure to bacterial products, KCs secrete cytokines, ROS and growth factors that encourage the expansion of preneoplastic hepatocytes (Roberts *et al*, 2007; Capece *et al*, 2013). KCs can also be activated by hepatocyte damage following the expansion of early neoplastic lesions, hence releasing inflammatory cytokines that support hepatocellular growth and allow the formation of macroscopic tumor masses (Vansaun *et al*, 2013; Wu *et al*, 2012).

At later stages of the disease, HCC can reprogram KCs to act as tumor associated macrophages (TAMs), supporting tumor progression, invasion, and immune escape (Figure 3b). TAMs can directly promote HCC growth by secretion of various cytokines and chemokines, such as IL-1β, IL-6, TNF, CCL2 and CXCL10, increasing cancer cell proliferation and resistance to apoptosis (Wan *et al*, 2015; Ju & Tacke, 2016; Capece *et al*, 2013). Furthermore, they can express many pro-angiogenic growth factors, as VEGF, PDGF, FGF and TGFβ, as well as angiogenesis-modulating enzymes cyclooxygenase-2 (COX-2) and matrix metalloproteinases (MMPs), which promote the vascularization of the tumor mass and the reshaping of its niche, allowing the tumor macroscopic expansion and invasion of nearby tissues (Wan *et al*, 2015; Afik *et al*, 2016; Capece *et al*, 2013). Finally, TAMs can impair adaptive anticancer immunity by engaging immunosuppressive Th2 and Treg cells, and by disrupting cytotoxic T cells activity inducing their senescence, secreting immunosuppressive molecules, or overexpressing PD1 co-inhibitory molecules (Ilkovitch & Lopez, 2009; Zhao *et al*, 2012; Li *et al*, 2012; Mantovani *et al*, 2009; Makarova-Rusher *et al*, 2015).

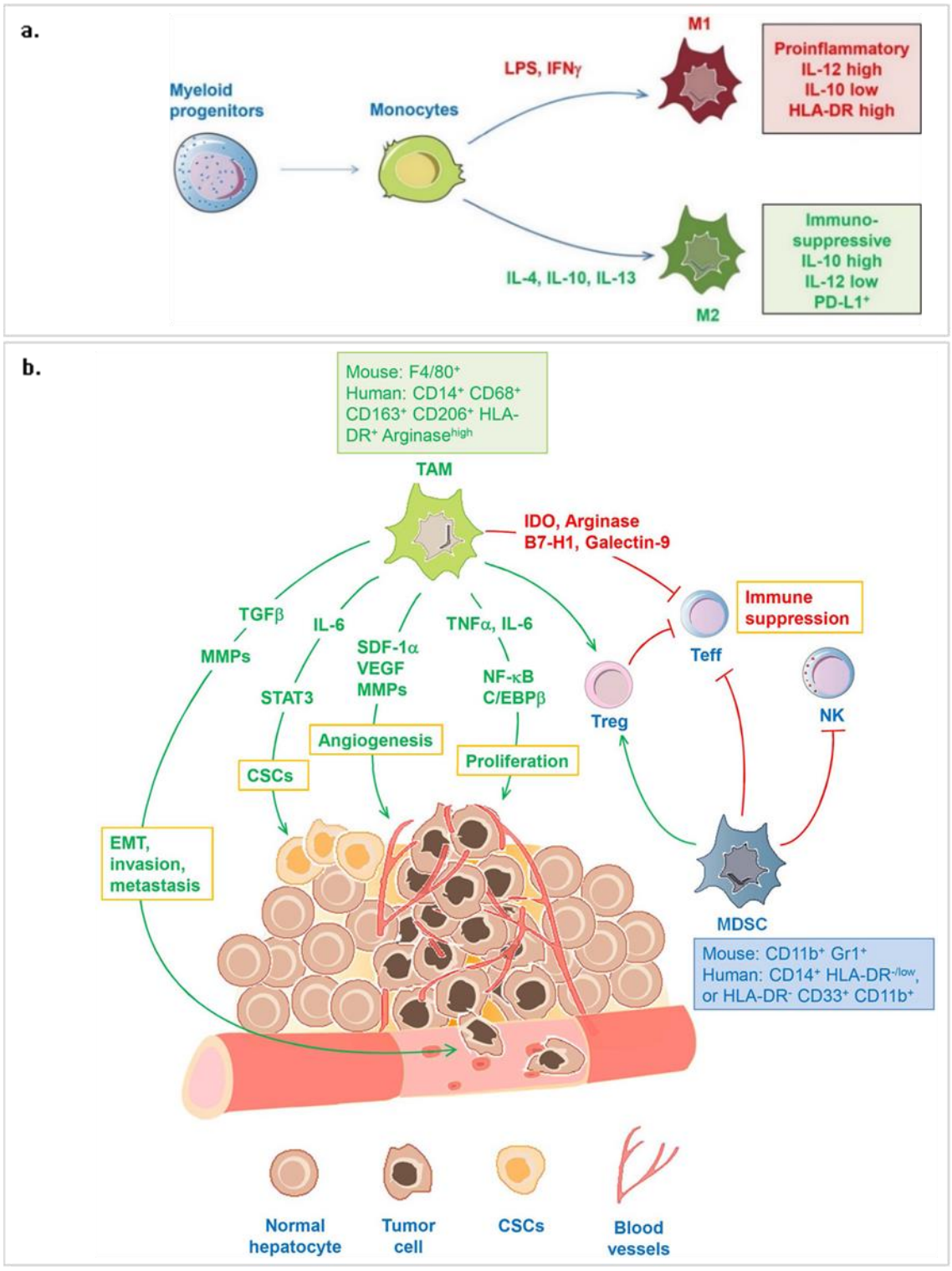


Figure 3 (a) Classically activated M1 and alternatively activated M2 macrophages *Macrophages typically originate from circulating myeloid progenitors or monocytes. Under different environmental stimuli they can differentiate into a range of phenotypes whose extremes are the classical activation state (M1) and the alternative activation state (M2).*
(b) TAMs functions in HCC *TAMs contribute to HCCs progression by promoting angiogenesis invasion/metastasis and cancer cell proliferation through a variety of mechanisms. Moreover, the collaborate with MDSCs to suppress immune-mediated antitumoral responses. (adapted from Wa et al, 2015; permission to reproduce from Wolters Kluwer Health, Inc. under license numbe 5686000121255)*

Similarly, KCs display ambivalent role in liver metastasis, exerting antitumoral or protumoral functions depending on the stage of the metastatic process, tumor burden, and interactions with other immune cells. During the early stages of metastatic dissemination, KCs limit liver colonization by releasing oxygen metabolites, cytotoxic cytokines, and proteases, as well as by directly engulfing cancer cells that extravasate in the liver (Gardner *et al*, 1991; Bayón *et al*, 1996; Wang *et al*, 2000; Seki *et al*, 2011; Kimura *et al*, 2016). This antitumoral activity is sustained by the recruitment of other immune cells, and in particular natural killer (NK) cells, which secrete inflammatory factors such as granulocyte macrophage colony stimulating factor (GM-CSF) and interferon γ (IFNγ) promoting KCs tumoricidal activity (Timmers *et al*, 2004). However, efficient tumor clearance by KCs is limited to the very early phases of metastatic dissemination, during cancer cell adhesion to the KCs into the liver sinusoids and following the first 24h of their entry in the parenchyma (Bayón *et al*, 1996; Matsumura *et al*, 2014). Subsequently, if immunosurveillance fails to halt the establishment of liver metastasis, KCs are reprogrammed by cancer cells to act as TAMs, again promoting cancer cell proliferation, favoring angiogenesis and tissue remodeling (Nielsen *et al*, 2016; Shimizu *et al*, 2017; Jiang *et al*, 2021).

This dual role of KCs in tumorigenesis is evident in colorectal cancer (CRC) liver metastasis murine models, in which the depletion of KCs before tumor induction resulted in increased tumor burden during early stages but proved beneficial in later stages, reducing tumor growth, VEGF signaling, and promoting immune-mediated cancer clearance by enhancing T cell and iNOS-expressing cell infiltration (Wen *et al*, 2013). Therefore, reversing the reprogramming of KCs towards an antitumoral phenotype is a key step to reactivate the immune system against liver metastasis and support immune-mediated cancer clearance.

1.3 microRNAs as regulators of gene expression

MicroRNAs (miRNAs) are the most abundant subset of small non-coding RNAs. They are short (~22 nt), single-stranded RNAs, and they are often highly conserved among species (Bartel, 2009). They are found in viruses, protists, and eukaryotes, but they are particularly relevant in higher organism, accounting for 1–2% of all genes in mammals (Bartel, 2004; Kozomara *et al*, 2019).

MiRNAs play a pivotal role in gene expression regulation, acting at both transcriptional and post-transcriptional level. In most cases miRNAs bind to the 3' UTR of target mRNAs to suppress their expression, but they can also interact with the 5' UTR or coding region, or even with gene promoters within the nucleus to regulate transcription (Vasudevan, 2012; Broughton *et al*, 2016; Makarova *et al*, 2016).

They are required for normal animal development and are involved in virtually every biological process, including cell proliferation, differentiation, metabolism and stress responses (Gebert & MacRae, 2019; Kozomara *et al*, 2019; Xu *et al*, 2021). Furthermore, many miRNAs display tissue and cell-specific expression patterns that, when deregulated, may lead to various pathological conditions, including cancer (Bartel, 2009).

1.3.1 Biosynthesis

MiRNAs can be transcribed either by RNA polymerase II or III depending on their genomic location in respect to other genes and the presence of an independent promoter. About half of annotated miRNAs are processed from introns, or less frequently exons, of protein coding genes, and as such share the same promoter and undergo the same transcriptional regulation of their host genes (Kim & Kim, 2007; De Rie *et al*, 2017). Conversely, other miRNAs are transcribed independently from protein coding genes, as individual genes or as clusters of multiple miRNAs coded by the same transcript (Tanzer & Stadler, 2004).

The unprocessed RNA derived from the transcription of miRNA genes takes the name of primary (pri)-miRNA. It is typically long over 1 kb and characterized by a hairpin structure composed of a 33–35 bp long stem embedding the mature miRNA sequence, a terminal loop and two single-stranded RNA segments at its 5′ and 3′ ends. This structure is recognized and processed at nuclear level by RNase III Drosha and its essential cofactor DGCR8, which together form a complex known as Microprocessor. The positioning of microprocessor onto

the hairpin is a crucial step of miRNA biosynthesis, and it is mediated by multiple structural and sequence-based features of the pri-miRNA (Han *et al*, 2006; Zhang & Zeng, 2010; Ma *et al*, 2013; Auyeung *et al*, 2013; Roden *et al*, 2017). Through the recognition of such features, DGCR8 binds the apical loop of the pri-miRNA, directing Drosha onto its stem and allowing the enzyme to cleave in the correct position: approximately 11bp from the stem base and 22 bp away from the junction with the apical loop (Han *et al*, 2006; Zeng *et al*, 2005).

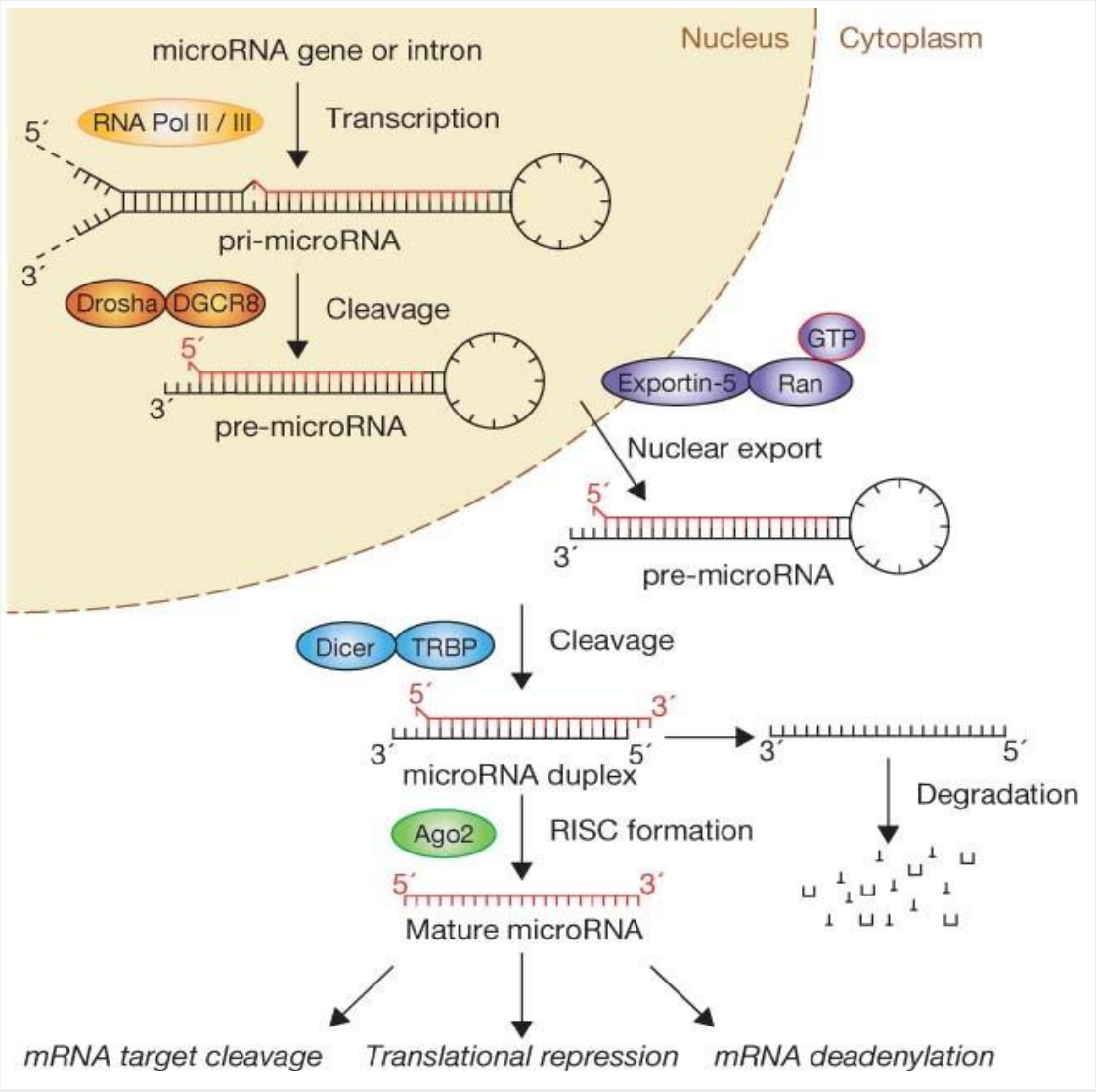


Figure 4 Canonical miRNA processing pathway *miRNAs are transcribed as pri-miRNA by RNA pol II or III, which is subsequently cleaved in the nucleus by the components of the microprocessor complex (DGCR8 and Drosha). The resulting precursor, known as pre-miRNA, is exported to the cytoplasm by Exportin-5 and nuclear GTPase RAN-GTP. Once in the cytoplasm, the pre-miRNA is further processed by RNAse Dicer and its cofactor TRBP, which cleave the terminal loop leaving a microRNA duplex. This precursor is finally loaded onto an AGO protein (eg. Ago2), which selects the guide strand and with it forms the RISC complex. The mature miRNA will provide the RISC complex with sequence specificity, allowing for its target-specific repressive function. (Winter et al, 2009; permission to reproduce from Springer Nature under license number 5686000291356)*

Following the pri-miRNA cleavage by the microprocessor, the lower stem and the single-stranded overhangs are dropped, and a shorter (~65 nt) hairpin structure is formed, known as precursor (pre)-miRNA. This intermediate is loaded onto a transport complex composed of exportin 5 and the GTP-binding nuclear protein RAN-GTP, which translocate it into the cytoplasm, where miRNA maturation can be completed (Yi *et al*, 2003; Lund *et al*, 2004; Bohnsack *et al*, 2004).

The pre-miRNA is then bound by cytoplasmic RNase III Dicer, which recognizes the two-nucleotide-long 3' overhang left by Drosha, and in turn cleaves the hairpin near its terminal loop (Park *et al*, 2011). The position of the Dicer cleavage site is fixed and depends on the species and the type of protein involved in the miRNA processing, but for mammals is generally located 22 nt away from pre-miRNA 5' end (MacRae *et al*, 2006, 2007; Park *et al*, 2011). Dicer processing can be influenced by various RNA-binding proteins, which associate to the pre-miRNA terminal loop and act as cofactors to increase its efficiency and regulate the length of mature miRNAs, or conversely interfere with its action (Heo *et al*, 2008; Trabucchi *et al*, 2009; Lee *et al*, 2013).

The product of this second cleavage is a small RNA duplex, which is loaded onto an Argonaute (AGO) to form the RNA-induced silencing complex (RISC) (Tabara *et al*, 1999; Hammond *et al*, 2001; Mourelatos *et al*, 2002). Humans and mice express four different type of AGO (AGO1-4), which bind almost indistinguishable sets of miRNAs, but differ in terms of repressive activity on the miRNA target (Huntzinger & Izaurralde, 2011). Following miRNA duplex loading, the AGO protein selects one of the two RNA strands, which will become the mature miRNA (i.e. guide strand), and discard the other (aka passenger or star strand), which is rapidly degraded. Guide strand selection is determined on the basis of thermodynamic stability and sequence, with a preference for strands with unstable 5' terminus or uracil at first nucleotide position (Schwarz *et al*, 2003; Khvorova *et al*, 2003). However, this process is not completely strict, and the un-favored strand can be selected with varying frequency in different tissues or under different developmental phases (Chiang *et al*, 2010). The directionality of the chosen strand will then determine the name of the mature miRNA: 5p originates from the 5' end of the original hairpin, and 3p from its 3' end.

Apart from the canonical miRNA processing just described, various alternative pathways can generate miRNAs or miRNA-like small RNAs in a Microprocessor or Dicer independent

manner. For instance, miRNAs embedded in introns can use mRNA splicing to bypass Drosha processing, producing a lariat that directly refolds into a pre-miRNA like structure (Berezikov *et al*, 2007; Ruby *et al*, 2007). Similarly, Drosha processing is dispensable for miRNA derived from endogenous short hairpin RNAs, tRNAs or tRNA-like precursors, small nucleolar RNAs (snoRNAs), or small nuclear RNA-like viral RNAs, whose structure is short enough to be processed directly by Dicer (Babiarz *et al*, 2008; Ender *et al*, 2008; Cazalla *et al*, 2011). There have also been reports of Dicer-independent miRNA biogenesis, as for the case of miR-451 processing, which exploits the catalytic activity of AGO2 to get rid of the apical loop (Cheloufi *et al*, 2010).

1.3.2 Mechanism of action

As previously mentioned, miRNAs biological function in regulating gene expression is accomplished through their interaction with AGO proteins to form the RISC complex. The miRNA act as a guide for target recognition, mediated by the base-pairing between it and the target. The AGO protein then recruits various interactors to the target to regulate its expression. The biological effect of the miRNA-target interaction can vary depending on the extent of miRNA-target complementarity, the endonuclease activity of the AGO protein and the nature of the miRNA target.

MiRNAs have been canonically associated to the negative regulation of their mRNA targets through the interaction with their 3' UTR. In this model base-pairing between the guide strand and the target is often limited to the seed region of the miRNA (residues 2-8 at its 5' end) plus some sporadic pairing at its 3' end to stabilize the bond (Doench & Sharp, 2004; Brennecke *et al*, 2005). This interaction promotes the RISC-mediated recruitment of various factors for mRNA destabilization, including CAF1-CCR4-NOT1 deadenylase complex and Dcp1/2 decapping complex, or leads to ribosome detachment by steric hindrance (Rehwinkel *et al*, 2005; Behm-Ansmant *et al*, 2006; Chekulaeva *et al*, 2011; Nishihara *et al*, 2013). Alternatively, in presence of extensive complementarity between the guide miRNA and the target mRNA, the latter can be directly cleaved by the endonuclease activity of AGO2 (Liu *et al*, 2004; Meister *et al*, 2004). In either case, the interaction of the miRNA with its target results in the translational repression of the mRNA and a reduced protein output.

This simplistic view of miRNA functions is being challenged by a growing body of evidence supporting alternative roles of miRNAs in gene expression regulation. In some cases,

miRNAs have been reported to exert a positive regulation on their targets, augmenting mRNA stability by competing with the mRNA degradation machinery, or by increasing their translation by competing with repressive proteins (Ma *et al*, 2010; Murphy *et al*, 2010; Eiring *et al*, 2010).

Furthermore, it is now clear that the RISC complex can shuttle between the cytoplasm and the nucleus thanks to the activity of different nuclear transporters, such as Importin 8 and Exportin 1, and thus can regulate gene expression in both cellular compartments (Nishi *et al*, 2013; Wei *et al*, 2014). For instance, miRNAs can exert their repressive function on nucleic RNAs targets such as long-non-coding RNAs or miRNA precursors (Tang *et al*, 2012; Leucci *et al*, 2013). MiRNAs can also bind mRNAs in the nucleus both post- and co-transcriptionally, inducing their degradation or influencing their processing, for example by regulating the splicing process (Alló *et al*, 2014; Havens *et al*, 2014; Bottini *et al*, 2017; Pitchiaya *et al*, 2017; Nishi *et al*, 2013).

Lastly, miRNA can regulate gene expression binding to enhancer or promoter region of other genes, repressing their transcription or inducing their overexpression thanks to mechanism that are not yet entirely clear (Li *et al*, 2017; Zhang & Zhang, 2017; Zheng *et al*, 2017a; Zhang *et al*, 2014; Morris *et al*, 2008; Matsui *et al*, 2013; Schwartz *et al*, 2008; Huang *et al*, 2012; Meng *et al*, 2016; Xiao *et al*, 2017). One model suggests that RISC-promoter interaction may happen at RNA level, with the miRNA targeting non-coding RNAs spanning regulatory regions or the antisense transcript resulting from bidirectional promoters and acting as a scaffold to recruit additional epigenetic factors (Huang *et al*, 2012; Schwartz *et al*, 2008; Matsui *et al*, 2013; Pisignano *et al*, 2017; Morris *et al*, 2008). Another model proposes that miRNA might bind directly to the single strand-DNA as the double helix unfolds during transcription initiation, altering histone modification signatures and/or the binding of transcription factors to the promoter region (Meng *et al*, 2016; Zheng *et al*, 2017a; Zhang *et al*, 2014; Li *et al*, 2017; Zhang & Zhang, 2017).

1.3.3 microRNA role in macrophage biology

MiRNAs play a fundamental role in the development and functions of macrophages, acting at different levels to regulate cell fate commitment, maturation, and activation (Squadrito et al, 2013; Roy, 2016).

Firstly, miRNAs are known to participate in hematopoietic stem cell (HSC) biology, regulating the equilibrium between self-renewal and differentiation. On the one hand, the miRNA cluster composed by miR-125a, miR-99b, and let-7e is preferentially expressed by long term HSC, and miR-125a was proved sufficient to increase the stem cell pool by targeting proapoptotic factors BAK1, KLF13 and BMF (Guo *et al*, 2010). On the other hand, miR-126, abundantly expressed in HSCs, controls stem cell expansion by targeting PI3K/AKT/GSK3β pathway, thus restraining cell cycle progression (Lechman *et al*, 2012).

MiRNAs can also regulate HSCs commitment towards specific lineages. For instance, the transcription factor PU.1 induces the expression of a subset of four miRNAs (miR-146a, miR-342, miR-338, and miR-155) as an initial step towards lymphoid-myeloid progenitor development (Ghani *et al*, 2011). Ectopic expression of miR-146a alone can drive HSCs commitment towards monocyte/macrophage lineage (Ghani *et al*, 2011), while the balance between miR-342 and its host gene Evl is thought to be fundamental in HSCs cell fate decision, driving respectively myelopoiesis or lymphopoiesis (Herbst *et al*, 2021).

Other miRNAs can balance granulocytes versus monocytes/macrophages output from common myeloid progenitors. Among them, miR-21, miR-196b, and miR-424 promote monocyte differentiation, while miR-17-5p, miR-20a and miR-106a drive granulopoiesis (Rosa *et al*, 2007; Fontana *et al*, 2007; Velu *et al*, 2009). Interestingly, these miRNAs are involved in feedback loops with well-known transcription factors regulating myeloid progenitor lineage commitment, with miR-21 and miR-196b being downregulated by pro-granulocytic factor GFI1, and miR-17-5/20a/106a being repressed by RUNX1, the same transcription factor that upregulates CSF-1R and thus drives monocyte development (Fontana *et al*, 2007; Velu *et al*, 2009).

Finally, miRNAs are involved in macrophage function and polarization, with specific signatures associated to M1 or M2 macrophages. For instance, miR-155, miR-181, and miR-451 are upregulated during M1 polarization, and miR-146a, miR-125a, and miR-145-5p during M2 polarization (Graff *et al*, 2012; Zhang *et al*, 2013).

In particular, miR-155 has been the subject of extensive investigation in the field of macrophage polarization and inflammation. Mir-155 is not only a M1 macrophage marker, but it directly drives classical macrophage activation by regulating the expression of approximatively 650 genes (Cai *et al*, 2012; Jablonski *et al*, 2016). Its expression can be

triggered by TLR agonists and pro-inflammatory cytokines, while it is downregulated by IL10 (Tili *et al*, 2007; O'Connell *et al*, 2007; Koch *et al*, 2012; McCoy *et al*, 2010). In turn, miR-155 inhibits negative regulators of the TLR signaling and enhances TNF-α production, in a positive feedback loop to boost M1 polarization (O'Connell *et al*, 2009; Androulidaki *et al*, 2009a; Tili *et al*, 2007). Furthermore, it inhibits IL-13 receptor α1 (IL13Rα1) expression, which normally drives the signaling to express M2-related genes, which are hence indirectly downregulated by miR-155 (Martinez-Nunez *et al*, 2011; Zhang *et al*, 2016).

MiR-155 is not the only miRNA mechanistically linked to macrophage polarization and pro-inflammatory responses. MiR-125a is known to positively regulate NF-κB pathway, a key regulator of macrophage classical activation, as well as TNF-α production and IFN-γ signaling, both pro-inflammatory mediators that can trigger M1 polarization (Androulidaki *et al*, 2009b; Chaudhuri *et al*, 2011; Kim *et al*, 2012); while miR-378-3p is expressed following IL4 stimulation and represses AKT1 signalling, limiting the alternative activation of macrophages (Rückerl *et al*, 2012). Conversely, miR-146 is associated to M2 phenotype and anti-inflammatory functions (Li *et al*, 2016; Huang *et al*, 2016; Hou *et al*, 2009). Its expression can be triggered by both anti- and pro-inflammatory stimuli, creating a feedback loop that keeps inflammation in check, preventing excessive responses (Taganov *et al*, 2006; Hou *et al*, 2009; Curtale *et al*, 2013). MiR-146, together with miR-219 and miR-21, is also upregulated

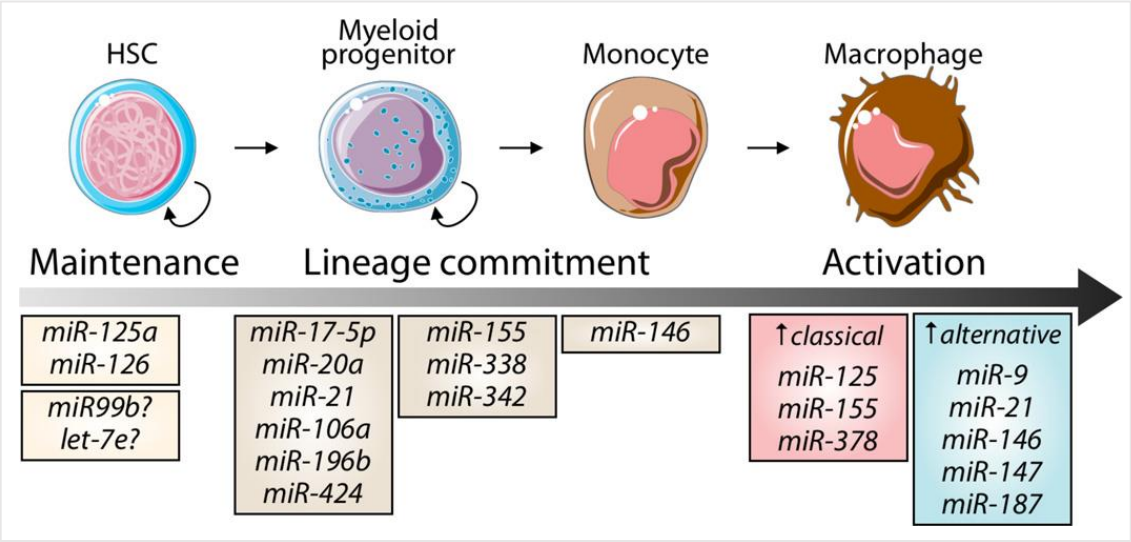


Figure 5. Overview of miRNAs involved in macrophage development and function *miRNAs play a role in virtually every aspect of macrophage biology: from HSCs and myeloid progenitor maintenance, to lineage commitment, to monocyte maturation and macrophage activation. (Squadrito et al, 2013; permission to reproduce from Elsevier under license number 5686000417812)*

by resolving D1 (RvD1), an endogenous lipid mediator regulating the resolution phase of inflammation (Recchiuti *et al*, 2011). Mir-21 has also been mechanistically linked to wound healing thanks to its role in regulating macrophage function by promoting efferocytosis and supporting macrophage polarization towards M2-like phenotypes (Das et al, 2014).

The ones provided are only few examples of an ever-growing list of miRNA associated to various macrophage functions, from activation to efferocytosis and phagocytosis, to regulation of the inflammatory response (Roy, 2016; Squadrito et al, 2013).

1.3.4 microRNA, cancer, and TAMs

A decade of experimental evidence has shown how miRNA expression is dysregulated in many human cancers, and can affect various aspects of tumor biology, including sustained proliferation, evasion of programmed cell death, promotion of invasiveness and metastasis, and therapy resistance (Peng & Croce, 2016; Si *et al*, 2019; Pan *et al*, 2021). Under different conditions, miRNAs can act as both tumor suppressors or oncogenes, and they have even been proposed as potential cancer therapeutics or diagnostic biomarkers. However, miRNAs significance in tumor biology is not limited to cancer cells themselves, but can also influence the tumor microenvironment, promoting TAMs development and action as well as tumor-TAMs crosstalk.

Most TAMs display a tolerogenic, M2-like phenotype, in accordance with their pro-tumoral and immunosuppressive functions. As discussed in the previous chapter, miRNAs can play a major role influencing macrophage polarization, and can influence TAMs activation pushing forward more immune-suppressive phenotypes. For instance, miR-146 regulates M2 polarization in TAMs associated with breast cancer, and when knocked down in macrophages it can inhibit tumor growth in vitro (Li *et al*, 2015). Conversely, miR-155 knockdown impairs macrophages classical activation, reducing their potential to secrete inflammatory cytokines and preventing them from mounting an effective antitumor response in mice (He *et al*, 2009; Zonari *et al*, 2013a). Interestingly, some studies indicate that it may be possible to reprogram them towards a pro-inflammatory M1-like phenotype by modulating the expression of specific miRNAs (Baer *et al*, 2016; Squadrito *et al*, 2012). Such reprogramming would impair TAM pro-tumoral functions and restrain tumor progression, and thus present an intriguing therapeutic strategy.

MiRNAs can also play a role in the recruitment of monocytes and TAMs at the tumor site, regulating the release of chemoattractant molecules from cancer cells. Such impact on chemotaxis has been observed in various setting, among which miR-375 in breast cancer, miR-125b in testicular germ cells tumors, and miR-148b and miR-26a in hepatocellular carcinoma (Chai *et al*, 2015; Batool *et al*, 2018; Frank *et al*, 2019; Ke *et al*, 2019). Not only that, but miRNAs can also regulate TAMs response to those chemokines, as in the case of miR-222, that when overexpressed in TAMs can inhibits chemotaxis by disrupting CCR4-CXCL12 axis (Li *et al*, 2015).

On the other hand, tumor-TAMs crosstalk can also be mediated by exosomal miRNAs, which can convey information between the two, as well as to other components of the tumor microenvironment. MiR-21-5p seems to have a particular relevance in this process, as TAM-derived exosomes packed with this miRNA have been shown to promote cancer cell migration and invasion, chemotherapy resistance, and an immunosuppressive environment in a number of different human cancers (Zheng *et al*, 2017b; Zhou *et al*, 2018; Lan *et al*, 2019). Other miRNAs enriched in TAM-derived exosomes are miR-365, which induces chemoresistance in pancreatic adenocarcinoma, and miR-223, which promotes breast cancer invasion and chemoresistance (Binenbaum *et al*, 2018; Yang *et al*, 2011; Zhu *et al*, 2019). The opposite process is also true, with miRNAs delivered by cancer cell-derived exosomes inducing a range of phenotypes in TAMs, notably pushing towards M2 polarization or increasing their pro-tumoral functions (Ying *et al*, 2016; Chen *et al*, 2017; Cooks *et al*, 2018; Hsu *et al*, 2018; Park *et al*, 2019).

1.4 Gene therapy: a promising tool to tackle human disease

1.4.1 Gene therapy approaches and platforms

Gene therapy allows the transfer of genetic material to recipient cells to replace a defective gene, or to equip them with new therapeutic functions (Naldini, 2015). Gene therapy has long fascinated the scientific community as it offers the opportunity to permanently cure several human diseases acting at their genetic root and using a single dose of treatment, as opposed to conventional interventions, which often require the repetitive administration of pharmacological compounds that act on relieving the symptoms of the disease. Most prominent in the field of gene therapy is its application to monogenic genetic disorders, which can sometimes be corrected by inserting a copy of the wild type gene into target cells. This is the case of some severe, life-long diseases such as inherited immunodeficiencies or some skin conditions as epidemolisis bullosa (Naldini, 2011; Jayarajan *et al*, 2021). However, the field is rapidly evolving, and now several clinical trials are applying similar gene-transfer strategies to the treatment of cancer and infectious diseases (Naldini, 2015).

Gene therapy strategies can be roughly divided into *ex vivo* and *in vivo* approaches. *Ex vivo* gene therapy is based on the collection of target cells from the patient, which are then engineered and expanded *ex vivo* before reintroduction into the individual. This strategy is most suited to easily collectible cell types and progenitor which are cultivable *ex vivo*, such as T cells, mobilized hematopoietic stem and progenitor cells (HSPCs) or keratinocytes (Naldini, 2011; Jayarajan *et al*, 2021). *Ex vivo* strategies allow a tight spatial and temporal control of the engineering process, but require a specific expertise in collecting and handling the target cells, and are thus extremely time and cost intensive (Elverum & Whitman, 2020). On the other hand, *in vivo* gene therapy relies on the direct administration of the gene delivery vehicle to the patient, offering the intriguing opportunity of an off-the-shelf approach. Obviously, this strategy necessitates a careful design of the gene therapy platform, as well as thorough investigation of its pharmacodynamics and biodistribution in order to ensure safe and selective engineering of the cell population of interest and prevent off-target gene expression that may lead to adverse events (van Haasteren *et al*, 2018).

Several platforms were developed to allow efficient genetic material transfer into recipient cells, divided mainly into two types of gene delivery vehicles: viral and non-viral vectors. Non-viral vectors can be constituted of nanoparticles with different chemistries, such as gold

nanoparticles, polymers of various origin or, more commonly, lipid nanoparticles, which are complexed to the nucleic acid (DNA or RNA) that needs delivering into the target cell/tissue. They are highly customizable and have gained considerable attention thanks to their low cytotoxicity and non-immunogenicity (Patil *et al*, 2019). However, non-viral vectors still face the problem of a generally lower gene transfer capability compared to viral vectors, which are the most employed in clinics, thanks both to their efficiency and well-characterized safety profile (Bulcha *et al*, 2021). Viral vectors are constituted of non-pathogenic and non-replicating viral particles, thus exploiting the intrinsic capacity of viruses to deliver genetic material into host cells. Currently, the most common types of viral vectors are based on adenoviruses (Ads), adeno-associated viruses (AAVs) or lentiviruses (LVs) (Bulcha *et al*, 2021).

Ads and AAVs vectors are non-integrating, with genomes flanked by inverted terminal repeats (ITRs) that persist as episomes in transduced cells, being gradually diluted in daughter cells upon cell division. For this reason, these viral vectors are employed in clinical settings in which transient gene expression is sufficient or desired, and for the targeting of non-proliferating cell populations. Ads-based viral vectors are largely employed thanks to their efficiency in infecting both replicating and non-replicating cells and their large cargo capacity, with the newer generations accommodating up to ~36 kb of space for transfer genes (Alba *et al*, 2005). Nevertheless, *in vivo* employ of these vectors tend to be compromised by the high prevalence of Ads infections in the human population, with most people carrying neutralizing antibodies against one or more human Ads serotypes, including those employed in gene therapy (Mast *et al*, 2010; Barouch *et al*, 2011). Furthermore, Ads trigger stronger immunological responses and toxicity events in recipients compared to other commonly used viral vectors (Bulcha *et al*, 2021). On the other hand, AAVs are much less immunogenic and offer a wide variety of serotypes, allowing selective tropisms for specific cell types/tissues and overcoming issues with pre-existing immunity. Their cargo capacity, however, is much more modest, allowing the packaging of transgene of a maximum length of ~4.5 kb.

LVs are integrating vectors and permit long-term gene expression that is transmitted to daughter cells. They are part of the retroviridae family, being characterized by a single strand RNA genome flanked by long terminal repeats (LTRs) which is retrotranscribed and integrated in the recipient genome upon target cell infection. They are preferred to other genera of retroviruses thanks to their capacity to efficiently transduce non-dividing cells, as well as for

their favorable safety profile (Bulcha *et al*, 2021). In fact, even if viral genome integration is not immune to risks deriving from insertional mutagenesis, LVs integration into the host cell genome appears to be biased towards benign integration sites (Biffi *et al*, 2011). Under these premises, random integration of Ads or AAVs vectors, despite relatively rare, represents a more concerning occurrence, as ITRs can transactivate gene elements in close proximity to the viral integration site and lead to oncogenesis (Nault *et al*, 2015, 2016; Dalwadi *et al*, 2021). Apart from granting stable transduction of proliferating and non-proliferating cells, LVs also display a large cargo capability, packaging transgenes of 9-10kb of length, and a low level of pre-existing immunity (Bulcha *et al*, 2021). The most commonly used LVs for gene therapy are based on human immunodeficiency 1 virus (HIV), which is not only has a low prevalence, but it is also scarcely immunogenic, with only about 20% of HIV infected people developing neutralizing antibodies against the virus, accounting for a total of 0.16% of the human population (Doria-Rose *et al*, 2010; Cantore & Naldini, 2021). All these characteristics make LVs-derived vectors particularly suited to *in vivo* applications, and as such they are currently under investigation for several therapeutic purposes.

1.4.2 Regulatory elements in gene therapy

As previously discussed, gene therapy requires a tight spatiotemporal regulation in order to ensure safe and selective expression of the transgene from the target cells. This can be achieved by acting at different levels to restrict off-target transduction, gene expression or protein translation.

When pursuing *in vivo* approaches, a first level of specificity is granted by the selection of a delivery route and a vector with the desired biodistribution, allowing for near exclusive transduction of the cell population of interest. For instance, viral vectors can be administered as hydrogels, aerosols or injected following different routes to reach the target organ as efficiently as possible. Furthermore, cellular receptors on the viral surface can confer more or less restrictive tropism for specific cell types or tissues, and thus can be selected or engineered in order to achieve high specificity towards the target. In LVs, envelope proteins are the main determinants of viral tropism, as they enable recognition and binding to the target cell, as well as promoting viral entry thanks to their fusogenic properties. In order to achieve the desired tropism, it is possible to equip HIV virus with engineered cellular receptors or with envelope proteins from non-related viruses, in a process termed pseudotyping (Frank & Buchholz,

2019; Gutierrez-Guerrero *et al*, 2020). Most commonly, LVs are pseudotyped with envelop proteins from the vesicular stomatitis virus glycoprotein (VSV-G), which gives rise to a broad tropism and a high infectivity (Hastie *et al*, 2013). On the other hand, AAVs do not display an envelope, and the proteins composing their capsids cannot be as easily engineered to create chimeric viruses. However, AAVs naturally occur in a wide range of serotypes with a variety of different tropism profiles, and thus can be selected to achieve the desired biodistribution (Gao *et al*, 2002, 2003, 2004).

A second layer of regulation is given by the transgene expression cassette inserted into the gene delivery vector. Particularly important is the choice of regulatory elements, as enhancers or promoters, with the desired expression profile, which can restrict the transcription of the transgene to the cell lineages of interest even in presence of off-target transduction (Poletti & Mavilio, 2021). Furthermore, promoter choice can influence the kinetics of transcription, preventing transgene expression in progenitor cells and in successive maturation states, or in a quantitative way, enhancing transgene output in presence of desired phenotypes/polarization states. Transgene expression can also be regulated at post-transcriptional level thanks to the incorporation of miRNA target sequences (miRT) into the vector design (Geisler & Fechner, 2016). As previously described, miRNAs can bind mRNA targets to prevent their translation by various mechanisms of RNA interference. Thus, including tandem miRT sequences downstream of the transgene can abrogate its expression even in transduced cells in which the selected promoter is active, as long as they also express the miRNA in question. Once again, this additional level of regulation can fine tune transgene expression in a spatiotemporal fashion, eliminating residual expression deriving from off-target transduction or allowing translation only in the presence of the correct maturation state/phenotype. For instance, miRT-122a has been exploited to abrogate expression in hepatocytes for *in vivo* gene therapy applications (Annoni *et al*, 2009). At the same time, miRT-126 can transiently turn down transgene output in the context of engineered HSPCs transplantation, inhibiting its expression in early progenitors, while preserving it in their progeny (Gentner *et al*, 2010).

1.4.3 In vivo gene therapy: the liver example

The liver has long been an enticing target for *in vivo* gene therapy approaches, both for its central role in metabolism and its accessibility to blood-borne particles. As previously mentioned, the liver receives an abundant blood supply and it is characterized by particularly

permeable vessels, the hepatic sinusoids, which allow the quick and efficient extravasation of particles from the bloodstream to the hepatic parenchyma. Thanks to its filtering activity, a significant fraction of any gene therapy vector that reaches the blood flow will eventually end up in the liver and be accessible to hepatic cell populations (van Haasteren *et al*, 2018). Among them, hepatocytes are long-lived and efficient protein factories, and thus could be ideally targeted by gene replacement strategies for treating many inherited metabolic diseases. Sustained transgene expression and release from hepatocytes could be beneficial not only in the context of hepatic disorders, but also to tackle enzyme deficiencies in distant districts, as well as plasma protein deficiencies (Naldini, 2015; Cantore & Naldini, 2021). Under these premises, hepatic *in vivo* gene therapy approaches are under investigation in the context of various human diseases, and there are already some clinical trials for the treatment of severe hemophilia using AAV vectors administered via intramuscular or intravenous injection (Nathwani *et al*, 2014; Perrin *et al*, 2019; Leebeek & Miesbach, 2021).

Currently, the majority of liver-directed gene therapy approaches are based on the use of AAV vectors, and in particular on AAV8, which is considered the canonical hepato-specific serotype. However, AAVs present some limitations due to the rates of pre-existing immunity in the population and their nature of non-integrating vectors, which leads to transgene dilution over time following liver growth and regeneration, thus preventing their employment in pediatric settings. Conversely VSV-G pseudotyped LVs, albeit non-hepatocyte specific, have been suggested as an alternative to AAV for *in vivo* liver gene therapy, as they grant stable transgene expression and transmission to daughter cells. Several biodistribution studies in mice and non-human primates have demonstrated that intravenous administration of VSV-G pseudotyped LVs leads to efficient and abundant transduction of the liver, and limited targeting of the spleen (Peng *et al*, 2001; Milani *et al*, 2019). Hepatic targeting is mostly granted by the high expression of LDL receptor on the surface of hepatocytes, which serves as an entry receptor for VSV-G, and by active phagocytosis of the viral particles into the hepatic sinusoids (Tao *et al*, 2001; Cantore & Naldini, 2021). This enables the efficient transduction of several hepatic cell populations, including KCs and plasmacytoid dendritic cells (pDCs), and to a lesser extent hepatocytes and LSECs. Nevertheless, hepatocyte transduction can be enhanced by employing phagocytosis-shielded VSV-G pseudotyped LVs that incorporate high levels of protein CD47 on their surface, a “don’t eat me” signal that inhibits KC-mediated viral particle uptake (Milani *et al*, 2019). The clinical relevance of LV-

based gene therapy approaches for liver targeting was further demonstrated by the successful, long-term treatment of hemophilic dogs with a systemic injection of VSV-G pseudotyped LVs for the expression of canine factor IX (Cantore *et al*, 2015). Interestingly, the same study evaluated the risk of insertional mutagenesis in three different tumor-prone mouse-models, detecting no events of genotoxicity from the LV treatment. Thanks to their favorable safety and biodistribution profile, as well as their capacity to induce sustained transgene expression, VSV-G pseudotyped LVs thus constitute a promising tool for liver-directed gene therapy approaches.

1.4.4 Gene therapy approaches in oncology

Gene therapy has been exploited for decades for the treatment of inherited diseases by gene repair or gene transfer into the affected cells. However, in recent years similar approaches have been applied to the context of other human diseases, for example in the field of oncology, with remarkable clinical success in the treatment of some tumors types. In this context, gene therapy approaches may directly target cancer cells, delivering suicide genes or regulating the expression of tumor suppressors of oncogenes to promote tumor regression (Griffith *et al*, 2009; Jia *et al*, 2012). Alternatively, one could induce the expression of highly immunogenic antigens from the cancer cells to promote their clearance at the hand of the immune system (Das *et al*, 2015). More interestingly, some approaches have focused on the tumor microenvironment, and in particular on the engineering of immune cells to enhance their antitumoral function or equip them with new features that enable efficient cancer cell clearance.

Chimeric antigen receptor (CAR) T cells are the most famous and clinically relevant example of gene therapy-based immunotherapy. They consist of armored T cells, which are usually collected from the peripheral blood of the oncologic patient and engineered *ex vivo* to express a synthetic cellular receptor against a desired tumor antigen. CARs act as surrogate tumor-specific T cell receptors, recognizing desired tumor antigens in an MHC-independent fashion and initiating an intracellular signaling cascade that activates the effector function of the T cell. Thus, once reinfused into the patient, CAR-T cells are potentially able to trigger a potent and sustained antitumoral immune response. This has been shown in the context of hematological malignancies (Cappell *et al*, 2020), while CAR-T cells efficacy remains modest in the context of solid tumors. Among the factors impeding the efficacy of CAR-T cells in

solid tumors there are accessibility issues, tumor antigen heterogeneity leading to antigen escape, and the immunosuppressive effect of the tumor microenvironment (TME), which triggers exhausted phenotypes in CAR-T cells (Marofi *et al*, 2022). To try and overcome some of these issues, similar strategies are under development for the engineering of other immune cell types, subsequently termed CAR-NK or CAR-macrophages (Pan *et al*, 2022).

Finally, gene therapy has been exploited to engineer cells in the TME to express immune-activating molecules or checkpoint inhibitors, thus reactivating antitumoral immune responses. One take on this approach developed in Naldini's lab focused on the use of TAMs to express the immune-activating cytokine IFNα in the TME. In this context, HSPCs are collected and engineered *ex vivo* with a VSV-G pseudotyped LV carrying an expression cassette for IFNα under the transcriptional control of *Tie2*-promoter, a gene selectively expressed by monocytes and macrophages in the TME. In different tumor types, mice undergoing HSPCs transplant with cells engineered to express IFNα reconstituted all hematopoietic cell lineages, but they showed selective IFNα expression only in the TME (De Palma *et al*, 2003). This platform was further developed to better restrict transgene output in a spatiotemporal fashion, and its efficacy in reducing tumor burden was demonstrated in the context of several different malignancies (De Palma *et al*, 2008; Escobar *et al*, 2014b, 2014a; Catarinella *et al*, 2016; Birocchi *et al*, 2022). In these studies, tumor regression was associated to TME reprogramming and re-activation of antitumoral immunity, with enhanced polarization of macrophages towards M1 phenotypes and a reduced exhaustion of the T cell compartment. Interestingly, this strategy has been proved to synergize with CAR-T cell therapy in the context of murine leukemia, since IFNα proved effective in overcoming TME immune-repressive action on CAR-T cells (Escobar *et al*, 2018). Based on these promising preclinical results, an open label phase I/IIa clinical trial was authorized and it's currently ongoing for the treatment of glioblastoma multiforme patients with this platform (NCT03866109, https://clinicaltrials.gov/).

2 Aim of the work

In this work, we aimed to identify the cell populations transduced upon intravenous injection of VSV-G-pseudotyped lentiviral vectors (LVs). Conducting extensive biodistribution studies is of pivotal importance for *in vivo* gene therapy approaches, which require stringent targeting of cell populations of interest to ensure safe and selective transgene expression. Identifying cell populations transduced by systemically delivered LVs would allow us to explore limits and potential of LV-based in vivo gene therapy approaches through the discovery of novel biological targets for cell engineering, but also potential off-target cell populations.

After identification of the cells targeted by LVs, we dissected active gene networks via thorough transcriptomic analyses. Defining differentially expressed genes among target and off-target populations allowed us to identify differentially active regulatory elements (i.e. promoters, miRNAs) which can be exploited in LV platform design to restrict transgene expression to desired cell population, or to regulate it in a spatiotemporal fashion. This allows for a greater flexibility of LV-based platforms, whose specificity is not limited by VSV-G broad tropism, since selective cell engineering can be reached upon transgene expression cassette design. Furthermore, characterizing the transcriptomic profile of LV-targeted cell populations can give insights on which gene networks are relevant for their development and function, and on the impact that their deregulation may have on their biology.

In the second part of our work, we focused on a miRNA that we found strongly and selectively active in myeloid cells: miR-342-3p. Consistently with its activity pattern, miR-342-3p is implicated in myeloid lineage development and macrophage function (Herbst et al, 2021; Czimmerer et al, 2016; Solomon et al, 2017; Wang et al, 2019). Interestingly, a rich scientific literature also describes miR-342-3p activity in human cancers, however whether its antitumoral action is restricted to cancer cells or if it also regulates TAMs function is unclear. By investigating miR-342-3p expression regulation in TAMs and by modulating its levels in KCs, we aimed to characterize miR-342-3p functions in macrophage biology, in particular in the liver metastasis setting. Identifying miR-342-3p direct targets and gene networks indirectly impacted by its modulation will help us characterize the biological mechanism behind miR-342-3p antitumoral function, and eventually leverage this knowledge for novel antitumoral therapeutic approaches.

3 Results

3.1 Characterization of splenic and hepatic populations preferentially transduced upon VSV-G pseudotyped LVs systemic delivery

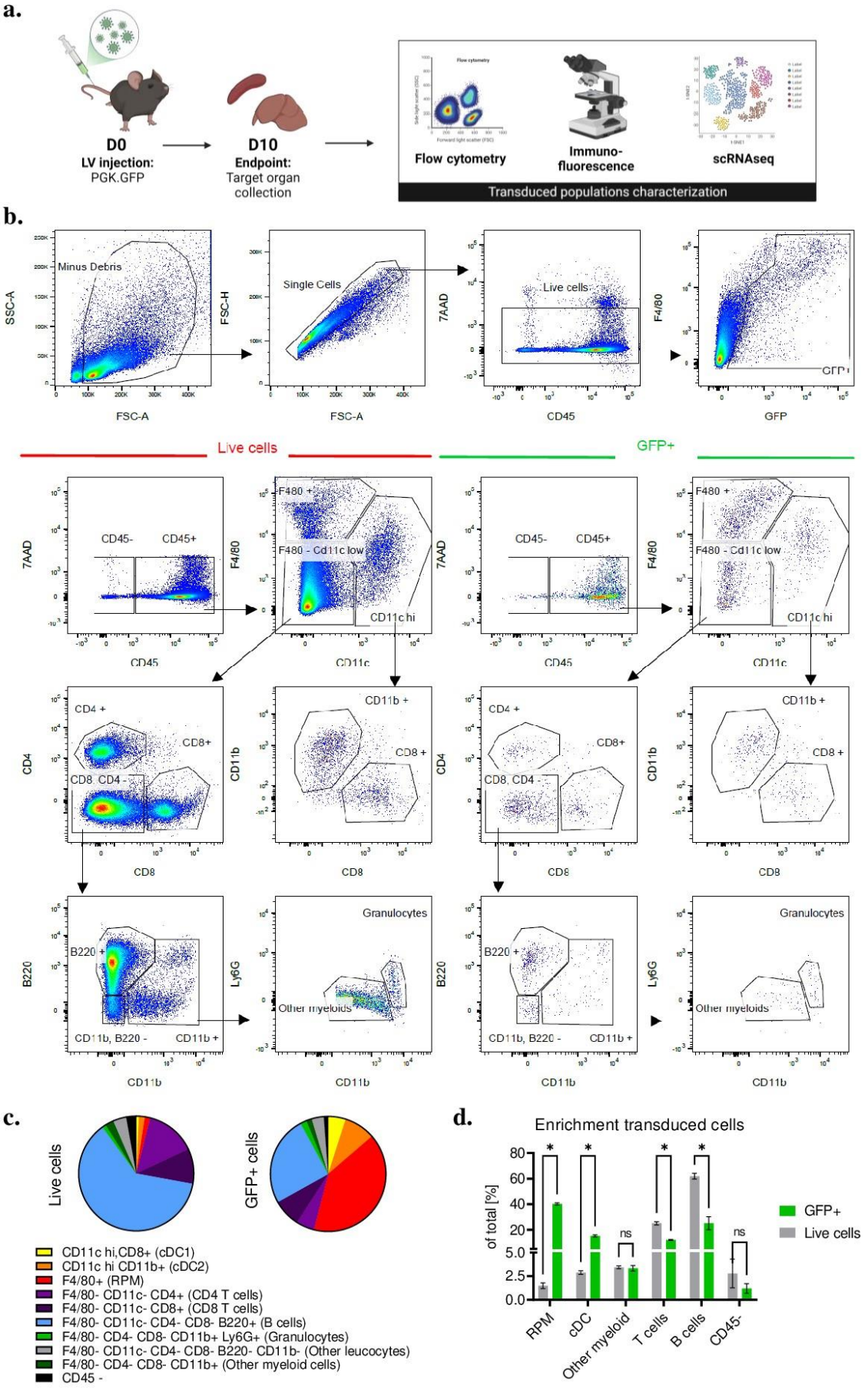
As previously mentioned, VSV-G pseudotyped lentivirus (LVs) biodistribution upon intravenous injection has been extensively studied. Within the liver, the most efficiently transduced organ, KCs, hepatocytes, and LSECs have been described as the cell populations most abundantly targeted by VSV-G pseudotyped LVs (Peng *et al*, 2001; Milani *et al*, 2019). In the same studies, spleen has been regarded as the second most transduced organ after liver, however, little is known about the splenic population targeted by systemically delivered LVs. Identifying these cell populations and differentially active gene networks between them is of pivotal importance to increase the spatiotemporal specificity of *in vivo* gene therapy approaches, thus limiting potentially detrimental off-target expression. To do so, we performed an in-depth biodistribution study aimed at identifying splenic cell populations targeted by LVs intravenous injection and characterize their protein coding and small transcriptome.

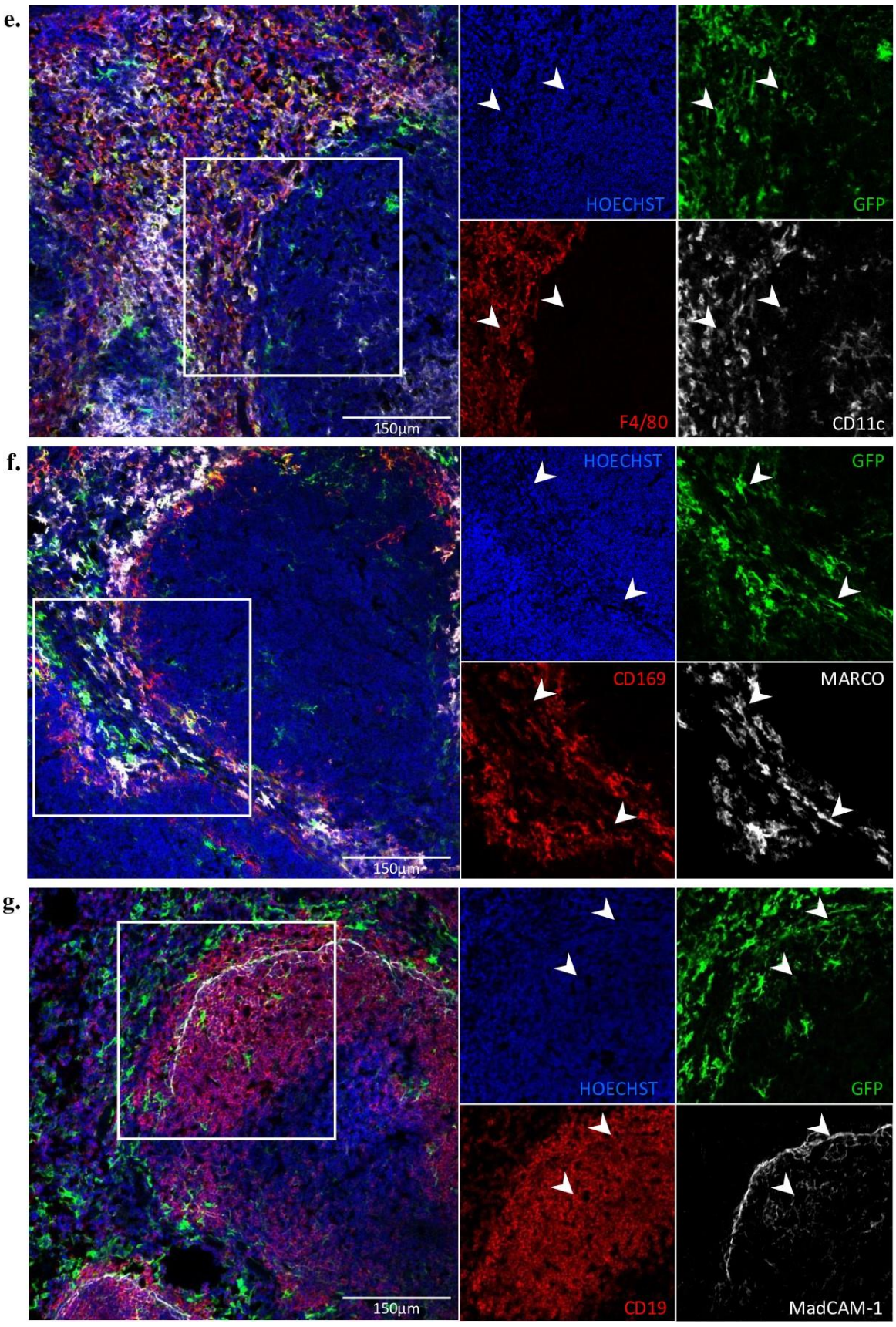
3.1.1 Biodistribution study of intravenously injected VSV-G pseudotyped LVs

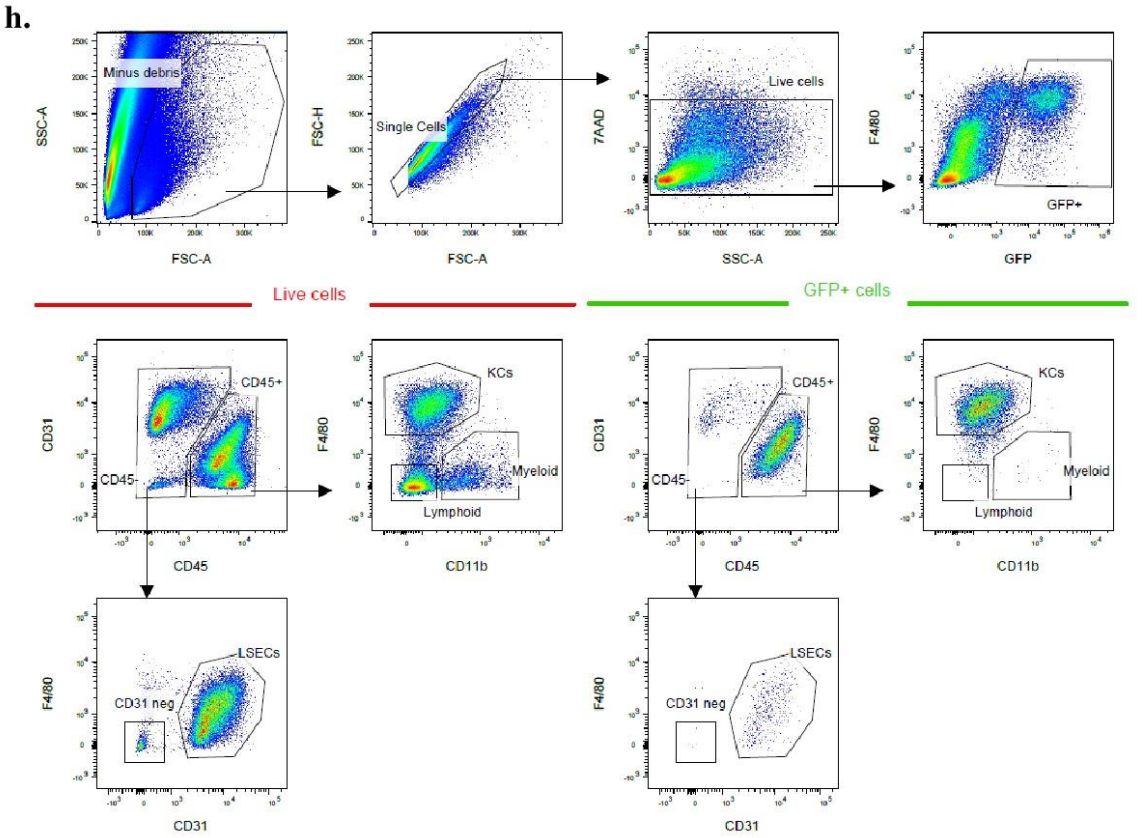
We intravenously injected n=3 5 week old C57bl/6 female mice with 3E+08 TU/mouse LVs carrying a PGK.GFP expression cassette. These vectors drive the fluorescent protein expression under a ubiquitous promoter, and thus allow the targeting of all transduced cells. After 10 days from LV injection mice were sacrificed, and liver and spleen were collected for flow cytometry and immunofluorescence analysis (Figure 6a).

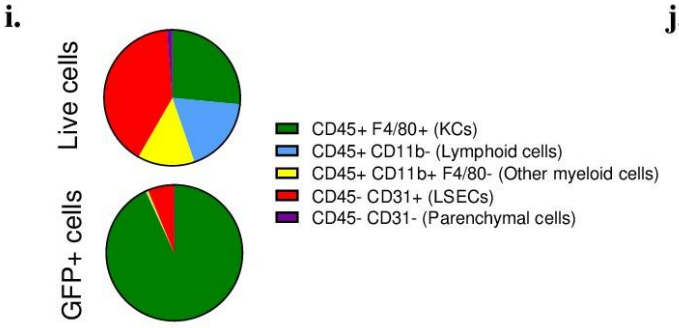
To characterize splenic LV-transduced populations, we set-up a flow cytometry panel to distinguish between B cells (CD45+ B220+), T cells (CD45+, CD11c-, CD4/8+) and various subsets of myeloid cell populations, including cDCs (CD11c hi, CD8/CD11b+), RPM (F4/80+) and granulocytes (CD11b+ Ly6G+) (Figure 6b). As expected, B and T cells accounted for the majority of splenic cell populations, making up to about 85% of live cells. Nonetheless, they showed negligible transduction levels. On the other hand, myeloid cells, although a minority, showed much higher transduction rates. In particular, RPM and cDCs, which accounted for less than 5% of live cells, made up to more than half of all GFP+ cells (Figure 6c). Interestingly, we found small percentages of transduced non-leucocytic cell

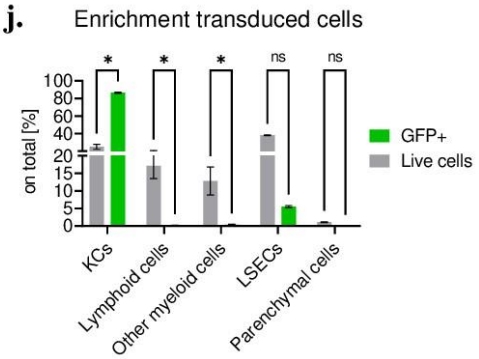
Figure 6.


a.
D0
LV injection:
PGK.GFP
D10
Endpoint:
Target organ
collection
Flow cytometry
Immuno-
fluorescence
scRNAseq
Transduced populations characterization
b.
Minus Debris
SSC-A
FSC-A
FSC-H
Single Cells
7AAD
Live cells
CD45
F4/80
GFP
Live cells
GFP+
CD45-
CD45+
F480 +
F480 - Cd11c low
CD11c hi
CD11c
CD4 +
CD8+
CD8 -CD4 -
CD11b +
B220 +
CD11b, B220 -
Granulocytes
Other myeloids
Ly6G
B220
c.
Live cells
GFP+ cells
CD11c hi,CD8+ (cDC1)
CD11c hi CD11b+ (cDC2)
F4/80+ (RPM)
F4/80- CD11c- CD4+ (CD4 T cells)
F4/80- CD11c- CD8+ (CD8 T cells)
F4/80- CD11c- CD4- CD8- B220+ (B cells)
F4/80- CD4- CD8- CD11b+ Ly6G+ (Granulocytes)
F4/80- CD11c- CD4- CD8- B220- CD11b- (Other leucocytes)
F4/80- CD4- CD8- CD11b+ (Other myeloid cells)
CD45 -
d.
Enrichment transduced cells
of total [%]
80
60
40
20
5.0
2.5
0.0
*
ns
RPM
cDC
Other myeloid
T cells
B cells
CD45-
GFP+
Live cells


e.
HOECHST
GFP
F4/80
CD11c
150µm
f.
HOECHST
GFP
CD169
MARCO
150µm
g.
HOECHST
GFP
CD19
MadCAM-1
150µm


h.
Minus debris
SSC-A
FSC-A
Single Cells
FSC-H
FSC-A
Live cells
7AAD
SSC-A
F4/80
GFP+
GFP
Live cells
GFP+ cells
CD45+
CD45-
CD31
CD45
KCs
Myeloid
Lymphoid
F4/80
CD11b
LSECs
CD31 neg
F4/80
CD31


i.
Live cells
GFP+ cells
CD45+ F4/80+ (KCs)
CD45+ CD11b- (Lymphoid cells)
CD45+ CD11b+ F4/80- (Other myeloid cells)
CD45- CD31+ (LSECs)
CD45- CD31- (Parenchymal cells)


j.
Enrichment transduced cells
on total [%]
100
80
60
40
20
15
10
5
0
*
*
*
ns
ns
GFP+
Live cells
KCs
Lymphoid cells
Other myeloid cells
LSECs
Parenchymal cells

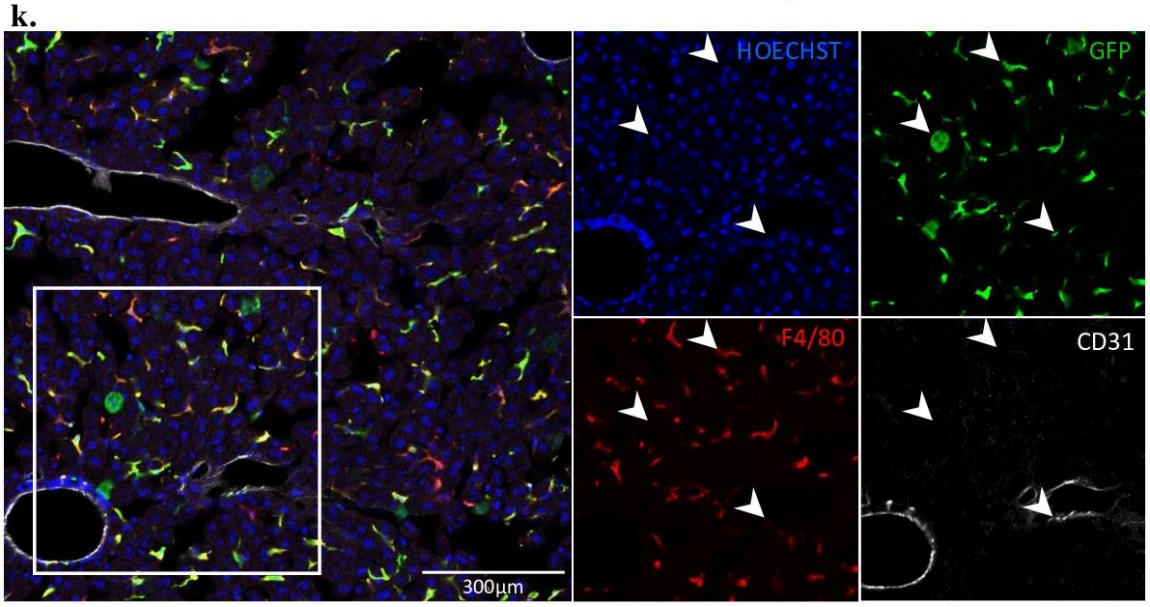

k.
HOECHST
GFP
F4/80
CD31
300µm

Figure 6 VSV-G pseudotyped LV biodistribution experiment *(a) Experimental setting. n=3 mice were injected with 3E+08 TU/mouse with a VSV-G LV coding for a PGK.GFP expression cassette. After 10 days spleen and liver were collected and analyzed by flow cytometry, immunofluorescence and scRNA-seq. (b) Gating strategy for splenic population analysis by flow cytometry. (c) Composition of all live cells versus transduced (GFP+) cells in the spleen, as measured by flow cytometry. (d) Frequence of splenic populations in the live cell fraction compared to the transduced (GFP+) fraction. Statisticts with Mann-Withney test. *: p <0.05 (e-g) Representative immunofluorescent image of spleen sections stained with Hoechst for nuclear staining, and antibodies targeting GFP (green), F4/80 (red) and CD11c (white) for (e), CD169 (red) and MARCO (white) for (f), and CD19 (red) and MadCAM-1 (white) for (g). Magnifications of selected regions (white squares) are displayed as single channels on the right, single marker pos cells are highlighted by arrows. (h) Gating strategy for hepatic population analysis by flow cytometry. (i) Composition of all live cells versus transduced (GFP+) cells in the liver, as measured by flow cytometry. (j) Frequence of each hepatic population in the live cell fraction compared to the transduced (GFP+) fraction. Statisticts with Mann-Withney test. *: p <0.05 (k) Representative immunofluorescent image of liver sections stained with Hoechst for nuclear staining, and antibodies targeting GFP (green), F4/80 (red) and CD31 (white). Magnifications of selected regions (white squares) are displayed as single channels on the right, single marker pos cells or double neg cells are highlighted by arrows.*

populations, as well as some non-identified leucocytes and myeloid cells. Among transduced cell populations, only RPM and cDC showed a statistically significant enrichment in the GFP+ fraction, while lymphoid cells were significantly depleted (Figure 6d).

To better characterize these cell populations, as well as to identify cells, that may not be easily analyzed by flow cytometry (e.g. stromal cells which are hardly retrieved by tissue dissociation), we also performed some immunofluorescent staining with specific cell markers. We were then able to confirm RPM (F4/80+), cDCs (CD11c+) and B cells (CD19+) transduction, and to identify some new splenic cell populations targeted by systemically delivered LVs (Figure 6e-g). In particular, we identified different subsets of splenic macrophages residing in the marginal zone, an intermediate region of the spleen parenchyma between the red and the white pulp. Among them, we found properly said marginal zone macrophages (MARCO+) and marginal metallophilic macrophages (CD169+) (Figure 6f). Furthermore, different subsets of CD45- cells were found to be transduced both in the white pulp and at the marginal zone-white pulp interface. For instance, we identified a MadCAM-1+ subset of dendritic cells of non-hematopoietic origin, termed follicular dendritic cells (FDCs) for their localization in the B cell region of the white pulp, particularly in correspondence to germinal centers. Another LV-targeted non-leucocytic cell population is constituted by marginal reticular cells (MRCs), similarly characterized by MadCAM-1 expression, but located at the interface between marginal zone and the B cell region of the white pulp, forming the marginal sinus (Figure 6g).

We also experimentally confirmed what was reported in the literature regarding liver targeting by systemically delivered LVs. Upon flow cytometric analysis of the livers of PGK.GFP LV transduced mice, we identified KCs (CD45+ F4/80+) and LSECs (CD45- CD31+) as the most abundantly transduced populations, with some minor contribution by other myeloid cells (potentially plasmacytoid DCs) and non-leucocytic cells (probably hepatocytes) (Figure 6i). The only cell population that was significantly enriched in the transduced (GFP+) fraction were KCs, while lymphoid and other myeloid cells appeared to be significantly depleted (Figure 6j). It is important to notice that hepatocytes are not easily analyzed by flow cytometry due to their size, fragility and high autofluorescence, and that they were likely mostly lost or damaged following our protocol for tissue dissociation, which also accounts for the high number of cellular debris detected (Figure 6h). Therefore, the composition of live/GFP+ cells reported in Figure 6i is likely not representative of that of the intact organ. For this reason, we performed some immunofluorescent staining on the liver, which confirmed the transduction of both KCs (F4/80+), LSECs (CD31+) and hepatocytes (F4/80- CD31-), characterized by their big size and a round morphology (Figure 6k).

3.1.2 scRNA-seq unravels heterogeneity of LV-targeted splenic populations

Following our initial biodistribution study we performed a scRNA-seq analysis of the transduced cell population in mouse spleen in order to characterize more in depth the variety of leucocytic and non-leucocytic populations that are transduced upon systemic LV delivery. Taking into consideration publicly available datasets of murine spleen scRNA-seq analysis, and in particular those generated by the Broad institute for the ImmGen consortium (https://www.immgen.org/Databrowser19/SingleCell.html), we decided to enrich our reference sample for non-B non-T cell populations in order to have a more detailed picture of non-lymphoid cell composition.

Once again, we intravenously injected n=3 5 weeks old C57bl/6 female mice with 3E+08 TU/mouse of PGK.GFP LVs. After 10 days we collected their spleens and processed them to obtain a single-cell suspension, then stained the samples with anti-CD19, anti-CD3 antibodies and performed cell hashing to identify the origin of the sample (Mouse 1, 2 or 3). This technique enables sample demultiplexing and super-loading of scRNA-seq platforms through the use of oligo-tagged antibodies against ubiquitously expressed surface proteins (hashtag antibodies). Labelling each mouse sample with unique hashtag antibodies allowed the pooling

Figure 7.

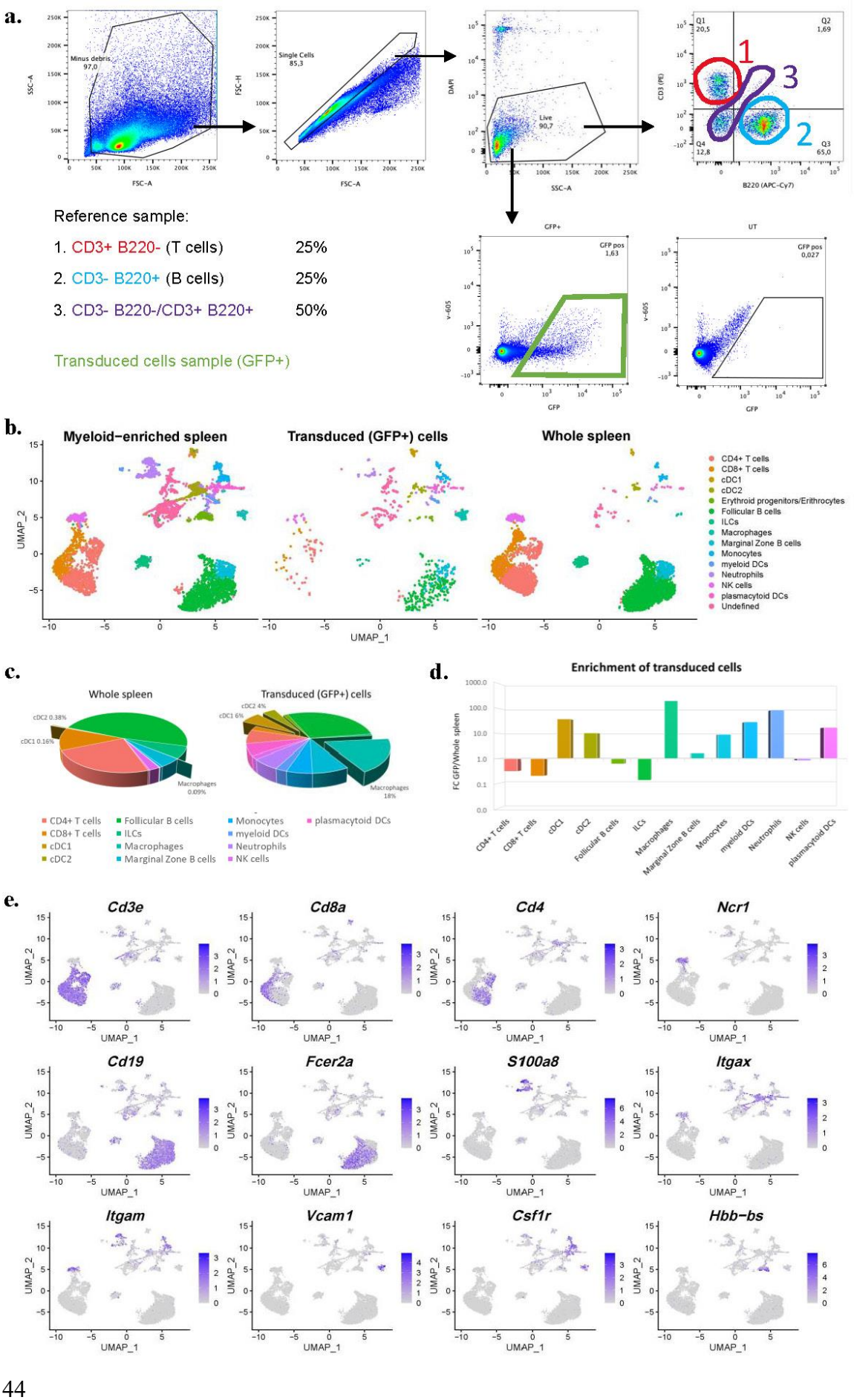

a.
Minus debris
97,0
Single Cells
85,3
Live
90,7
Q1
20,5
Q2
1,69
Q4
12,8
Q3
65,0
1
2
3
Reference sample:
1. CD3+ B220- (T cells) 25%
2. CD3- B220+ (B cells) 25%
3. CD3- B220-/CD3+ B220+ 50%
Transduced cells sample (GFP+)
GFP+
GFP pos
1,63
UT
GFP pos
0,027
b.
Myeloid−enriched spleen
Transduced (GFP+) cells
Whole spleen
UMAP_1
UMAP_2
CD4+ T cells
CD8+ T cells
cDC1
cDC2
Erythroid progenitors/Erithrocytes
Follicular B cells
ILCs
Macrophages
Marginal Zone B cells
Monocytes
myeloid DCs
Neutrophils
NK cells
plasmacytoid DCs
Undefined
c.
Whole spleen
Transduced (GFP+) cells
cDC2 0.38%
cDC1 0.16%
Macrophages 0.09%
cDC2 4%
cDC1 6%
Macrophages 18%
d.
Enrichment of transduced cells
FC GFP/Whole spleen
e.
Cd3e
Cd8a
Cd4
Ncr1
Cd19
Fcer2a
S100a8
Itgax
Itgam
Vcam1
Csf1r
Hbb−bs

Figure 7 scRNA-seq analysis of LV transduced spleen *(a) Gating strategy for FACS of the different cell populations analyzed by scRNA-seq. The reference population was divided based on CD3 and B220 expression, sorted separately and re-composed post-sorting in 25-25-50% ratio. Transduced (GFP+) cells were sorted separately. (b) Umap representation with cluster annotation and classification into the indicated populations based on an unsupervised clustering split into the three samples: our reference population of myeloid-enriched spleen (left), transduced cells (middle) and whole spleen reference sample from the Broad institute dataset (right). (c) Composition of reference whole spleen sample versus transduced (GFP+) cells in the spleen, as measured scRNA-seq clustering. (d) Enrichment of single populations in the transduced (GFP+) sample compared to the whole spleen. For each population is reported the fold change between the percentage in the GFP+ sample versus that in whole spleen. (e) Level of gene expression of different population marker genes in the umap representation*

multiple samples into one scRNA-seq run, which were then demultiplex by hashtag label. We sorted viable cells collecting CD3- B220+, CD3+ B220- and CD3+B220+/CD3-B220- cells in separated tubes, and prepared a pool in an approximate ratio of 25%-25%-50% among cell populations for each mouse. Starting from these samples, we then prepared a second pool with a 33%-33%-33% ratio between each mouse (Figure 7a). We also sorted separately GFP+ cells, also preparing a single pool with a 33%-33%-33% ratio between each mouse. We then prepared two scRNA-seq libraries, one for the myeloid-enriched reference population and one for the GFP+ sorted cells.

Upon scRNA-seq data analysis, we included the Broad dataset described in the first paragraph of this chapter as a whole spleen control, as it was performed on mice with same sex, strain and comparable age to mice employed in our experiment, and libraries were prepared with the same scRNA-seq technology (10x Chromium 3' library kit). We performed a harmonization of the data and unsupervised clustering, based on which we manually annotated 15 different cell populations, including different subsets of B and T cells, DCs and macrophages (Figure 7b). Upon comparison of different biological replicates we did not found significant variations, therefore we proceeded the analysis taking into account a pool of the three mice. Our reference population showed a significant enrichment in myeloid cell population compared to Broad whole spleen dataset, as expected, which further highlighted the heterogeneity of the leucocytic cell populations in the murine spleen. Myeloid cell populations were also highly enriched in the transduced cell sample, with macrophages reaching up to 100 fold increase compared to the whole spleen (Figure 7c-d). Interestingly, scRNA-seq analysis revealed a much more heterogeneous composition of GFP+ cells than previously expected, including low levels of transduced T and NK cells, as well as neutrophils, granulocytes, and monocytes.

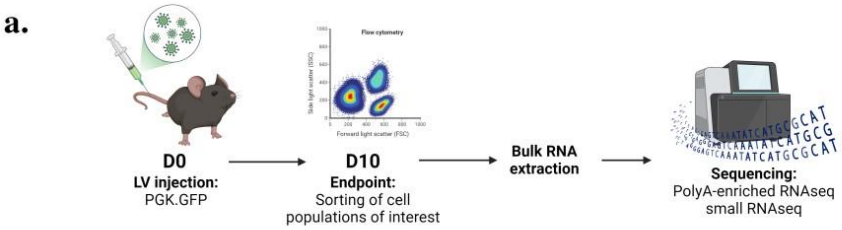
3.1.3 Characterization of active gene networks in preferentially transduced hepatic and splenic cell populations

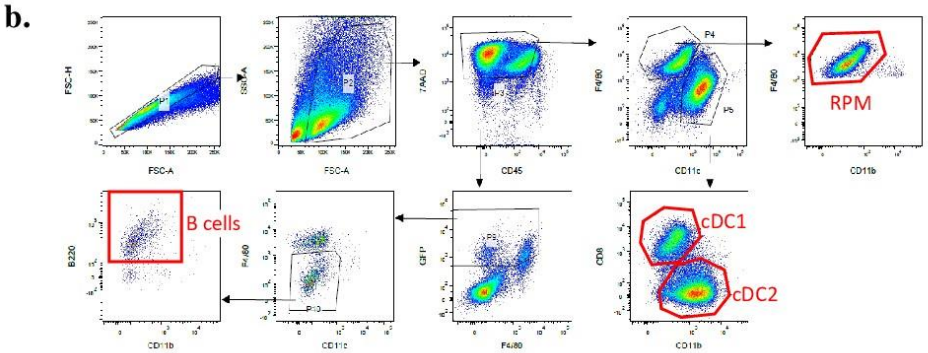
Following splenic and hepatic LV-targeted cell identification we wanted to more in depth characterize the cell populations predominantly transduced by LVs. Given the absence of scRNA-seq technology for small RNA sequencing, and aiming at reaching a higher depth of sequencing, we opted for sorting selected cell populations and perform bulk RNA extraction and a coupled polyA-enriched and small RNA sequencing (Figure 8a). We injected n=3 mice with PGK.GPF encoding LVs and sorted transduced B cell subset, RPM and cDCs for spleen and LSECS and KCs for liver. Sorting strategies for spleen and liver were based on previous flow cytometric analysis, and are reported respectively in Figure 8b and 8c.

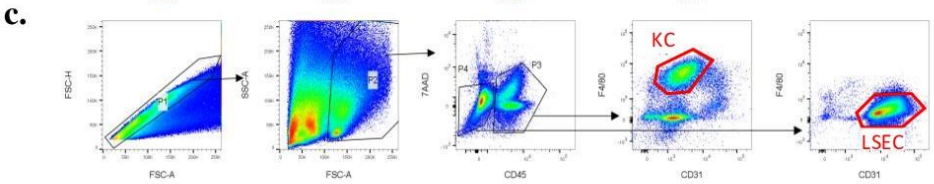
PolyA-enriched RNA-seq analysis confirmed the identity and purity of sorted populations, which displayed expected lineage markers (Figure 8d). Furthermore, we were able to determine that the subset of transduced B cells expresses both antibody isotype Ig2G, pointing towards more progressed states of maturation and activation. Whether these states are more receptive to LV entry or they are induced upon transduction is yet to be defined. Another particularly interesting feature emerging from the polyA-enriched RNA-seq differential gene expression analysis (DGE) was the striking similarity between RPM and KCs, which were the two populations more closely related, even more than the two subsets of cDCs included in the panel (Figure 8e).

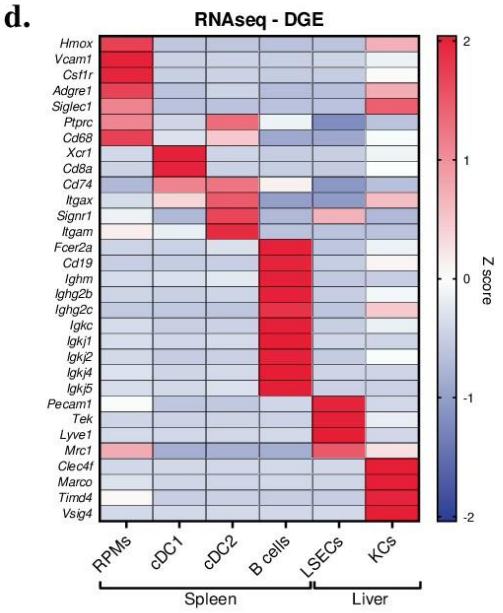
We also performed small RNA-seq to identify miRNAs that were preferentially expressed in the distinct cell types. We initially filtered miRNAs based on their expression level and fold change between the different populations (Figure 8f), and manually curated the resulting list selecting 16 miRNAs highly and differentially expressed between target cell populations or organs. We grouped the resulting miRNAs into families, and checked the overall expression of all the members of the families in the selected populations (Figure 8g). Members of a miRNA family generally derive from a common ancestor, and thus share the same seed region. They usually act redundantly on the same mRNA targets and share common biological functions, so we excluded from further testing miRNAs belonging families which contained highly ubiquitously expressed members, or whose members had an inverse trend inside a single population. For instance, we discarded miR-15b-5p and miR-322-3p, which belonged to the same miRNA family of ubiquitously expressed miR-16-5p.

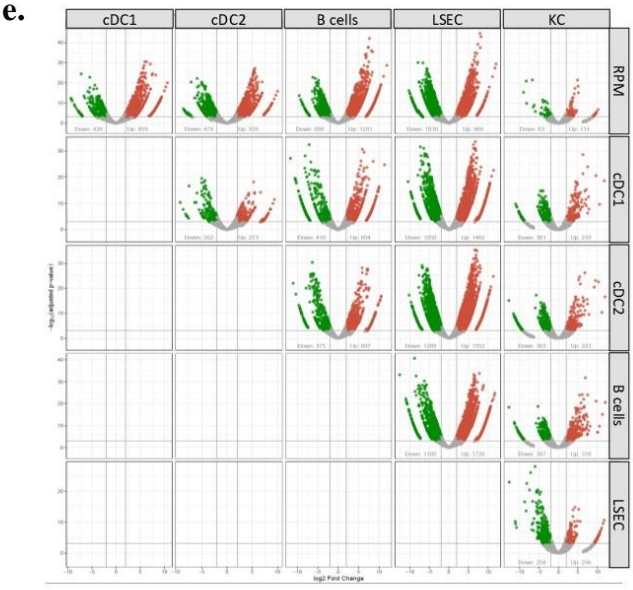
Figure 8.

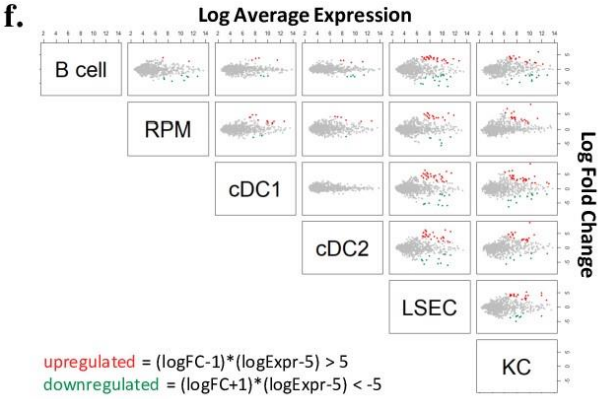

a.
D0
LV injection:
PGK.GFP
D10
Endpoint:
Sorting of cell
populations of interest
Bulk RNA
extraction
Sequencing:
PolyA-enriched RNAseq
small RNAseq


b.
RPM
B cells
cDC1
cDC2


c.
KC
LSEC


d.
RNAseq - DGE
Hmox
Vcam1
Csf1r
Adgre1
Siglec1
Ptprc
Cd68
Xcr1
Cd8a
Cd74
Itgax
Signr1
Itgam
Fcer2a
Cd19
Ighm
Ighg2b
Ighg2c
Igkc
Igkj1
Igkj2
Igkj4
Igkj5
Pecam1
Tek
Lyve1
Mrc1
Clec4f
Marco
Timd4
Vsig4
Z score
RPMs
cDC1
cDC2
B cells
LSECs
KCs
Spleen
Liver


e.
cDC1
cDC2
B cells
LSEC
KC
RPM
cDC1
cDC2
B cells
LSEC


f.
Log Average Expression
B cell
RPM
cDC1
cDC2
LSEC
KC
Log Fold Change
upregulated = (logFC-1)*(logExpr-5) > 5
downregulated = (logFC+1)*(logExpr-5) < -5

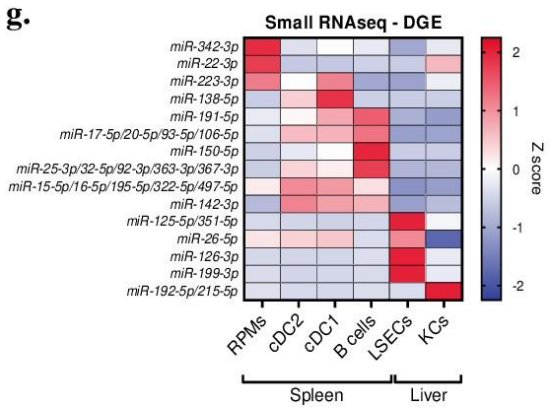

g.
Small RNAseq - DGE
miR-342-3p
miR-22-3p
miR-223-3p
miR-138-5p
miR-191-5p
miR-17-5p/20-5p/93-5p/106-5p
miR-150-5p
miR-25-3p/32-5p/92-3p/363-3p/367-3p
miR-15-5p/16-5p/195-5p/322-5p/497-5p
miR-142-3p
miR-125-5p/351-5p
miR-26-5p
miR-126-3p
miR-199-3p
miR-192-5p/215-5p
Z score
RPMs
cDC2
cDC1
B cells
LSECs
KCs
Spleen
Liver

Figure 8 In depth characterization of the transcriptional landscape of LV-targeted cell populations *(a) Experimental setting. n=3 mice were injected with 3E+08 TU/mouse with a VSV-G LV coding for a PGK.GFP expression cassette. After 10 days spleen and liver were collected and selected populations purified by FACS. After bulk RNA extraction, both polyA-enriched and small RNA-seq analysis was performed on all samples. (b) Gating strategy for splenic populations purification by FACS. (c) Gating strategy for hepatic populations purification by FACS. (d) Heatmap showing the expression of manually selected marker genes from polyA-enriched RNA-seq analysis. Color scale represents the Z score of gene expression for each gene. (e) NxN volcano plot of all comparisons for polyA-enriched RNA-seq DGE analysis. (f) NxN MA plot of all comparisons for small RNA-seq analysis (g) Heatmap showing the expression of differentially expressed miRNAs from small RNA-seq analysis. Color scale represents the Z score of gene expression for each gene.*

3.2 Evaluation of miRNA activity in LV-targeted cell populations in different pathophysiological conditions

We next sought to evaluate the activity of some of the miRNAs identified in the previous analysis. In order to efficiently repress their targets, miRNAs need to reach specific levels of expression, but it's often difficult to define *a priori* a threshold of expression over which the miRNA is biologically active. To evaluate miRNA activity *in vivo* we exploited miRNA reporters LVs. These are viral vectors containing a bidirectional expression cassette, which promotes the expression of two fluorescent proteins (e.g. GFP and mCherry) under the transcriptional regulation of a constitutive promoter (e.g. PGK). While both cassettes are simultaneously transcribed, only one of them is under the post-transcriptional control of a miRNA of interest thanks to the incorporation of miRNA targeting sites (miRT) downstream of its sequence. In this way the ratio between the two fluorescent proteins, evaluated by flow cytometry or immunofluorescence, gives an indirect measure of miRNA silencing activity (Figure 9a).

3.2.2 Bidirectional LVs allow for miRNA-activity tracking in healthy liver and spleen

To produce miRNA reporter LVs for the miRNAs of interest, we cloned 4 x miRT sequences for different miRNAs of interest downstream of GFP in a miRNA reporter LV encoding for mCherry as a transduction reporter. We intravenously injected n=3/4 5 weeks old C57bl/6 female mice per group with 3E+08 TU/mouse of either one of the miRNA reporter LVs or a No miRT control LV. After 10 days we collected liver and spleen, and analyzed them by flow cytometry and immunofluorescence, as described in chapter 3.1. We confirmed the activity pattern suggested by the literature for some of the miRNAs tested, and in particular for miR-142-3p, specific for cells of hematopoietic origin, and miR-223-3p, specific for

Figure 9.

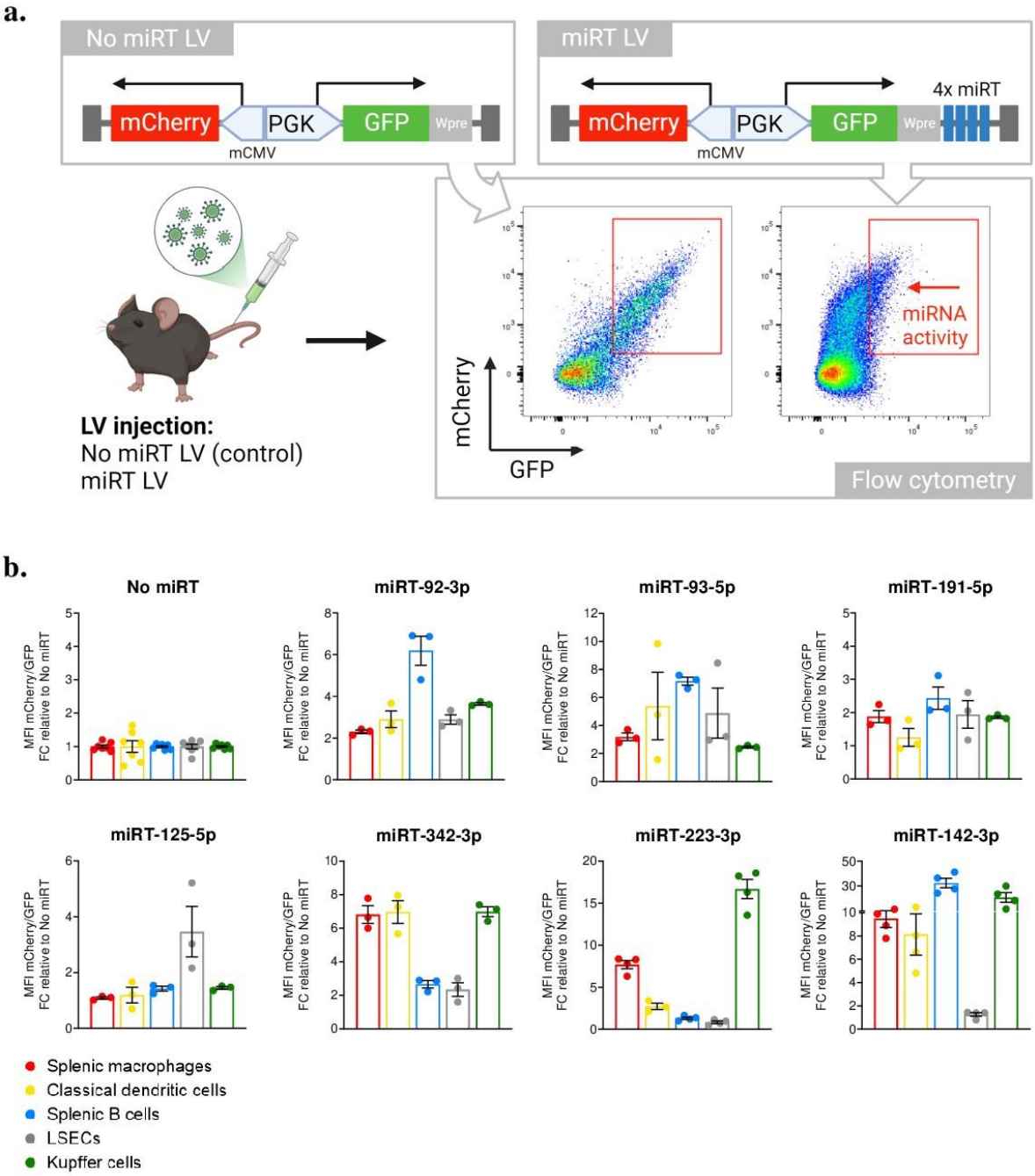
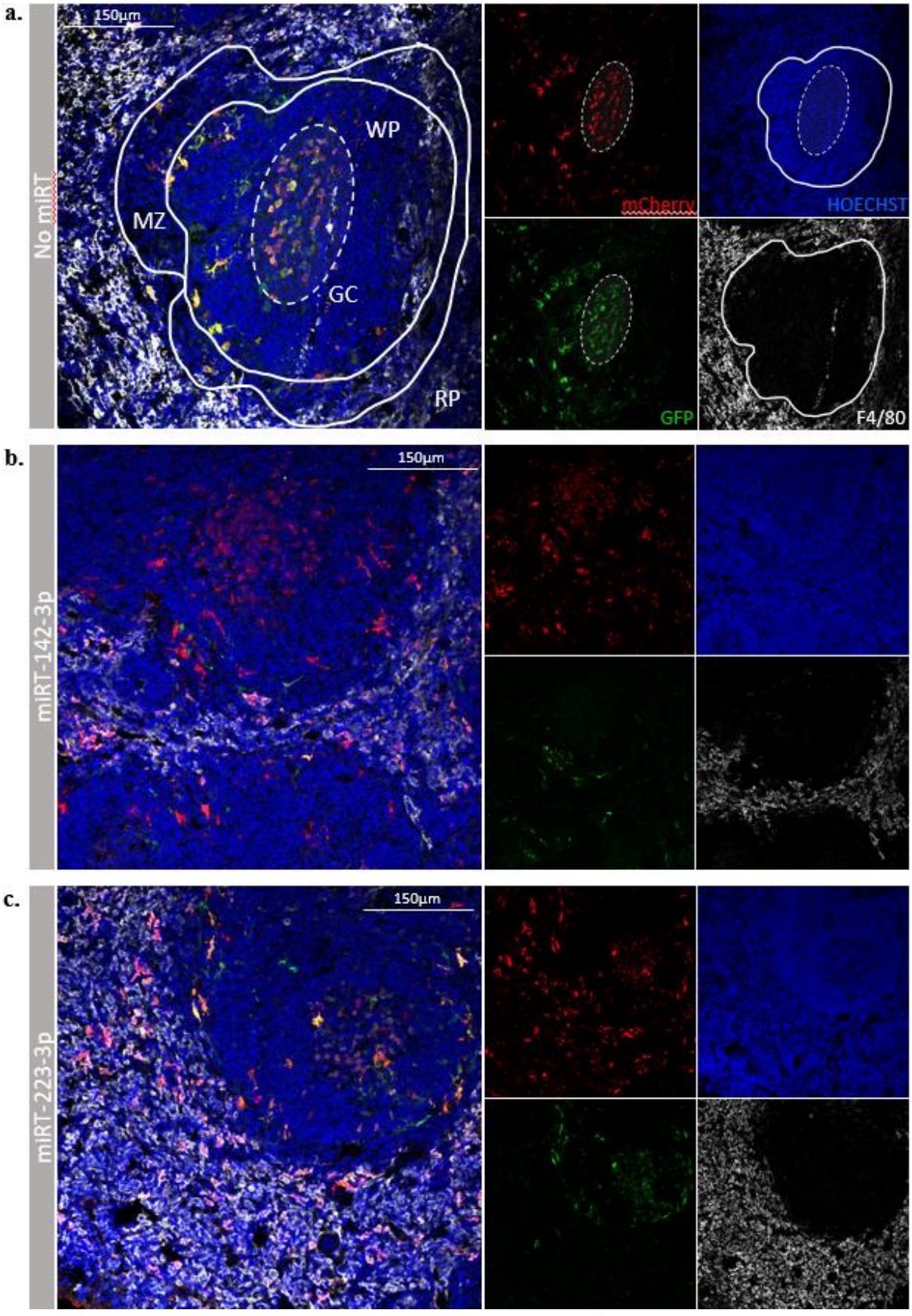
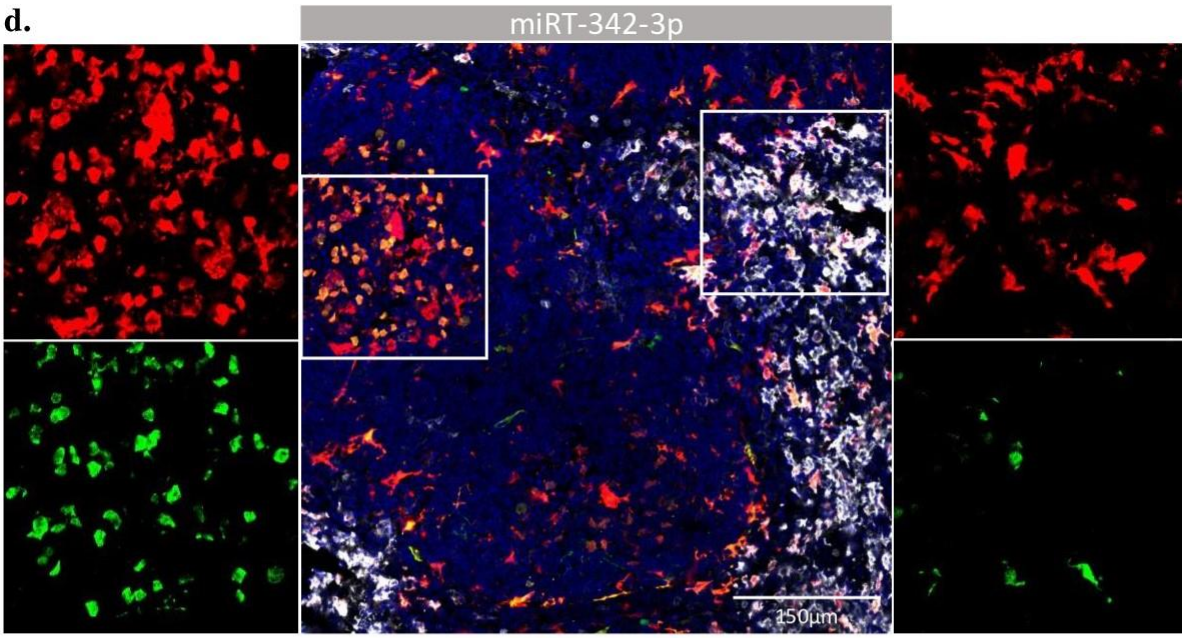
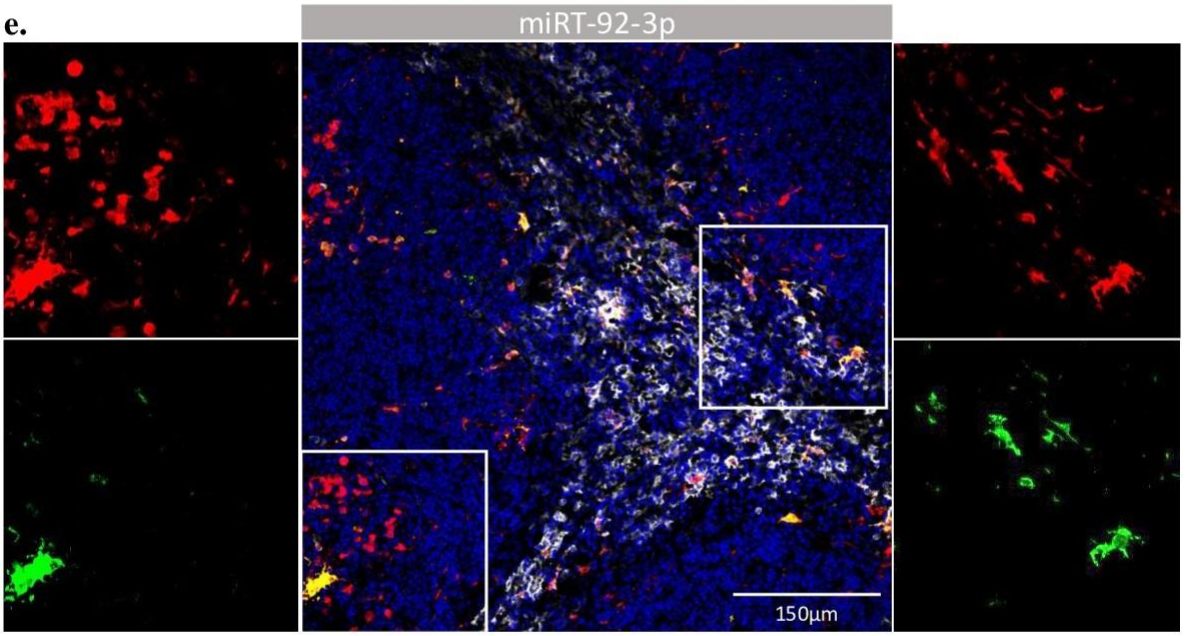


Figure 9 Flow cytometry analysis of miRNA reporter LVs assay *(a) Schematics of the miRNA reporter LVs mechanism of action. mCherry and GFP are co-transcribed by a bidirectional promoter, but GFP is post-transcriptionally regulated by the incorporation of miRT sequences downstream of its coding sequence. In presence of the miRNA of interest, mCherry expression is preserved while GFP expression is downregulated following the strength of miRNA activity. (b) Readout of miRNA activity in different cell populations expressed as the ratio between mCherry MFI and GFP MFI measured by flow cytometry. n=3/4 mice per group.*

Figure 10.


a.
No miRT
150µm
WP
MZ
GC
RP
mCherry
HOECHST
GFP
F4/80
b.
miRT-142-3p
150µm
c.
miRT-223-3p
150µm


d.
miRT-342-3p
150µm


e.
miRT-92-3p
150µm

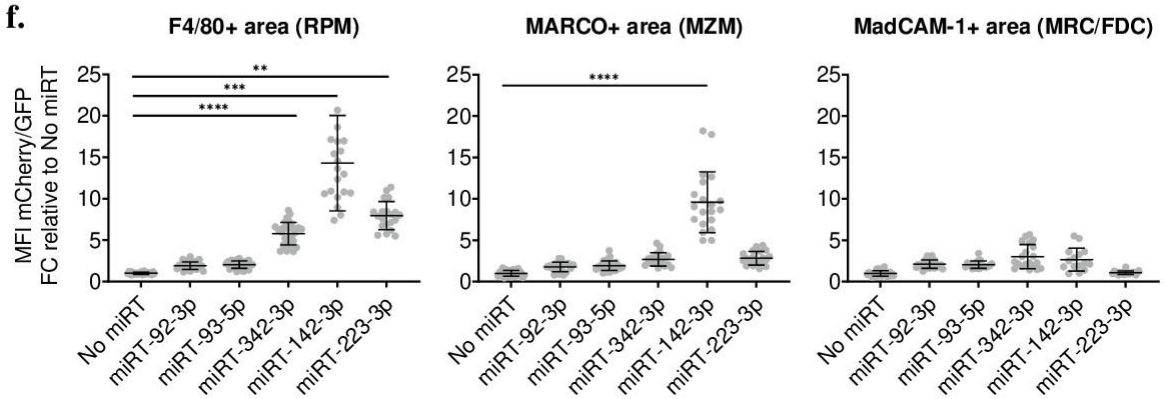

f.
F4/80+ area (RPM)
MARCO+ area (MZM)
MadCAM-1+ area (MRC/FDC)
MFI mCherry/GFP
FC relative to No miRT
**
***
****
****
No miRT
miRT-92-3p
miRT-93-5p
miRT-342-3p
miRT-142-3p
miRT-223-3p

Figure 10 Immunofluorescence analysis of miRNA reporter LVs assay *(a-c) Representative immunofluorescent images of spleen sections stained with Hoechst for nuclear staining, and antibodies targeting mCherry (red), GFP (green) and F4/80 (white). The composite image is displayed on the left, single-channel images for all colors on the right. Spleen in panel (a) was transduced with No miRT LV and is annotated with different anatomical regions of the murine spleen: red pulp (RP) defined as the F4/80+ area, white pulp (WP) corresponding to the regions with high cellular density, germinal centers (GC) are the elliptic areas within the WP with more sparse cellularity, and the marginal zone (MZ) is the area in between RP and WP. Panels (b) and (c) show respectively spleens transduced with a miRT-142-3p LV and a miRT-223-3p LV. (d-e) Representative immunofluorescent images of spleen sections stained with Hoechst for nuclear staining, and antibodies targeting mCherry (red), GFP (green) and F4/80 (white). The composite image is displayed in the middle, magnifications of highlighted areas in the RP or GC (white squares) are shown as single channels for GFP and mCherry on the sides. (f) Readout of miRNA activity in areas positive for different cell populations markers expressed as the ratio between mCherry MFI of the and GFP MFI measured by immunofluorescence within the marker+ mCherry+ area. Groups were composed by 3-4 mice, 5-10 images per mouse were acquired, each dot representing a single image. Statistics on the average per mouse with One-way ordinary Anova. *: p <0.05; **: p <0.01; ***: p <0.001; ****: p <0.0001*

myeloid cells. In fact, miR-142-3p activity was not detected by flow cytometry in LSECs in the liver (Figure 9b), neither was active in MRCs and FDCs in the spleen (Figure 10b). On the other hand, while miR-223-3p was highly active in KCs and RPMs (Figure 9b), its expression seemed to be insufficient to completely abrogate GFP expression in cDCs and MZM (Figure 9b, 10c).

Other miRNAs whose activity profile matched the expression pattern reported in our small RNA-seq analysis were miR-125-5p, which showed a modest activity in LSECs, miR-93-5p and miR-92-3p, which seemed to be B cell specific, and miR-342-3p, which conversely was myeloid specific (Figure 9b). On the other hand, miR-191-5p didn't show any appreciable activity in the cell populations tested.

Upon closer inspection of the miRNA activity in splenic cell populations employing immunofluorescent confocal imaging, miR-92-3p and miR-93-5p showed an inverse activity pattern as compared to miR-342-3p: the formers abrogated GFP expressions in the B cells in the germinal centers but mostly preserved it in the red pulp, while the latter diminished drastically GFP expression in the RPM, but not in the white pulp (Figure 9d-e). We were also able to evaluate miRNA activity in the splenic populations that could not be evaluated by flow cytometry. In this case a mask was drawn around a Marker+ mCherry+ area, and pixel intensity for mCherry and GFP was measured inside of the region of interest. Interestingly, none of the tested miRNAs were found active in the MRC/FDC, and only miR-142-3p was active in the MZM (Figure 10f).

3.2.3 miR-342-3p activity in KCs diminishes in close proximity to CRC liver metastases

We then moved to the evaluation of miRNA activity in the context of CRC liver metastasis. For this analysis our choice fell on miR-342-3p, which showed the most robust and selective activity pattern in myeloid cells, suggesting a functional relevance in these populations. The literature also hints to miR-342-3p relevance in myeloid cell fate decision and macrophage function, and its antitumoral and antiproliferative role in cancer cells is extensively documented. However, little is known about the role of miR-342-3p in the regulation of macrophage function in the TME, and whether its antitumoral effect could expand to TAMs.

To address this question, we first repeated our miRNA reporter assay in presence of CRC liver metastasis to detect any change in miR-342-3p activity which could be suggestive of its role in this context. To induce liver metastasis, we intra-splenically implanted 30.000 AKTPF cells/mouse in n=10 6 week old C57bl/6 female mice. These cells derive from spontaneous colorectal tumors developed by genetically modified C57bl/6 mice harboring 5 commonly found mutations in human CRC (*APCΔ716*, *KrasG12D*, *Trp53R270H*, *Tgfbr2-/-*, *Fbxw7-/-*). When injected intra-splenically, these cells have the potential to form multifocal hepatic metastasis that closely recapitulate the human disease, without seeding in the spleen. Ten days after tumor injection n=4 mice per group were injected either with 3E+08 TU/mouse of miRT-342-3p LV or a No miRT LV as a control, while two mice were left untransduced for gating purposes. After an additional 11 days, 3 weeks after tumor implant, mice were sacrificed, and liver collected for immunofluorescence analysis (Figure 11a).

Upon analysis, most of transduced hepatic cells were F4/80+, either located in the parenchyma or infiltrating the metastatic lesions (Figure 11b). Although miR-342-3p activity was preserved in the intact parenchyma, activity quickly diminished in close proximity to the tumor foci, decreasing more than twofold in the tumor and in the area within a perimeter of 300 μm from the tumor border (Figure 11c). This finding suggests a tumor-mediated reprogramming of the TME to downregulate miR-342-3p expression in TAMs, thus hinting to a potential immune stimulating or antitumoral role in these cells.

Figure 11.

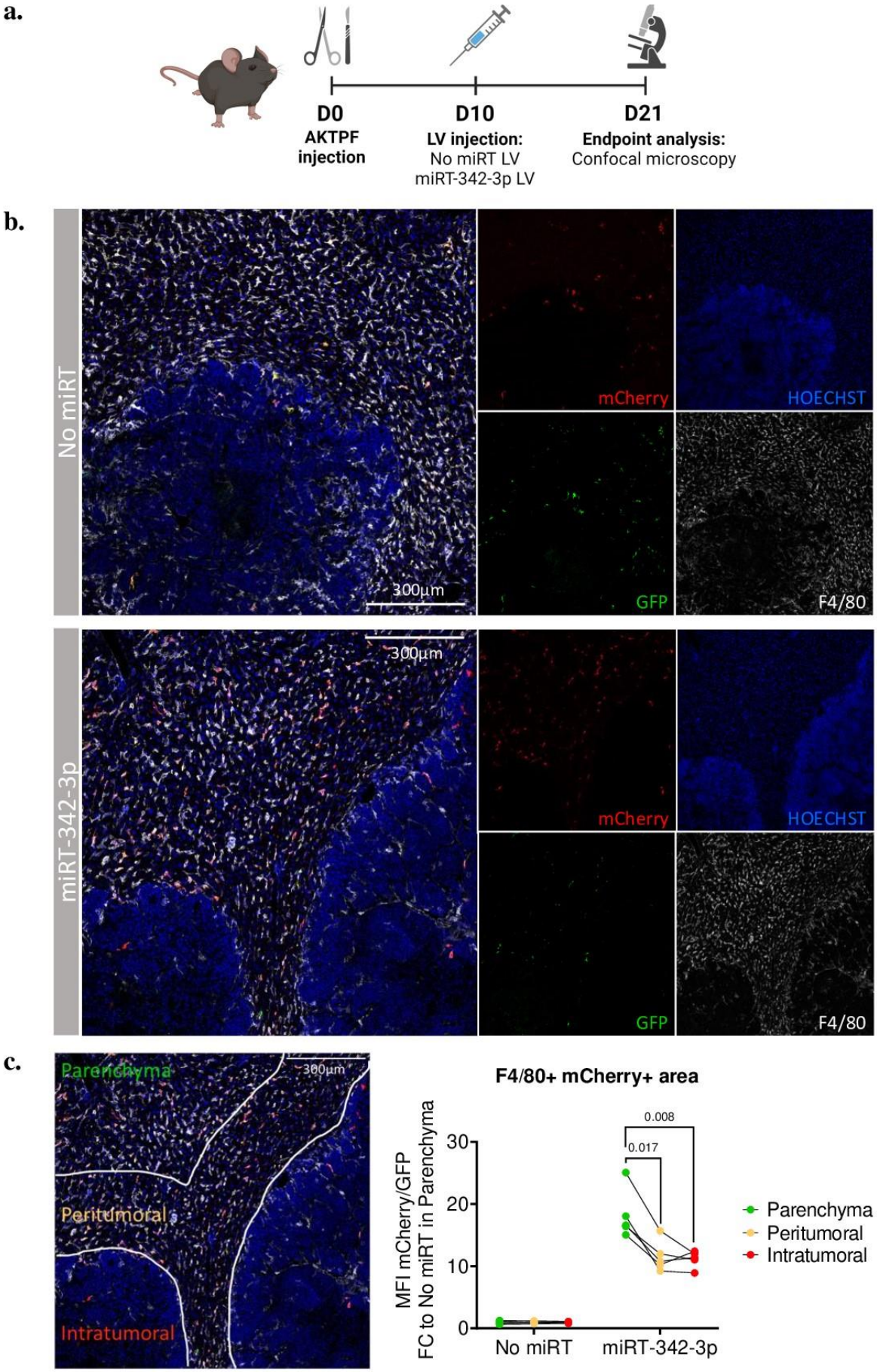

a.
D0
AKTPF injection
D10
LV injection:
No miRT LV
miRT-342-3p LV
D21
Endpoint analysis:
Confocal microscopy
b.
No miRT
mCherry
HOECHST
GFP
F4/80
300µm
miRT-342-3p
mCherry
HOECHST
GFP
F4/80
300µm
c.
Parenchyma
Peritumoral
Intratumoral
300µm
F4/80+ mCherry+ area
MFI mCherry/GFP
FC to No miRT in Parenchyma
0.008
0.017
30
20
10
0
No miRT
miRT-342-3p
Parenchyma
Peritumoral
Intratumoral

Figure 11 miR-342-3p activity detection in CRC liver metastasis model *(a) Experimental setting. AKTPF cells were implanted intra-splenically in mice. After 10 days mice were injected with 3E+08 TU/mouse with miRNA reporter LVs. At day 21 post tumor injection mice were sacrificed and liver was collected for immunofluorescence. (b) Representative immunofluorescent images of liver sections stained with Hoechst for nuclear staining, and antibodies targeting mCherry (red), GFP (green) and F4/80 (white). The composite image is displayed on the left, single-channel images for all colors on the right. Upper panel shows No miRT control, lower panel miRT-342-3p LV transduced liver. (c) Representative image of the different areas in which miR-342-3p activity was measured, with peritumoral area extending 300um around of the tumor mass (left). Readout of miRNA activity expressed as the ratio between mCherry MFI and GFP MFI measured by immunofluorescence as pixel intensity within the F4/80+ mCherry+ area (right). Groups were composed by 4 mice, 4 images per mouse were acquired and mean between the images was plotted. Statistics: Mann-Whitney test.*

3.3 Enforcing miRNA expression in LV-targeted cell populations

As discussed in the introduction, some studies suggest the possibility of remodeling TAMs phenotype through the modulation of specific miRNAs that trigger antitumoral responses. The next step of the project was then aimed at modulating miRNA expression in TAM-like KCs in the context of liver metastasis. To do so, we chose to employ LVs to overexpress *in vivo* some miRNAs of interest: miR-155-5p, associated to pro-inflammatory M1-like phenotypes, antitumoral miR-511-3p, as well as the newly identified miR-342-3p.

3.3.1 Development and validation of a miR-342-3p overexpression cassette

We generated a miR-342-3p expression cassette by amplifying a region of about 300 bp around *Mir342* locus and cloning it into an LV transfer plasmid under the transcriptional regulation of SFFV promoter. The amplified region was inserted within a copy of human *EF-1a* first intron to allow the co-expression of a reporter transgene (e.g. mOrange) inserted downstream of it (Amendola *et al*, 2009) (Figure 12a). Together with the LV coding for miR-342-3p, we also produced an empty intron control (hereon referred as Intron LV) and some vectors already validated for the overexpression of miR-155-5p or miR-511-3p (Zonari et al, 2013; Squadrito et al, 2012). We used these LVs to transduce a *bona fide* in vitro model of KCs (KC1) obtained through the immortalization of C57bl/6 mouse-derived KCs through their transduction with an LV coding for SV40 large T antigen. These cells recapitulate many of the features displayed by KCs *in vivo*, notably their morphology and the possibility to polarize towards M1-like and M2-like phenotypes upon appropriate stimulation. However, they do not express some typical KCs markers (e.g. CLEC4F), potentially due to the lack of interaction with the hepatic niche.

Figure 12.

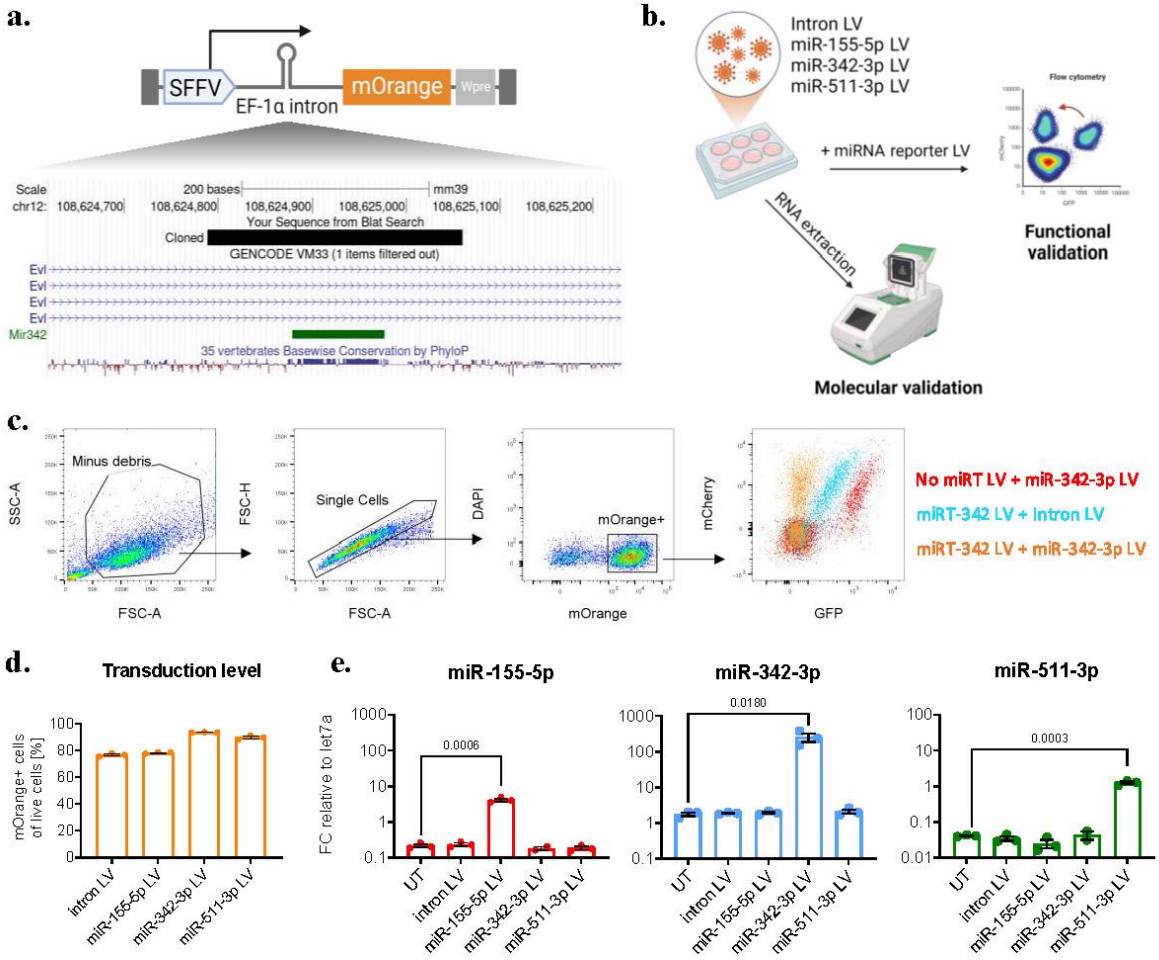


Figure 12 miR-342-3p overexpression LV design and validation *(a) Overview as displayed in UCSC genome browser of the region cloned into SFFV.EF1a intron.mOrange.Wpre transfer plasmid for miRT-342-3p LV generation. (b) Experimental setting for miRNA overexpression LVs validation. KC1 cells were transduced with miRNA overexpression vectors or Intron LV control, then co-transduced with associate miRNA reporter LV to track increased functionality of miRNA of interest, or RNA was extracted to measure the miRNA levels in the cell at molecular level. (c) Gating strategy and results of miR-342-3p LV functional validation by flow cytometry. (d) Levels of transduction of KC1 transduced with various miRNA overexpression vectors or control LV. (e) Results of ddPCR analysis on RT of RNA extracted from transduced KC1 cells. Level of miRNA expression is expressed in terms of fold change compared to let7a expression. Statistics: Unpaired t test*

Following KC1 transduction with miRNA overexpression vectors we checked their level of transduction by flow cytometry, confirming that the percentage of mOrange+ cells was high enough to grant stable miRNA overexpression in the majority of cells (Figure 12d). Finally, we validated miR-342-3p overexpression LV both from a functional and molecular standpoint, either through the co-transduction with miRT-342-3p LV to check for the miRNA repressive activity or by directly measuring miRNA levels. miR-342-3p activity in KC1 was endogenously high, as highlighted by the fact that a reduction in GFP MFI was observable even in Intron LV-transduced cells, however a gain of function could be achieved by miR-

342-3p LV transduction, which completely abrogated GFP expression from the cells (Figure 12c).

Upon bulk RNA extraction and small RNAs retrotranscription, we could evaluate miRNA levels in the cDNA by ddPCR with specific TaqMan assays. We included let7a as a normalizer, and measured each miRNA in every condition to verify that unrelated miRNA processing affected by the overexpression. Transduced cell populations showed comparable levels of unrelated miRNAs compared to the untransduced control. miR-342-3p basal level was the highest, with an expression comparable to that of let7a, while miR-155-5p and miR-511-3p were significantly lower, respectively 5 and 20 times lower that let7a. All miRNA overexpression LVs could induce an increase in the level of the respective miRNA, however miR-342-3p LV seemed to be the most efficient both in terms of overall expression and fold change compared to the basal level (Figure 12e). This can be partially related to the slightly higher transduction level, but also to more efficient miRNA processing, given that miR-342-3p seems to be the only one to be endogenously expressed by KC1, among the tested miRNAs.

3.3.2 Overexpression of selected miRNAs in a model of CRC liver metastasis

Once all miRNA overexpression LVs were validated, we evaluated their impact on the phenotype of KCs in a CRC liver metastasis model. We intra-hepatically implanted 100.000 MC38 cells/mouse in n=30 6 week old C57bl/6 female mice. MC38 is a murine CRC cell line with a background in the C57bl/6 strain; upon implant into the mouse liver, it forms a single bulky, rapidly proliferating tumor mass whose growth can easily be evaluated weighting it or measuring it with a caliber. We weighted the mice at day 2 post tumor injection and divided them into 4 groups equally distributing their initial body weight to account for potential differences in the level of transduction. At day 3 post tumor implant we intravenously injected n=7 mice per group with 3E+08 TU/mouse of either miR-155-5p LV, miR-342-3p LV, miR-511-3p LV or Intron LV. Two mice were left untransduced for gating purposes.

Disease progression and acute toxicity events linked to miRNA overexpression were monitored by weighting the mice twice a week and by analyzing the blood count at 7 and 14 days post LV injection (Figure 13a). All groups showed a comparable weight gain, with an average increase of 1,5 – 2 g during the 15-day monitoring (Figure 13b). Blood count revealed no significant difference among groups, all of which displayed a slight anemia and mono/neutrophilia that progressed from week 1 to week 2 post LV injection and was likely

Figure 13.

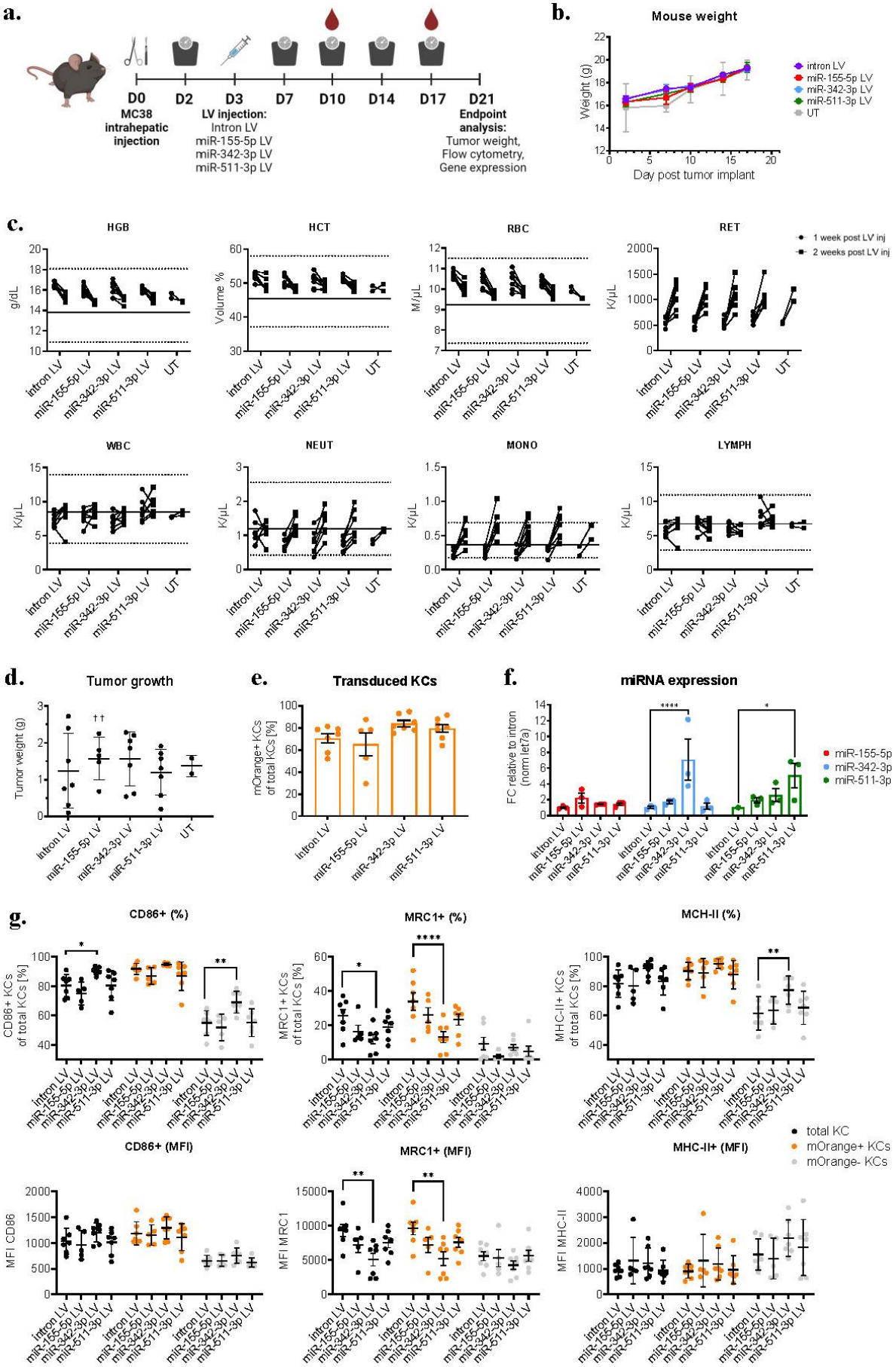

a.
D0
D2
D3
D7
D10
D14
D17
D21
MC38 intrahepatic injection
LV injection: Intron LV miR-155-5p LV miR-342-3p LV miR-511-3p LV
Endpoint analysis: Tumor weight, Flow cytometry, Gene expression
b.
Mouse weight
Weight (g)
Day post tumor implant
intron LV
miR-155-5p LV
miR-342-3p LV
miR-511-3p LV
UT
c.
HGB
HCT
RBC
RET
WBC
NEUT
MONO
LYMPH
1 week post LV inj
2 weeks post LV inj
d.
Tumor growth
Tumor weight (g)
e.
Transduced KCs
mOrange+ KCs of total KCs [%]
f.
miRNA expression
FC relative to intron (norm let7a)
miR-155-5p
miR-342-3p
miR-511-3p
g.
CD86+ (%)
MRC1+ (%)
MCH-II (%)
CD86+ KCs of total KCs [%]
MRC1+ KCs of total KCs [%]
MHC-II+ KCs of total KCs [%]
CD86+ (MFI)
MRC1+ (MFI)
MHC-II+ (MFI)
MFI CD86
MFI MRC1
MFI MHC-II
total KC
mOrange+ KCs
mOrange- KCs

Figure 13 miRNA enforced expression in MC38 tumor model *(a) Experimental setting. MC38 cells were implanted intra-hepatically in mice. After 2 days mice were weighted, and the following day they were injected with 3E+08 TU/mouse of miRNA overexpression LV. For the following two weeks mice were weighted twice per week and a blood analysis was performed at days 7 and 14 post LV injection. At day 21 post tumor injection mice were sacrificed and liver and tumor were collected for flow cytometry. (b) Weight charts of mice during the monitoring. (c) Blood analysis results performed 1 week (circle) or 2 weeks (square) post LV injection. Levels of hemoglobin (HGB) and hematocrit (HCT) were tested, as well as performing the counts of red blood cells (RBC), reticulocytes (RET), white blood cells (WBC), neutrophils (NEUT), monocytes (MONO), and lymphocytes (LYMPH). (d) Tumor weight at sacrifice. Two mice of miR-155-5p group perished before the endpoint, and are indicated with crosses. (e) Level of transduction of KCs in liver parenchyma assessed by flow cytometry. (f) miRNA expression levels mOrange+ KCs purified by FACS from the liver of transduced mice and analysed by ddPCR on RT. Statistic: 2 way Anova with Dunnet correction. *: p <0.05; **: p <0.01; ***: p <0.001; ****: p <0.0001 (g) CD86 (left), MRC1 (middle) and MCH-II (right) expression in KCs in the liver parenchyma, expressed both as percentage of marker+ cells on the total population (upper panels) or MFI of the marker in the marker+ population (lower panels). All parameters were measured independently for the whole population (black), only for the mOrange+/transduced KCs (orange) or for the mOrange-/untransduced KCs (grey). Statistics: 2 way Anova with Dunnet correction. *: p <0.05; **: p <0.01; ***: p <0.001; ****: p <0.0001. n=7 mice per group, 2 UT mice.*

caused by the inflammatory state associated with tumor progression (Figure 13c). Two mice in the miR-155-5p LV group perished in the days preceding experimental endpoint, while the others were sacrificed 21 days after tumor implant.

We evaluated tumor weight at sacrifice and found no significant difference between the groups (Figure 13d). We collected both tumor and liver for flow cytometric analysis, as well as the liver of three mice per group for FACS of transduced KCs. Flow cytometric analysis revealed that mice were evenly transduced among groups, with the exception of one mouse in the miR-155-5p LV group (Figure 13e). Transduced KCs showed an increase in respective miRNA expression, as demonstrated by ddPCR TaqMan assays performed on the RNA from sorted KCs (Figure 13f). miR-342-3p LV once again reached the higher overexpression of the related miRNA, which was associated with a remodeling of KCs towards M1-like and immune-active phenotypes, as demonstrated by the significant increase in CD86 and MHC-II expression and the reduction in MRC1 expression (Figure 13g). Interestingly, these remodeling wasn't limited to transduced KCs, but involved also mOrange- KCs, suggesting some level of TME reprogramming or a positive feedback between transduced and untransduced cells mediated by soluble factors.

3.3.3 Overexpression of miR-342-3p in a more relevant CRC liver metastasis model hints to an antitumoral activity

Building on the results of the previous experiment, we decided to repeat miR-342-3p overexpression in a more relevant CRCLM model. Although MC38 liver metastases are a convenient murine tumor model, as they are easy to quantify and do not require MRI monitoring, they are highly aggressive and do not recapitulate human disease progression and histopathological characteristics. As previously discussed, AKTPF CRCLM more closely resemble the human disease, as cells are spread hematogenously through the portal vein to seed into the liver, creating multifocal lesions. On the one hand, the presence of multiple smaller tumor masses determines a bigger liver parenchyma-tumor interface, which provides an ideal platform to test strategies based on the reprogramming of the TME. Moreover, the presence of multifocal, slowly proliferating lesions allows each mass to accumulate mutations independently from the others, creating heterogeneous cancer cell populations that better recapitulate human pathogenesis.

We repeated the experiment employing AKTPF tumor model, implanting intra-splenically 30.000 cells/mouse in 6 weeks old C57bl/6 female mice and injecting intravenously 3E+08 TU/mouse of miR-342-3p LV or Intron LV at day 3 after tumor implant (Figure 14a). Tumor volume was evaluated 3 weeks after tumor injection by MRI, and we found it to be particularly small, with several mice in both groups that appeared to be tumor free (Figure 14c). The unexpectedly low tumor burden may be the result of an IFN-mediated response to the LV injection, which was likely performed when tumor cells were still in the early phases of hepatic seeding, triggering their clearance. Nevertheless, a nearly significant trend was observed, with miR-342-3p LV-injected mice displaying a lower tumor burden compared to controls (Figure 14b). This observation was in agreement with the enhanced pro-inflammatory and anti-tumoral activation of TAMs upon miR-342-3p enforced expression observed in the previous experiment using MC38-based CRCLM.

Experimental endpoint was set at 28 days after tumor injection, collecting liver for vector copy number (VCN) and flow cytometry. Both analyses confirmed that mice were evenly transduced in both groups, discounting the possibility that miR-342-3p LV injected mice increased tumor clearance was determined by a higher vector dose (Figure 14d-e). Flow

Figure 14.

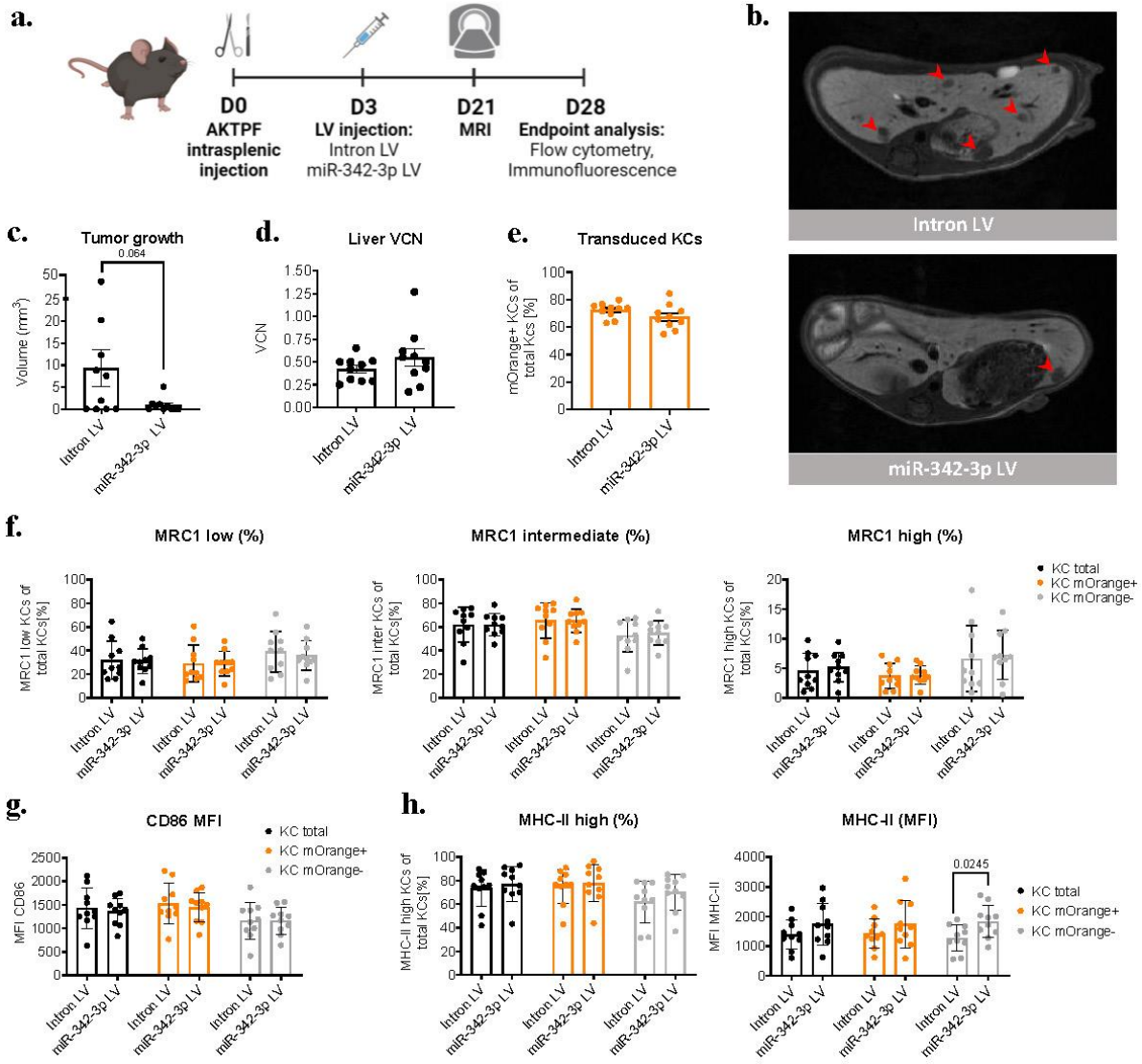


Figure 14 miR-342-3p enforced expression in AKTPF tumor model: early injection *(a) Experimental setting. AKTPF cells were implanted intra-splenically in mice. After 3 days mice were injected with 3E+08 TU/mouse with miRNA reporter LVs. Tumor growth was monitored by MRI 21 days after tumor injection. Mice were sacrificed 28 days after tumor implant and liver was collected for flow cytometry. (b) MRI images of mice with the highest tumor burden in each experimental group. Liver metastases are indicated by red arrows. (c) Tumor volume measured by MRI at day 21 post tumor implant. Statistics: Mann-Whitney test. (d) Lever of transduction of the liver measured by VCN analysis. (e) Level of transduction of KCs assessed by flow cytometry. (f-h) Study of the phenotype of KCs in the liver parenchyma by flow cytometry. MRC1 expression (f), CD86 expression (g), and MHC-II expression (h) were measured independently for the whole population (black), only for the mOrange+/transduced KCs (orange) or for the mOrange-/untransduced KCs (grey). Statistics: Mann-Whitney test.*

cytometry analysis revealed that KCs in the liver were skewed mainly towards an M2-like phenotype, as expected for this kind of tumor compared to MC38 tumors, in which both M1 and M2-like TAMs are present at substantial levels. Therefore, no significant differences in terms of polarization were detected between miR-342-3p LV and Intron group (Figure 14f-g).

However, a trend towards an increased MHC-II expression in KCs of mice from miR-342-3p LV group was observed, reaching statistical significance in untransduced cells (Figure 14h).

3.4 Evaluating miR-342-3p impact on KCs biology and antitumoral activity

Following on the promising results of the previous experiment, we chose to investigate the molecular mechanism behind miR-342-3p-driven KC reprogramming more in depth. To do so we generated LVs for miR-342-3p modulation with specific associated controls and used them to evaluate the miRNA impact on KCs transcriptional profile *in vitro* and *in vivo*. We also evaluated miR-342-3p overexpression impact on newly discovered pathways at higher tumor burden, characterizing the tumor infiltrate and validating the miRNA effect on tumor growth.

3.4.1 Development and validation of a miR-342-specific control and of miR-342-3p sponge LVs

We generated a matched control LV mutating the sequence cloned for miR-342-3p LV in the region corresponding to the miRNA duplex, maintaining CG content and paying attention not to introduce pre-existing miRNA seed regions. The sequence encoded by this miR-342 mut LV was otherwise identical to that of miR-342-3p LV, and coded for a pri-miRNA structure that was comparable to that of pri-miR342, and thus was expected to undergo a similar processing (Figure 15a,c). However, mutations introduced in the mature miRNA sequence prevent it from binding to miR-342-3p targets, rendering it inactive.

We also generated different LVs encoding for miRNA sponges, whose function is binding endogenous miRNAs (e.g. miR-342-3p) sequestering them from their targets and thus inhibiting their effect. We employed different strategies for miRNA sponge design, the easiest included a sequence perfectly complementary to miR-342-3p (perfect target, PT) repeated 8 x in tandem and separating each repetition with randomized 4 nt linkers. This structure would bind miR-342-3p with high affinity, however extensive complementarity is known to induce Ago2 endonuclease activity, eventually leading to sponge degradation. Alternatively, the sponge could be constituted by targets containing a central mismatch, creating a bulge between 11-14nt (bulge target, BT). Such peculiar conformation has been reported to induce the 3' trimming, tailing and degradation of miRNA, rather than the RNA target, in a process termed target-directed microRNA degradation.

Figure 15.

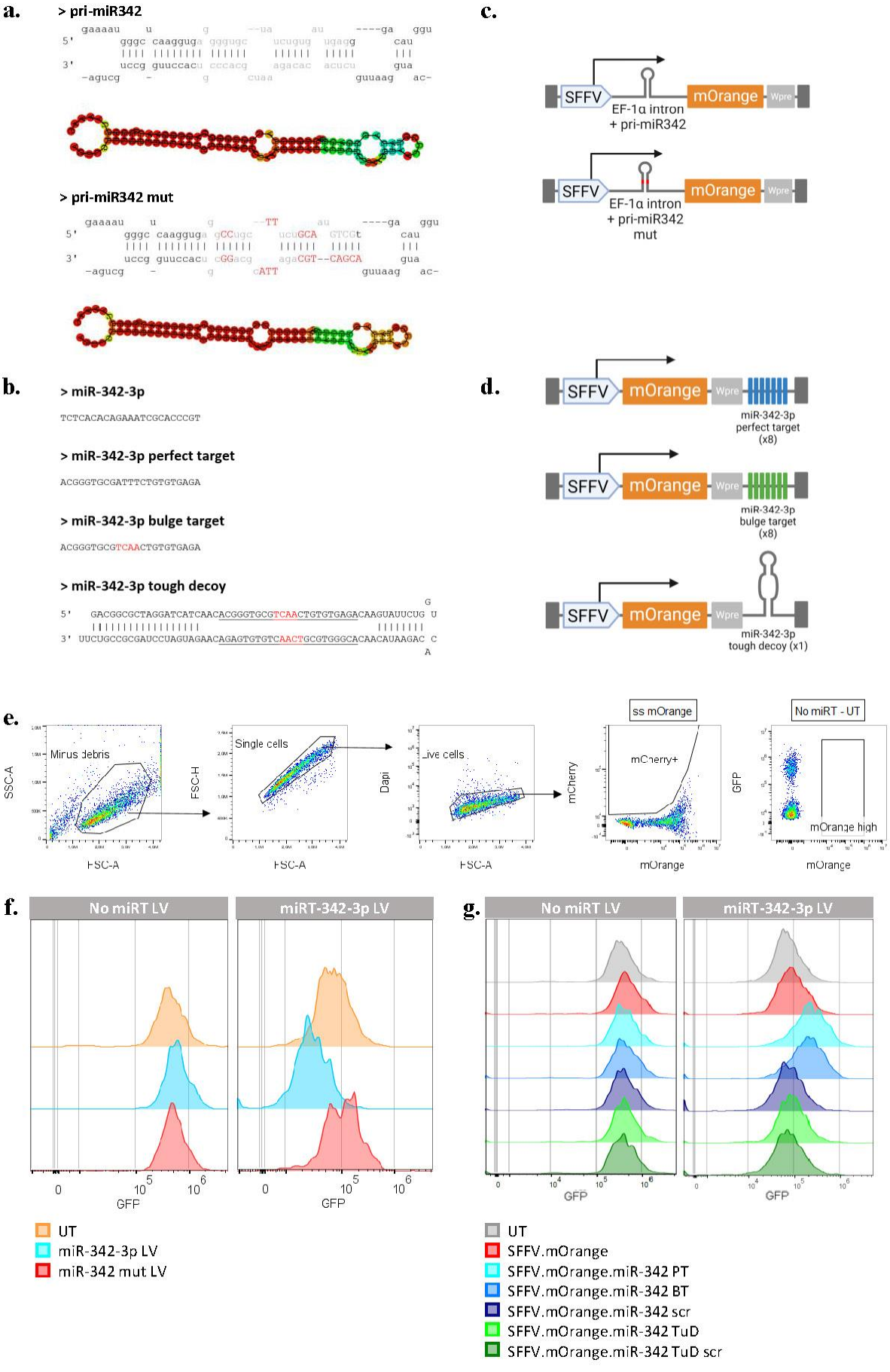

a.
> pri-miR342
> pri-miR342 mut
b.
> miR-342-3p
TCTCACACAGAAATCGCACCCGT
> miR-342-3p perfect target
ACGGGTGCGATTTCTGTGTGAGA
> miR-342-3p bulge target
ACGGGTGCGTCAACTGTGTGAGA
> miR-342-3p tough decoy
c.
SFFV
EF-1α intron
+ pri-miR342
mOrange
Wpre
SFFV
EF-1α intron
+ pri-miR342
mut
mOrange
Wpre
d.
SFFV
mOrange
Wpre
miR-342-3p
perfect target
(x8)
SFFV
mOrange
Wpre
miR-342-3p
bulge target
(x8)
SFFV
mOrange
Wpre
miR-342-3p
tough decoy (x1)
e.
Mirus debris
SSC-A
FSC-A
Single cells
FSC-H
FSC-A
Dapi
ive cells
FSC-A
ss mOrange
mCherry+
mCherry
mOrange
No miRT - UT
mOrange high
GFP
mOrange
f.
No miRT LV
miRT-342-3p LV
GFP
UT
miR-342-3p LV
miR-342 mut LV
g.
No miRT LV
miRT-342-3p LV
GFP
UT
SFFV.mOrange
SFFV.mOrange.miR-342 PT
SFFV.mOrange.miR-342 BT
SFFV.mOrange.miR-342 scr
SFFV.mOrange.miR-342 TuD
SFFV.mOrange.miR-342 TuD scr

Figure 15 miRNA overexpression control and miRNA sponge design and validation *(a) pri-miR342 and mutated pri-miR342 cloned inside of the SFFV.EF1a intron.mOrange.Wpre vector for miRNA overexpression. Sequence and secondary structure as predicted by the RNAfold web server are displayed on the left, schematics of LV design on the right. Inside of pri-miR sequence, miRNA duplex is displayed in grey and mutated bases in red. (b) Sequences for the target monomers composing the miRNA sponges (left) and relative schematics of the LV design (right). (e) Gating strategy employed during the validation of the miR-342 mut LV and the miR-342 sponge LVs by flow cytometry. (f-g) Histogram displaying GFP mFI mCherry+ mOrange+/UT cells for (f) miR-342 mut LV validation and (g) miR-342 sponges LV validation and relative SCR controls.*

Finally, we also generated a miRNA sponge contained in a hairpin structure with increased stability termed tough decoy (TuD). TuD are composed of a lower and upper stem, an apical loop, and a central region containing two miRNA targets, in our case the miR-342-3p BT. Compared to linear sponges, TuD are supposed to have a longer half-life and therefore be more efficient at inhibiting miRNA action, but their complex secondary structure may pose a challenge in vector production and viral RNA packaging. The expression of all constructs is driven by SFFV promoter, which also drives the expression of mOrange, which serves as a transduction control. Furthermore, we generated controls LVs both the linear sponge and TuD sponge, which contained scramble targets (SCR) instead of miR-342-3p target sequences.

All constructs were tested co-transducing KC1 with a No miRT LV or a miRT-342-3p LV to track miRNA activity, and with the mOrange-coding sponge or miRNA overexpression LV. As expected, miR-342-3p LV induced a GFP downregulation in the cells transduced with miR-342-3p reporter, while GFP level in miR-342 mut LV or untransduced groups was comparable (Figure 15f). Both miR-342-3p PT and BT sponge LV caused an increase in GFP MFI in cells transduced with miR-342-3p reporter, bringing it to comparable levels to No miRT controls (Figure 15g). On the other hand, miR-342-3p TuD sponge did not cause such shift in GFP MFI, which remained comparable to both untransduced cells and SCR controls (Figure 15g).

3.4.2 In vitro expression regulation of miR-342-3p in a bona fide KC model suggests its relevance in immune activation and macrophage biology

To better understand the molecular basis of miR-342-3p action in macrophages, we transduced KC1 *in vitro* either with the miR-342-3p LV or the sponge miR-342-3p BT LV and the relative controls (miR-342 mut LV and sponge SCR LV). We aimed at an average VCN lower than 1, to prevent overloading the transcription machinery of the cells, obtaining for each construct a population with 40-50% mOrange+ cells (corresponding to VCN 0.5-0.7).

We sorted viable mOrange high cells and extracted total RNA, on which we performed polyA-enriched RNA-seq.

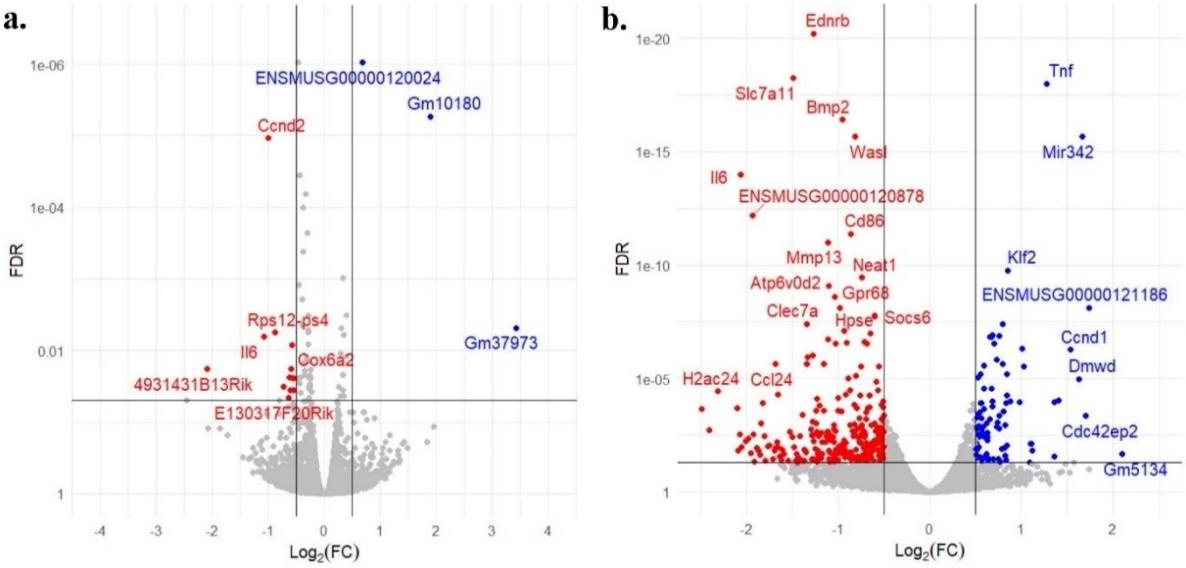
Upon DGE analysis we found sponge BT group gene expression to be similar to that of sponge SCR control, with less than 20 genes with FDR<0.05 and $|Log_2FC|>0.5$ (Figure 16a). On the other hand, miR-342-3p group showed a remarkable number of deregulated genes compared to miR-342 mut control. The majority of deregulated genes were downregulated, however we could also find some upregulated genes, notably *Mir342* and *Tnf* (Fig 16b).

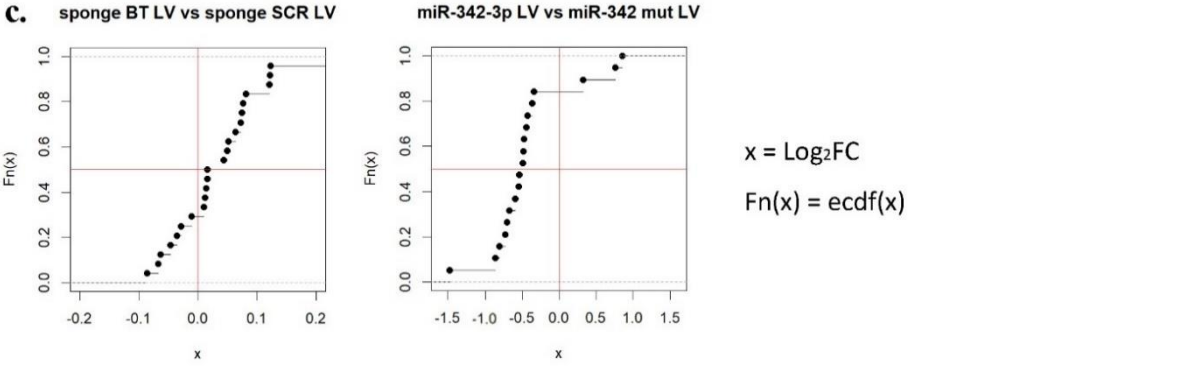
We then considered miR-342-3p targets reported by TargetScan prediction tool, selecting genes based on their Cumulative weighted context++ score, an index evaluating the downregulation potential of the miRNA on a target taking into account the number, position and affinity of the miRNA binding sites contained in its 3'UTR. The advantages and limitation of TargetScan use for target prediction will be further addressed in the Discussion section. When we checked the cumulative distribution of Log_2FC of miR-342-3p top targets in sponge BT versus sponge SCR group, we found the majority of them to be slightly upregulated. Conversely, the same set of genes was found quite strongly downregulated in miR-342-3p group compared to miR-342 mut control (Figure 16c). These findings were expected and confirmed the downregulation or upregulation of miR-342-3p induced by our LVs. However, the sponge BT effect was modest, potentially because of an

insufficient level of expression of the construct, therefore for the following analysis we only took into account the results of the DGE between miR-342-3p and miR-342 mut groups, and used the comparison between Sponge BT and SCR control as check validation.

We looked for direct miR-342-3p targets based on their downregulation in miR-342-3p group compared to miR-342 mut control, on TargetScan prediction variables, in particular the number and conservation of miRNA target sites, and on the associated entries in miRTarBase, an experimentally validated microRNA-target interactions database. The results of this preliminary analysis were manually curated, and 5 potential targets were selected for further testing. We repeated the *in vitro* miR-342-3p overexpression experiment in KC1, extracting the RNA from miR-342-3p or miR-342 mut LV and assessing the expression of the potential targets by ddPCR on the RT. 4 out of 5 of the tested genes were consistently downregulated in the second batch, although statistical significance wasn't reached for all of them.

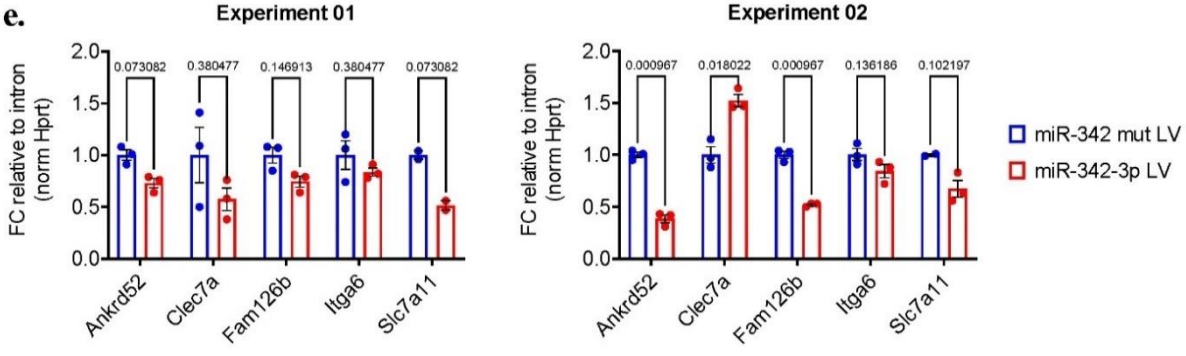
Figure 16.



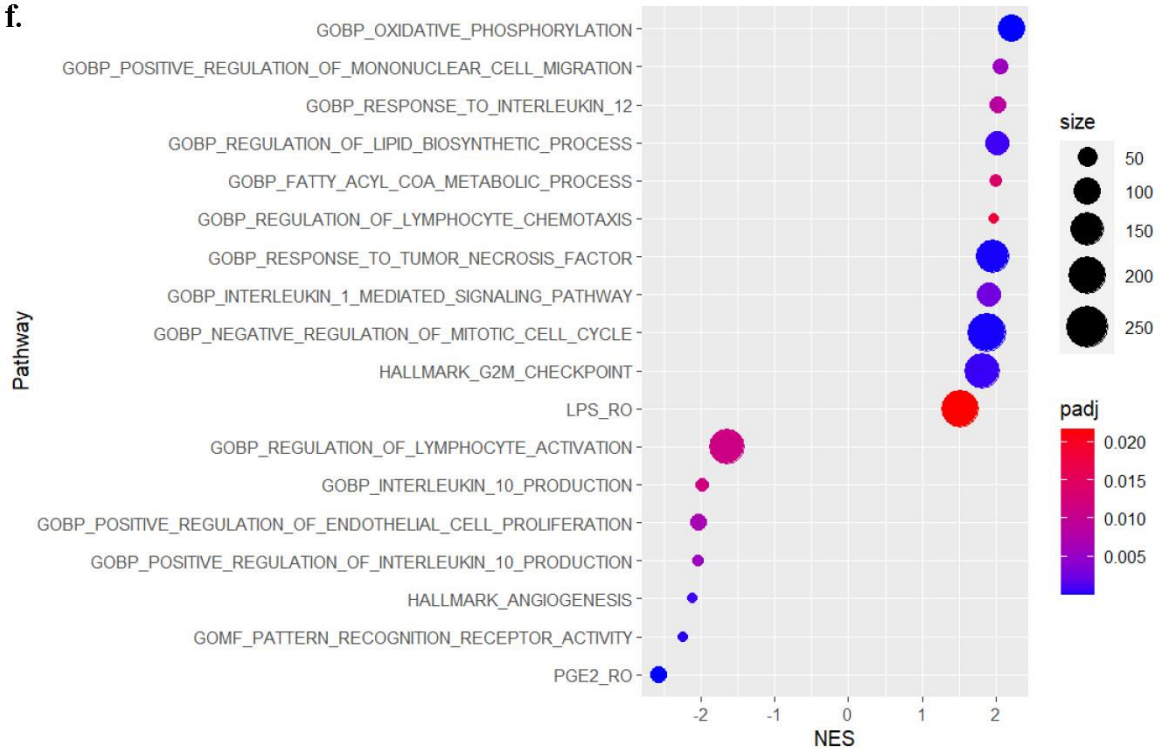


d.

				TargetScan8.0										miRTarBase	
Gene	logFC	logCPM	FDR	Conserved sites total	Conserved 8mer sites	Conserved 7mer-m8 sites	Conserved 7mer-A1 sites	Poorly conserved sites total	Poorly conserved 8mer sites	Poorly conserved 7mer-m8 sites	Poorly conserved 7mer-A1 sites	6mer sites	Cumulative weighted context++ score	ID	References (PMID)
Ankrd52	-0.60	7.05	5.85E-02	2	0	2	0	0	0	0	0	1	-0.07		
Clec7a	-1.34	5.62	3.96E-08	0	0	0	0	1	0	1	0	1	-0.01	MIRT604220	21258322
Itga6	-0.57	6.40	2.06E-03	1	1	0	0	1	0	0	1	1	-0.06		
Fam126b	-0.68	4.37	2.39E-02	1	0	0	1	3	1	1	1	2	-0.32		
Slc7a11	-1.49	4.70	5.65E-19	0	0	0	0	2	1	1	0	4	-0.27	MIRT580885	23597149, 21258322, 25083871



f.


GOBP_OXIDATIVE_PHOSPHORYLATION
GOBP_POSITIVE_REGULATION_OF_MONONUCLEAR_CELL_MIGRATION
GOBP_RESPONSE_TO_INTERLEUKIN_12
GOBP_REGULATION_OF_LIPID_BIOSYNTHETIC_PROCESS
GOBP_FATTY_ACYL_COA_METABOLIC_PROCESS
GOBP_REGULATION_OF_LYMPHOCYTE_CHEMOTAXIS
GOBP_RESPONSE_TO_TUMOR_NECROSIS_FACTOR
GOBP_INTERLEUKIN_1_MEDIATED_SIGNALING_PATHWAY
GOBP_NEGATIVE_REGULATION_OF_MITOTIC_CELL_CYCLE
HALLMARK_G2M_CHECKPOINT
LPS_RO
GOBP_REGULATION_OF_LYMPHOCYTE_ACTIVATION
GOBP_INTERLEUKIN_10_PRODUCTION
GOBP_POSITIVE_REGULATION_OF_ENDOTHELIAL_CELL_PROLIFERATION
GOBP_POSITIVE_REGULATION_OF_INTERLEUKIN_10_PRODUCTION
HALLMARK_ANGIOGENESIS
GOMF_PATTERN_RECOGNITION_RECEPTOR_ACTIVITY
PGE2_RO
Pathway
-2
-1
0
1
2
NES
size
50
100
150
200
250
padj
0.020
0.015
0.010
0.005

g.


GOBP_OXIDATIVE_PHOSPHORYLATION
GOBP_RESPONSE_TO_INTERLEUKIN_12
GOBP_NEGATIVE_REGULATION_OF_MITOTIC_CELL_CYCLE
HALLMARK_G2M_CHECKPOINT
GOBP_INTERLEUKIN_1_MEDIATED_SIGNALING_PATHWAY
GOBP_RESPONSE_TO_TUMOR_NECROSIS_FACTOR
LPS_RO
GOBP_REGULATION_OF_LYMPHOCYTE_CHEMOTAXIS
GOBP_POSITIVE_REGULATION_OF_MONONUCLEAR_CELL_MIGRATION
GOBP_REGULATION_OF_LIPID_BIOSYNTHETIC_PROCESS
HALLMARK_ANGIOGENESIS
GOBP_POSITIVE_REGULATION_OF_ENDOTHELIAL_CELL_PROLIFERATION
PGE2_RO
GOBP_FATTY_ACYL_COA_METABOLIC_PROCESS
GOBP_POSITIVE_REGULATION_OF_INTERLEUKIN_10_PRODUCTION
GOBP_REGULATION_OF_LYMPHOCYTE_ACTIVATION
GOMF_PATTERN_RECOGNITION_RECEPTOR_ACTIVITY
GOBP_INTERLEUKIN_10_PRODUCTION
size
20
40
60
Log2(FC)
1.5
1.0
0.5
0.0
-0.5
-1.0

Figure 16 In vitro analysis of miR-342-3p impact on KC1 transcriptional landscape *KC1 cells were transduced either with a vector for miR-342-3p overexpression (miR-342-3p LV) or for its downregulation (sponge BT LV9 and their respective controls (miR-342 mut LV and sponge SCR LV). Sorted cells were purified by FACS and used for an RNA-seq analysis. (a) Volcano plot of DGE analysis between sponge BT and sponge SCR. (b) Volcano plot of the DGE analysis between miR-342-3p and miR-342 mut LV. (c) Cumulative distribution of the FC of top miR-342-3p targets predicted by TargetScan for sponge BT-sponge SCR comparison (left) and miR-342-3p-miR-342 mut comparison (right). (d) Table annotating the characteristics of selected miR-342-3p targets. (e) Expression levels of selected target genes by ddPCR on RT from experiment 1 (on which RNA-seq analysis was performed) and experiment 2, its biological replicate. Statistics: Unpaired T test. (f) GSEA of the genes differentially expressed between miR-342-3p LV and miR-342 mut LV groups. Statistics: adjusted P-value based on an adaptive multi-level split Monte-Carlo scheme. (g) Cnetplot of the pathways reported in the GSEA of previous panel. Each dot represents a gene, dots connected to more than one pathway are shared among them. Colors of the dots reflect the FC from DGE analysis.*

We then tried to establish the pathways indirectly regulated by miR-342-3p overexpression in order to infer its biological effect on KCs. We performed a gene set enrichment analysis (GSEA) and selected pathways related to cell proliferation, macrophage function and polarization (Figure 16f). Interestingly, we were able to identify two main clusters of genes perturbed upon miR-342-3p overexpression, one of which was upregulated and the other downregulated (Figure 16g). The enriched cluster comprised genes related to cell cycle arrest, but also to many immune-related functions such as pro-inflammatory cytokine response, leukocyte chemotaxis and migration, and lipid biosynthetic processes related with M1 polarization. On the other hand, the downregulated cluster contained genes related mainly to the response and production of immunosuppressive cytokines and to angiogenesis. Of note, miR-342-3p overexpressing KC1 were showing an increase in LPS-response genes and reduction in PGE_2-response genes, previously defined by gene signatures generated following *in vitro* stimulation of bone-marrow derived macrophages (BMDMs) (Cilenti *et al*, 2021).

3.4.3 In vivo overexpression of miR-342-3p in a CRC liver metastasis model confirms its activity in TME remodeling

Finally, we repeated miR-342-3p overexpression experiment in AKTPF liver metastasis model delaying LV injection to increase tumor engraftment and using a control group which may enable measuring more specific transcriptional effects (miR-342 mut LV). We injected intra-splenically 30.000 cells/mouse in 6 weeks old C57bl/6 female mice, and waited one week before LV intravenous injection of 3E+08 TU/mouse. We measured tumor growth by MRI 3 weeks after tumor injection, and then sacrificed animal 2 days later, at 23 days post tumor implant (Figure 17a).

Figure 17.

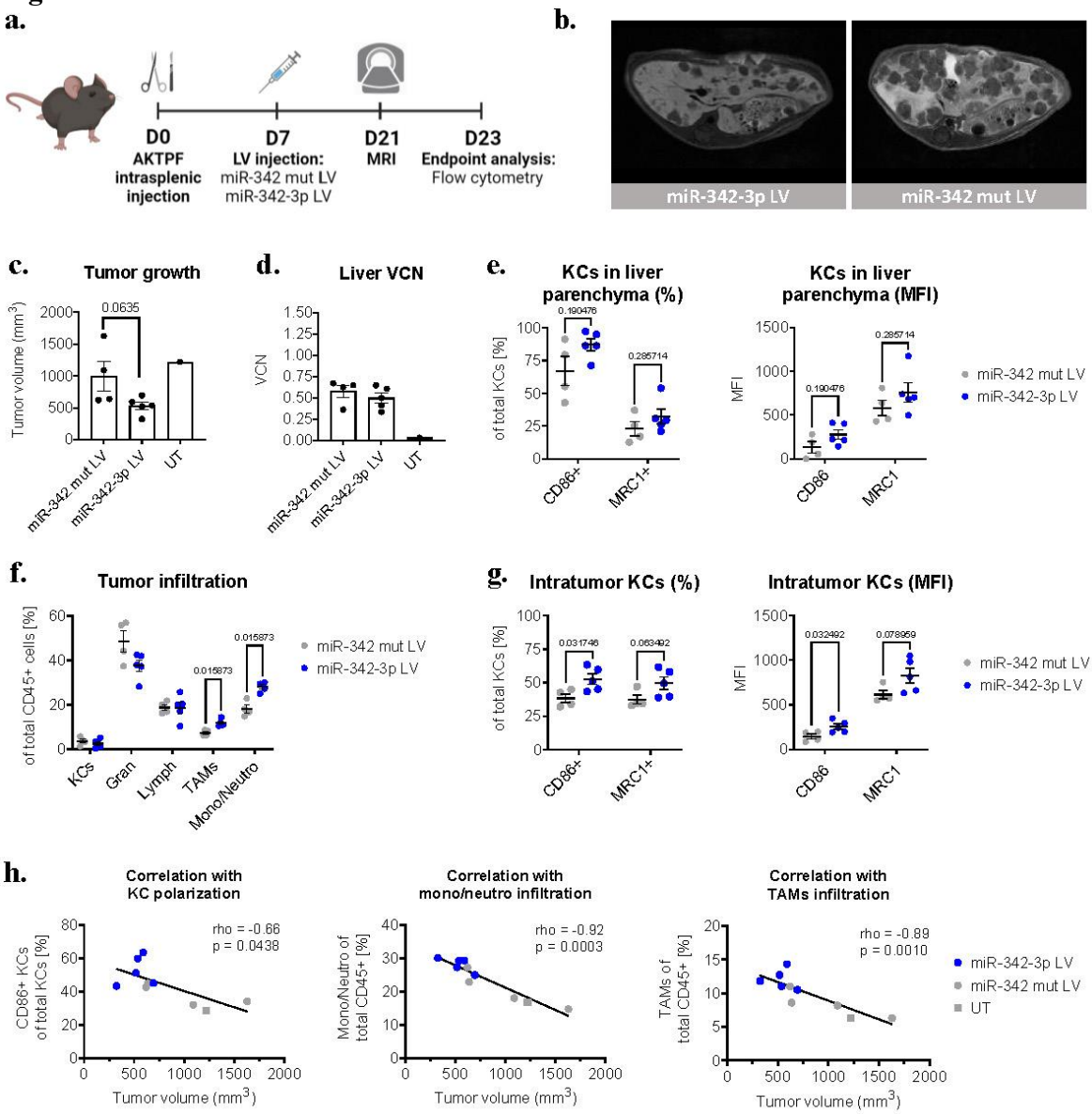


Figure 17 miR-342-3p enforced expression in AKTPF tumor model: late injection *(a) Experimental setting. AKTPF cells were implanted intra-splenically in mice. After 7 days mice were injected with 3E+08 TU/mouse with miRNA reporter LVs. Tumor growth was monitored by MRI 21 days after tumor injection. Mice were sacrificed 23 days after tumor implant. Liver and tumor were collected for flow cytometry. (b) Representative MRI images of mice injected with miR-342-3p or mut LV. (c) Tumor volume measured by MRI at day 21 post tumor implant. Statistics: Mann-Whitney test. (d) Lever of transduction of the liver measured by VCN analysis. (e) Polarization of KCs in the liver parenchyma by flow cytometry. Statistics: Mann-Whitney test. (f) Composition of the tumor infiltrate by flow cytometry. (g) Polarization of KCs infiltrating the tumor by flow cytometry. Statistics: Mann-Whitney test. (h) Correlation of tumor volume with CD86 expression in KCs (left) monocytes/neutrophils tumor infiltration (middle) or BMDM tumor infiltration (right). Statistics: Spearman's correlation.*

This time tumor volume was much more elevated than in the previous experiment, and in line with what we would expect for the normal progression of the model. Tumor growth was once again reduced in miR-342-3p LV group compared to controls, with an average tumor size that was about halved in treated mice compared to untransduced or miR-342 mut mice (Figure 17c). Thanks to the increased tumor burden we were able to collect both samples of healthy parenchyma and tumor tissue for DNA extraction and flow cytometric analysis.

Liver VCN analysis confirmed that mice in the two experimental groups were evenly transduced, once again excluding that detected differences were conducible to different vector doses (Figure 17d). Flow cytometric analysis revealed high levels of MRC1 expression in KCs in all conditions, and we detected a trend towards increased CD86 expression in miR-342-3p LV group that reached statistical significance in intratumor KCs (Figure 17e,g). Tumor infiltrate composition was also evaluated by flow cytometry, distinguishing between KCs (CD45+ F480+ Cd11b low), TAMs (CD45+ F480+ Cd11b high), granulocytes (CD45+ CD11b high Ly6G+), lymphocytes (CD45+ CD11b), and other myeloid cells, reasonably monocytes and neutrophils (CD45+ CD11b+ Ly6G- F4/80-). While lymphocytes and KCs infiltration were unvaried, we found a trend towards granulocytes decrease and a significant increase in TAMs and monocytes/neutrophils in miR-342-3p group compared to controls (Figure 17f). The percentage of CD86+ KCs, TAMs and monocytes/neutrophils infiltrating the tumors inversely correlated with tumor size in a significant manner, suggesting that monocytic compartment reprogramming could be implicated in the tumor growth delay observed in miR-342-3p group. As addressed in the Discussion section, a deeper transcriptional characterization may be required to identify the specific phenotypic characteristics of liver macrophages upon miR-342-3p enforced expression, as well as the impact on other LV-targeted populations.

4 Discussion

In recent years, *in vivo* gene therapy has gained increasing attention from the scientific community, as testified by the marketing authorization of several *in vivo* gene therapy products (Cantore *et al*, 2022). These approaches rely on the administration of gene delivery vectors directly to the patient, and thus require careful platform design to ensure safe and selective engineering of cells/tissues of interest (van Haasteren *et al*, 2018). This includes thorough biodistribution studies to identify and characterize targeted cell populations, in order to select appropriate regulatory elements that restrict transgene expression to the desired cell subset.

VSV-G pseudotyped lentiviral vectors (LVs) are preferentially employed in gene therapy thanks to VSV-G high infectivity and broad tropism, as well as their capacity to transduce proliferating and non-proliferating cells (Hastie et al, 2013; Gutierrez-Guerrero et al, 2020). Their biodistribution upon intravenous injection has been extensively studied in mice and non-human primates, identifying the liver as the most targeted organ, and within the liver, KCs, hepatocytes, and LSECs as the majorly transduced cell populations (Peng *et al*, 2001; Milani *et al*, 2019). In the same studies, spleen has been reported to be the second most transduced organ, however little is known about the splenic cell populations targeted by systemically delivered LVs.

In the first part of this work, we performed an in-depth characterization of cell populations transduced upon VSV-G LVs intravenous injection. We performed biodistribution studies systemically delivering PGK.GFP LVs and characterizing transduced populations by flow cytometry, confocal microscopy, and scRNA-seq. We were able to identify various splenic cell populations variably transduced by LVs, such as various subsets of splenic macrophages, dendritic cells, and B cells. Furthermore, we confirmed data regarding targeted hepatic cell populations. Interestingly, scRNA-seq analysis of transduced splenic cell populations revealed a significant enrichment in the myeloid lineage, while B and T cells were only marginally transduced. In fact, although VSV-G pseudotyped LVs have the potential to transduce nearly every cell type, most cell populations targeted upon *in vivo* administration were either phagocytic or strategically located within the vascular bed of filter organs. This suggests that both the nature of the cells and their localization contributes to the transduction bias observed

upon LVs intravenous injection, that could be overcome by employing different delivery routes, phagocytosis-shielded vectors or alternative pseudotyping.

Some of the LV-targeted cell populations observed in the spleen were not previously reported to be transduced upon systemic LV delivery and give us the chance to explore new therapeutic applications. Particularly interesting is the possibility to transduce B cells in the spleen, although at low percentages, since they could be exploited as cell factories for antibody therapy (Romani *et al*, 2017; Patel *et al*, 2020). For this purpose, one should select vectors with B cell-biased pseudotyping, and employ integration-deficient lentiviral vectors (IDLVs), which show comparable biodistribution to LVs, but allow transient transgene expression. Another cell population of interest is constituted by splenic dendritic cells, and in particular follicular dendritic cells (FDCs). These are non-hematopoietic DCs of stromal origin that have been implicated in germinal center formation and antigen presentation in both spleen and lymph nodes, and thus play a pivotal role in the development of humoral immunity (Heesters *et al*, 2014). For instance, one could envision applications in the field of (cancer) vaccination by triggering expression and presentation of antigens by this cell population. Conversely, current *ex vivo* gene therapy strategies targeting DCs could be reimagined as *in vivo* approaches aimed at the induction of systemic tolerance in the context of transplantation or immune diseases (Comi *et al*, 2020; Passeri *et al*, 2023; Fortunato *et al*, 2023).

We also performed an in-depth transcriptional analysis of some of the VSV-G LV-targeted cell populations, identifying differentially expressed genes by polyA-enriched and small RNA-seq. Our results highlight several genes whose promoters could be employed to drive preferential transgene expression in selected cell populations. We then validated some of the miRNAs identified in the DGE analysis by measuring their activity *in vivo* with miRNA reporter LVs (as described by Amendola et al, 2005), and identified several miRNAs which could abrogate transgene expression in specific LV-targeted cell populations. A partial disconnect between the results of small RNA-seq analysis and *in vivo* miRNA activity assay highlights the difficulty of defining *a priori* an actionable threshold of expression, which may vary for each miRNA and depend on the expression of its endogenous targets. Furthermore, the highly phagocytic nature of some of the cell populations of interest determines an additional confounding factor, since detected mRNAs may derive from phagocytosis of surrounding cells rather than gene transcription. This highlights the importance of validating

in vivo transcriptomic findings via other techniques, especially when working with phagocytic cell populations.

Taken together, these results constitute a helpful tool to design cell population-specific expression cassettes for virtually any LV-targeted cell population and for an array of *in vivo* gene therapy applications. For instance, the use of miRT-142-3p and previously described miRT-122-5p and miRT-126-3p (Annoni *et al*, 2009; Li *et al*, 2022) could restrict transgene expression solely to FDC for vaccination applications. Alternatively, a hematopoietic-specific promoter (e.g. *Ptprc*) combined with miRT-342-3p or miRT-223-3p could abrogate expression in non-hematopoietic and myeloid cells, while preserving it in B cells.

In the second part of this work, our focus shifted to the characterization of the function and regulation of a specific miRNA that emerged from our previous analysis: miR-342-3p. This miRNA is particularly active in myeloid cells, in accordance with its implication in both myeloid lineage commitment and in macrophage function (Herbst *et al*, 2021; Czimmerer *et al*, 2016; Solomon *et al*, 2017; Wang *et al*, 2019). Interestingly, a rich scientific literature describes miR-342-3p activity in a wide variety of cancers, in which it negatively regulates proliferation, migration, invasion, and even resistance to therapy (Lai *et al*, 2018; Romero-Cordoba *et al*, 2018; Xue *et al*, 2018; Xie *et al*, 2015; Wang *et al*, 2018; Tai *et al*, 2015; Chen *et al*, 2021; Liu *et al*, 2018; Li *et al*, 2014a, 2014b; Zhang *et al*, 2020; Zhao & Zhang, 2015; Wang *et al*, 2022; Yao *et al*, 2022; Huang & Chi, 2019; He *et al*, 2020). However, whether miR-342-3p antitumoral activity is limited to cancer cells or could also involve TAMs was yet to be investigated.

As previously discussed, KCs are efficiently and abundantly transduced upon LVs systemic delivery. Furthermore, they can contribute to antitumoral responses in early phases of liver carcinogenesis, but they are quickly reprogrammed towards TAM-like phenotypes upon cancer progression in both HCC and liver metastasis setting. Therefore, KCs constitute an ideal candidate for antitumoral *in vivo* gene therapy approaches, as well as a model to study the interactions between cancer cells and TAMs. We employed miRNA reporter LVs to measure miR-342-3p activity in a murine CRC liver metastasis model and found that miR-342-3p action was repressed in macrophages in close proximity and within the tumor masses in comparison to those in healthy liver parenchyma. Consistent with its antitumoral function, miR-342-3p is often found downregulated in many human malignances. We then speculated

that its downregulation in macrophages could be linked to the cancer cell-driven TAM reprogramming, thus suggesting its relevance in macrophage biology and a potential antitumoral function.

To better characterize miR-342-3p role in KCs, we modulated miR-342-3p levels in a *bona fide* model of murine KCs (KC1) by transduction with appropriate overexpression LVs or sponge LVs. The transcriptomic analysis of LV-transduced KC1 revealed a dramatic alteration of their transcriptomic profile upon miR-342-3p enforced expression. Apart from miR-342-3p predicted targets, whose average expression was downregulated compared to controls, several pathways were significantly altered in the test samples. For instance, several different gene sets related to cell cycle regulation and lipid metabolism were significantly enriched, as expected based on literature in cancer cells and macrophage progenitors. In fact, miR-342-3p has been described to inhibit the expression of E2F1, a transcription factor regulating cell cycle progression and lipid anabolism, hence this miRNA is able to indirectly regulate these processes (Tai *et al*, 2015; Lai *et al*, 2018; Solomon *et al*, 2017). This is particularly interesting given how lipid metabolism is tightly intertwined with macrophage polarization, being driven by common transcription factors, epigenetic signatures, and biochemical cues (Remmerie & Scott, 2018).

More surprisingly, miR-342-3p enforced expression also regulated several pathways related to immune function, and in particular response to and production of several chemokines and cytokines, among which TNFα, IL1, IL12, and IL10. Interestingly, miR-342-3p overexpressing KC1 showed an increase in LPS-response genes and reduction in PGE_2-response genes, as defined by gene sets previously generated upon BMDMs *in vitro* stimulation (Cilenti *et al*, 2021). As previously described, LPS is one of the main signals driving M1 polarization in macrophages, while PGE_2 has been linked to the development and sustenance of TAMs by cancer cells (Eisengart *et al*, 2000; Cilenti *et al*, 2021; Wei *et al*, 2022). Under these premises, miR-342-3p enforced expression should drive a pro-inflammatory phenotype in opposition to cancer-mediated KCs reprogramming. On the other hand, gene signatures associated to pattern recognition receptor activity were depleted in samples overexpressing miR-342-3p compared to controls, including receptors traditionally associated to M1 polarization like *Tlr4*. This apparent contradiction could be partially explained by non-canonical action of *Tlr4* in TAMs, or by negative feedback loops from LPS-response genes (Yao *et al*, 2018; Lv *et al*, 2017; Jiang *et al*, 2018).

Finally, the *in vitro* analysis revealed an underrepresentation of gene sets associated to angiogenesis in the samples overexpressing miR-342-3p compared to controls, which also included genes encoding for soluble molecules such as *Vegfa*. As previously described, TAMs can sustain tumor growth by promoting endothelial cell proliferation and vascularization of the neoplastic mass (Fu *et al*, 2020). Therefore, miR-342-3p overexpression in TAM-like KCs could once again impair their tumor-promoting activity. Furthermore, miR-342-3p has been reported to regulate angiogenesis acting on a number of other cell types, notably on cancer cells, fibroblasts or on endothelial cells themselves (Jiang *et al*, 2020; Cheng *et al*, 2018; Gao & Wang, 2021).

When tested in murine CRC liver metastasis models, miR-342-3p overexpression was well tolerated, and proved effective in reducing the tumor burden for multifocal, slowly proliferating tumor models (AKTPF cells), but not for more aggressive tumors forming a single hepatic mass (MC38). The presence of multifocal lesions in opposition to a single bulky mass allows for better tumor infiltration and a broader tumor-parenchyma interface in relation to tumor volume, therefore constituting a more suitable setting to test engineered KCs interaction with cancer cells. It's also important to notice that AKTPF tumor model more closely resembles the human disease compared to MC38 tumor model, since it better recapitulates its mutations, pathogenesis and histological characteristics. Therefore, we can speculate that the antitumoral effect observed in AKTPF tumor model more accurately predicts the therapeutic potential of TME reprogramming induced by miR-342-3p.

In accordance with *in vitro* findings, KCs showed an increase in M1 polarization markers expression and antigen presentation in all *in vivo* CRCLM murine models. Such skewing towards pro-inflammatory phenotypes was not limited to transduced cells, but interested the entirety of KCs, suggesting a TME reprogramming sustained at least in part by soluble factors. This is once again backed up by previous findings regarding miR-342-3p ability to increase pro-inflammatory cytokine production, and decrease that of immune-suppressive cytokines. As already mentioned, the *in vitro* analysis also highlighted an enrichment of genes regulating lymphocyte chemotaxis, which is in accordance with the increased levels of tumor-infiltrating TAMs and monocytes/neutrophils observed following *in vivo* miR-342-3p overexpression. Both KCs polarization and tumor infiltration correlated inversely with tumor burden and could potentially provide a mechanism underlying miR-342-3p antitumoral effect.

Taken together, these findings suggest how miR-342-3p overexpression could revert cancer-dependent KCs reprogramming towards TAM-like phenotype, which is normally associated to M2 polarization, and even reshape the TME altering the cytokine milieu toward a pro-inflammatory state, enhancing leukocyte infiltration and inhibiting angiogenesis. Despite a general understanding of the biological processes driving miR-342-3p antitumoral activity, the molecular players behind its functions remain elusive. We were able to identify some direct targets of miR-342-3p involved in TAMs function, notably *Slc7a11*, and *Clec7a* (Ishii *et al*, 2022; Tang *et al*, 2023a; Daley *et al*, 2017; Tang *et al*, 2023b), and for some of them we could even confirm a consistent downregulation in successive biological replicates. Nevertheless, the extent of gene expression deregulation observed upon miR-342-3p enforced expression in KC1 is hardly attributable to the action of these genes and would be more consistent with that of a transcription factor or another master regulator of gene expression.

The primary source of data for miRNA target analysis was TargetScan, a publicly available prediction tool that compiles lists of potential target genes based on number, location and characteristics of miRNA binding sites. TargetScan has the advantage of reporting, for each target gene, indexes of "quality" that account for binding stability and availability of the detected miRNA target sites. Furthermore, it contains both experimentally validated and bioinformatically predicted targets, allowing for target discovery. However, TargetScans only accounts for targets undergoing canonical miRNA regulation, that is to say containing miRNA target sites at the 3'UTR of the mRNA that can promote its destabilization and degradation. We tried to partially correct for this bias by including experimentally validated targets of miR-342-3p from miRTarBase database. Nevertheless, it's possible that we are overlooking novel targets whose deregulation is not reflected at RNA level, for instance mRNA whose translation is inhibited by miR-342-3p action, or targets for which the miR-342-3p action is exerted at transcriptional level, for which the miRNA binding sites would either be located in regulatory genomic regions or in the 5' UTR. Further proteomic and transcriptomic analysis *in vivo* may be required to address these issues and validate the findings of our *in vitro* analysis.

Another limitation of our approach overexpressing miR-342-3p is constituted by the intrinsic characteristics of the LV employed. Even if KCs constitute the main targets of systemically delivered LVs, and SFFV promoter is preferentially active in myeloid versus lymphoid cells (Zonari et al, 2013), the expression cassette employed in our experiments is not inherently KCs-specific, and thus miR-342-3p overexpression could be enforced in other

cell populations. This poses different kinds of challenges to our approach. Firstly, we cannot exclude the contribution of other transduced cell types to miR-342-3p antitumoral effect. This could be addressed by scRNA-seq or other transcriptomic analysis performed on targeted cell populations *in vivo* to better characterize the impact of miR-342-3p overexpression on each of them. Furthermore, the lack of spatial and temporal regulation of miR-342-3p overexpression cassette might make it, at least in part, unsuitable for clinical translation. Up to date, we are not employing LV platforms that allow selective expression of miRNAs from KCs upon systemic delivery. In fact, LV design for miRNAs overexpression poses some specific challenges, among which the necessity to employ extremely efficient promoters to reach actionable levels of expression and the impossibility to rely on miRT post-transcriptional regulation. However, we could leverage the findings on differentially active transcriptional networks in LV-targeted cell populations to select a KC-specific promoter among both protein coding or small-RNA genes.

In this context, identifying miR-342-3p targets isn't only crucial to deepen our understanding of the molecular mechanisms behind its antitumoral function, but would also provide some druggable genes that could be employed for translational therapeutics approaches. While we currently lack cell population-specific miRNA overexpression LVs, we have previously designed a transgene expression cassette that is able to drive selective expression of protein-coding genes in KCs in the proximity of liver metastases border (Kerzel *et al*, 2023). This platform is based on the use of *Mrc1* promoter, which is particularly active in M2-polarized macrophages and LSECs, and of miRT-122-5p and miRT-126-3p, which abrogate residual expression in hepatocytes and LSECs. As already mentioned, miRT sequences can't be employed to abrogate off-target expression from LSECs, and *Mrc1* promoter alone is neither specific nor strong enough to drive selective miRNA expression in KCs. However, this platform could be employed to express either one of the immune-modulating molecules positively regulated by miR-342-3p, or a genetic/epigenetic editor to disrupt the expression of key miR-342-3p targets.

Collectively, our work represents a rich source of information for the development of novel LV-based *in vivo* gene therapy strategies, deepening the understanding of active gene-networks in several hepatic and splenic cell populations. Furthermore, our work provides some insights on miR-342-3p activity in macrophages in the setting of cancer, opening the

field for further research into its antitumoral activity and the possibility to leverage its targets for therapeutic purposes.

5 Materials and methods

5.1 Molecular biology

5.1.1 Plasmid design cloning and amplification

The PGK.GFP LV transfer vector as well as the No miRT LV, miRT-142-3p LV, and miRT-223-3p LV transfer vector plasmids were already present in the lab (Amendola *et al*, 2005; Genovese *et al*, 2014). To generate the miRT-92-3p LV, miRT-93-5p LV, miRT-125-5p LV, miRT-191-3p LV, and miRT-342-3p LV we cloned four copies of the indicated miRT sequences separated by randomized linker sequences downstream WPRE sequence in No miRT LV.

The SFFV.EF1a intron.mOrange LV (Intron LV) transfer vector plasmid was already available in the lab, as well as those for miR-155-5p LV and miR-511-3p LV (Squadrito et al, 2012; Zonari et al, 2013). To generate miR-342-3p LV, the genomic region corresponding to *Mir342* was amplified from murine DNA by PCR with primers reported in Table 1 using Phusion High-Fidelity DNA Polymerase (Thermo Scientific/ F-530XL). The PCR product was purified with NucleoSpin Gel and PCR Clean-up kit (Macherey-Nagel/740609.50) and processed by enzymatic digestion with enzymes MluI and PmeI, and cloned inside of EF1a intron in the Intron LV.

The SFFV.mOrange LV was already available in the lab, and it was used as template for the generation of all sponge LVs, that were cloned downstream of WPRE sequence.

Ligation products for all constructs were transformed in bacteria by adding about 100 ng of ligation product to 50 µL of competent bacteria (Top10 cells/Invitrogen). The retransformation mix was carefully mixed, incubated for 30 minutes on ice, transferred to 42°C for 30 seconds followed by two additional minutes incubation on ice. 500 µL of Luria-Bertani (LB) medium was add and incubated for 30min at 37 °C. Bacteria were plated onto LB agar plates containing 100 µg/mL ampicillin and incubated over night at 37°C. Afterwards, single colonies were picked and transferred into 3mL LB medium containing 100 µg/mL of ampicillin and incubated overnight at 37°C shaking at 150 rpm. DNA was extracted from 2mL of the bacteria culture using the Wizard Plus SV Minipreps DNA Purification System kit (Promega/A1330). Plasmids derived from different clones were screened by analytical digest as well as Sanger sequencing to confirm plasmid sequence. To further amplify the plasmids,

the remaining 1 mL of the bacteria liquid culture from clones containing plasmids with the correct sequence were used to inoculate 500 mL of LB medium containing 100 µg/mL of carbenicillin which were subsequently left to grow overnight at 37°C shaking at 150 rpm. DNA extraction was performed using Nucleobond Xtra Maxi EF (Macherey-Nagel/740424.50) and the final plasmid resuspended in endotoxin-free TE.

5.1.2 Vector copy number determination

Genomic DNA was extracted from cell culture samples using the Maxwell RSC 48 Intrument (Promega/AS8500) with Maxwell RSC Cultured Cells DNA Kit (Promega/AS1620). Genomic DNA from whole tissue samples was extracted by using the DNeasy Blood and Tissue Kit (Qiagen/69504) according to manufacturer's instruction. LV copy number was determined using a QX200 Droplet Digital PCR System (Biorad) apparatus, and the digital droplet PCR was performed according to manufacturer's instructions.

Briefly, for each sample a reaction was prepared containing ddPCR Supermix for Probes (No dUTP) (Biorad/1863024), 10-50 ng of genomic DNA, primers at a final concentration of 900 nM, and the detection probes at 250 nM. Primers and probes for the detection of HIV genomes and Sema3a gene, employed as normalizer for murine samples, are reported in Table 1. As normalizer for human samples, a commercially available GAPDH expression assay was used (Invitrogen/Hs00894322_cn).

After droplet generation, the plate was sealed and amplified in a thermal cycler with the following protocol:

95°C	10 min	1x
94°C	30 sec	40x
60°C	1 min	
98°C	10 min	1x
4°C	∞	1x

Amplified droplets were acquired using the BioRad QX200 Droplet Reader and analysed by using the QuantaSoft software (Biorad). LV copies per genome were calculated by the formula: LV copies per genome = concentration HIV/concentration Normalizer *2

Primer/probe name	Sequence (5' to 3')
miR342 cloning Fw	AAAAAACGCGTTGCAAACATACCCCTCGCTT
miR342 cloning Rev	AAAAAAGTTTAAACCACACATCACGGCCACATTC
HIV primer Fw	TACTGACGCTCTCGACC
HIV primer Rev	TCTCGACGCAGGACTCG
HIV probe (FAM)	ATCTCTCTCCTTCTAGCCTC
Sema3a primer Fw	ACCGATTCCAGATGATTGGC
Sema3a primer Rev	TCCATATTAATGCAGTGCTTG
Sema3a probe (HEX)	AGAGGCCTGTCCTGCAGCTCATGG

Table 1. List of non-commercial primers and probes employed

Target	TaqMan assay ID
hsa-let-7a	000377
mmu-miR-155	002571
mmu-miR-511-3p	463069_mat
hsa-miR-342-3p	002260
Hprt	Mm03024075_m1
Clec7a	Mm01183349_m1
Itga6	Mm00434375_m1
Slc7a11	Mm00442530_m1
Fam126b	Mm00552956_m1
Ankrd52	Mm00555581_m1

Table 2. List of commercial TaqMan assays employed

5.1.3 Gene expression assays

For gene expression analysis, RNA was extracted from pelleted cell using the miRNeasy Micro Kit (Qiagen/217084).

For miRNAs, retrotranscription was performed according to manufacturer's instruction using TaqMan MicroRNA Reverse Transcription kit (Thermo Scientific/4366596) with specific TaqMan MicroRNA Assay, listed in Table 2. 1-100 ng of cDNA were used as input for the gene expression analysis.

For protein coding genes, retrotranscription was performed according to manufacturer's instruction using the SuperScript IV VILO (Invitrogen/11756050). 0,25-2,5 ng of cDNA were used as input for the gene expression analysis. TaqMan Gene Expression Assays from Invitrogen are listed in Table 2.

Data acquisition using ddPCR and analysis were performed as described in section 5.1.2.

5.2 Cell culture

5.2.1 HEK293T and MC38 cells

Human embryonic kidney 293T (HEK293T) cells were employed to produce and titer LVs, they were purchased from ATCC and their authenticity is supported by their capability to produce high titer LV stocks. MC38 cells were used to mimic CRC liver metastasis upon liver implantation, they were obtained from Amgen.

Both cells lines were cultured in adherence at 37°C in IMDM medium (Corning/10-016-CV) supplemented with 10% fetal bovine serum (FBS; HyClone/SH30066.03), 100 IU/mL penicillin, and 100 µg/mL streptomycin. Cells were split three times a week 1:5-1:10 by removing culture medium, washing cells with Phosphate Buffered Saline (PBS; Corning/21-031-CVR), and detaching them with a solution of 0.05% trypsin and EDTA (4mM) in PBS (ATV). Cells were then resuspended in fresh medium and transferred into a new plate.

5.2.2 AKTPF cells

AKTPF cells were employed to mimic CRC liver metastasis upon intrasplenic implantation. They were obtained from the laboratory of Masanobu Oshima.

Cells were cultured in adherence at 37°C in Advanced Dulbecco's Modified Eagle Medium (DMEM)/F12 medium (Gibco/12634-010) supplemented with 10% fetal bovine serum (FBS; HyClone/SH30066.03), 2% GlutaMAX supplement (Thermo Scientific/35050061), 100 IU/mL penicillin, and 100 µg/mL streptomycin. Cells were split three times a week 1:8-1:10 by removing culture medium, washing cells with Phosphate Buffered Saline (PBS; Corning/21-031-CVR), and detaching them with a solution of 0.05% trypsin and EDTA (4mM) in PBS (ATV). Trypsin solution was inactivated by adding fresh medium, cells were pelleted 5min 200g 4°C and resuspended in fresh medium before being transferred into a new plate.

5.2.3 Hepa-CSF100 cells and conditioned media production

Hepa 1-6 cells are available and routinely used in our institute. Hepa-CSF100 were obtained engineering Hepa 1-6 cells by transducing 50.000 cells/well in a MW6 plate with 500 µL media/well and hPGK.hCSF1 LV at MOI 100. The cell line thus produced was subsequently termed Hepa-SCF100, and used it to produce CSF containing cultured media for KC1 culture.

Hepa-CSF100 cells were cultured in adherence at 37°C in RPMI medium with L-Glutamine (Corning/10-040-CV) supplemented with 10% fetal bovine serum (FBS; HyClone/SH30066.03), 100 IU/mL penicillin, and 100 µg/mL streptomycin. Cells were split three times a week removing culture medium, washing cells with Phosphate Buffered Saline (PBS; Corning/21-031-CVR), and detaching them with a solution of 0.05% trypsin and EDTA (4mM) in PBS (ATV). Cells were then resuspended in fresh medium, counted, and seeded 5mln cells/plate into a 150mm dish with a total volume of 20ml of fresh medium.

After 48-72h, conditioned media was harvested and filtered with 0,20 µm pore size, then aliquoted and stored at -20°C until use.

5.2.4 Immortalized KCs (KC1 cells)

Our *bona fide in vitro* model of murine KCs was obtained by systemic injection of 5 weeks old female C57bl/6 mice with a 1,75E8 TU/mouse of LV enforcing the expression of SV40 Large T antigen under PGK promoter. Mice were sacrificed 7 days after LV injection, and liver was collected, smashed, and filtered through a 40 µm pore filter. Single cell suspension was pelleted at 30g for 5 min at room temperature to remove hepatocytes. Supernatant was collected and pelleted again at 300g for 5min at room temperature. Pellet was finally resuspended in RPMI medium with L-Glutamine (Corning/10-040-CV) supplemented with 10% fetal bovine serum (FBS; HyClone/SH30066.03), and 100ng/mL of mCSF (Peprotech/3015-02),

and kept in culture refreshing the media 3 times per week until non-immortalized cell were completely depleted. The cells thus obtained were termed KC1, and were used for subsequent *in vitro* experiments as a model of murine KCs.

For maintenance, cells were cultured in adherence at 37°C in RPMI medium with L-Glutamine (Corning/10-040-CV) supplemented with 10% fetal bovine serum (FBS; HyClone/SH30066.03), 100 IU/mL penicillin,100 µg/mL streptomycin, and 20% of Hepa-CSF100 conditioned media (see section 5.2.3). Cells were split twice a week 1:3-1:4 by removing culture medium, washing cells twice with Phosphate Buffered Saline (PBS; Corning/21-031-CVR), and detaching them with a solution of Trypsin-EDTA (0.25%) and phenol red in PBS (Gibco/25200056). Trypsin solution was inactivated by adding fresh RPMI 10%FBS 1% P/S, cells were pelleted 5min 300g 4°C and resuspended in fresh medium before being transferred into a new plate.

For experiments, cells were cultured as described above, but seeded 50.000 cells/well in a MW24 and final volume 0,5 mL/well, or 500.000 cells/plate in a 35mm dish in a final volume of 2,5 mL/dish. After cells adhered to the bottom of the plate (1-2h) culture medium was replaced with fresh medium containing the TU necessary for desired MOI.

5.2.5 LV production and titration

In this study, third generation VSV-G pseudotyped LVs were used. LV stocks were produced in laboratory scale as described previously in Soldi et al, 2020. The titer of the LV stocks was measured in HEK 293T cell-transducing units (TU/mL), as also described in Soldi et al, 2020.

5.3 Mouse procedures

In this study, we employed female C57Bl/6N mice purchased from Charles River Laboratory. All experiments and procedures were performed according to protocols approved by the Institutional Animal Care and Use Committee (IACUC) at San Raffaele Hospital animal facilities (IACUC number: 1098, 1108) and authorized by the Italian Ministry of Health and local authorities according to the Italian law. Mice were used between 5 and 10 weeks of age and were maintained in Specific Pathogen-free (SPF) animal research facilities with a 12h/12h dark/light cycle and standardized temperature (22 +/- 2C) and humidity (55 +/- 5%).

5.3.1 Intravenous injection

For systemic LV injection, LVs were diluted in PBS to obtain the desired TU to be injected per mouse in a volume ranging from 200 to 300 µL. Mice were warmed under an infrared/red-light lamp and the LVs were intravenously injected via the tail vein. All vectors were used between 1-1.5*10^{10} TU/kg. In all experiments untransduced (UT) mice were injected with a volume of PBS ranging from 200 to 300 µL.

5.3.2 MC38 tumor implant

We delivered MC38 cells by intrahepatic injection.

Briefly, mice were shaved and, immediately prior to surgery, they were injected with 50 µL carprofen (2.5 mg/mL) for pain management. Isoflurane (Iso-Vet/ 104331020) at a concentration of 3 % in flow of oxygen at 1.5 L/min was used to anesthetize the mice during surgery. 100,000 MC38 cells/mouse were injected in 5 µL/mouse of PBS with an Hamilton syringe, preferentially in the left liver lobe. Following surgery, mice were subjected to antibiotic treatment for one week by adding Baytril (Bayer) at a concentration of 0.5 mg/mL to the drinking water. Liver metastasis growth was measured by tumor weight (i.e. by dissecting the liver metastasis upon experiment termination and measuring its weight in a 10 mg precision digital bench scale).

5.3.3 AKTPF tumor implant

We delivered AKTPF cells by intrasplenic injection.

Briefly, mice were shaves and, immediately prior to surgery, they were injected with 50 µL carprofen (2.5 mg/mL) for pain management. During surgery, mice were anesthetized as in section 5.3.2. 30.000 AKTPF cells/mouse were resuspended in 50 µL/mouse Geltrex (Lige Tehnologies/A1413301) and carefully injected into the spleen using a precooled 0,5 ml syringe with 28 G needle. The peritoneum wall was sutured by using adsorbable stitches while the skin was closed by applying stainless steel wound clips. Following surgery, mice were subjected to antibiotic treatment as in section 5.3.2. Liver metastasis growth was measured by using magnetic resonance imaging (MRI), as described section 5.3.5.

5.3.4 Blood collection and analysis

Blood was withdrawn either from the retroorbital vein plexus and collected in Microvette with EDTA (Sarstedt/NC9990563). Hemocytometer analysis was performed on whole blood by using the ProCyte DXTM (IDEXX). For the collection of plasma, blood was centrifuged at 850g for 10 minutes at room temperature and precipitated red and white blood cells were discarded.

5.3.5 MRI analysis

A 7-Tesla preclinical scanner (Bruker, BioSpec 70/30 USR, Paravision 6.0.1), equipped with 450/675 mT/m gradients (slew-rate: 3400- 4500T/m/s; rise-time 140 ms) and a circular polarized mouse body volume coil with an inner diameter of 40 mm was used. During acquisition, mice were kept in anesthesia by inhaling isoflurane (Iso-Vet/ 104331020) at a concentration of 3 % in flow of oxygen at 1.5 L/min under a dedicated temperature control apparatus to prevent hypothermia. The breathing rate and the body temperature were continuously monitored (SA Instruments, Inc., Stony Brook, NY, USA). To aid liver lesion visualization, we used a hepatocyte-specific contrast agent, the Gd-EOB-DTPA (Primovist, Bayer Schering Pharma), at 0.05 mmol/g of body weight. Axial fat-saturated T2-weighted images (RARE-T2, Rapid Acquisition with Relaxation Enhancement, TR = 3000 ms, TE = 40 ms, voxel-size = 0.125 3 0.100 3 0.8 mm, averages = 4,) and axial fat-saturated T1-weighted sequences (RARE-T1: TR = 540 ms, TE = 7.2 ms, voxel size = 0.125 3 0.100 3 0.8 mm, averages = 4) were acquired during the hepatobiliary phase of Gd- EOB-DTPA enhancement (10 minutes after administration). Volume measurement was performed by using the Medical Image Processing, Analysis, and Visualization (MIPAV) software.

5.3.6 Sacrifice and necropsy

For endpoint analysis, mice were euthanized by cervical dislocation. The liver was perfused by injecting 10 mL of PBS containing 5 mM of UltraPure EDTA pH8 (Invitrogen/ 15575020) through the inferior vena cava and cutting the portal vein to allow exiting of the solution containing most circulating blood cells from the liver. In case flow cytometry (FC) but not immunofluorescence (IF) analysis was performed, 10 mL of IMDM (Corning) containing 0.35 mg/mL collagenase (Sigma-Aldrich) was injected through the inferior vena cava. All organs

were collected and immediately stored on ice (for FC and IF) or dry ice (for DNA/RNA extraction).

5.4 Flow cytometry (FC)

5.4.1 Sample preparation

For FC analysis of *in vivo* samples, organs were smashed into small pieces and then incubated 15min at 37°C in agitation with a tissue digestion solution composed of 1 mL IMDM (Corning) supplemented with 0.35 mg/mL collagenase type IV (Sigma-Aldrich/ SCR103), 1 mg/ml dispase II (Gibco/ 17105041) and 0.2 mg/ml DNAse (Roche/ 11284932001). The tissue was then further dissociated by pipetting and filtered using 40 µm cell strainers (Corning/ 352340). Single cell solution was washed with 30 mL of autoMACS Running Buffer (Miltenyi Biotec/130-091-221) and pelleted for 5min 300g 4°C to remove excess enzymes. Samples were transferred to FACS tubes and stained as described in section 5.4.2.

For FC analysis of in vitro samples, cells were collected as described in relative section of chapter 5.2, moved to FACS tubes and washed with 3-5 mL of autoMACS Running Buffer (Miltenyi Biotec/130-091-221) pelleting for 5min 300g 4°C to remove excess culture medium. Samples were stained with live/dead staining as described in section 5.4.2.

5.4.2 Sample staining

Upon single cell suspension preparation (see section 5.4.1), we added Fc Block (BD Pharmagen/ 553142) to the cells to prevent unspecific staining through binding of the FC receptor. For membrane bound antigens, samples were stained for 15 minutes on ice with antibodies and concentrations reported in table 3. After staining, cells were washed with 5 mL of autoMACS Running Buffer (Miltenyi Biotec/130-091-221) and resuspended in 100-500 µL of live/dead staining. Viability of cells was assessed by using either 7AAD (BioLegend/420404) or Dapi (BioLegend/422801) nuclear staining diluted in autoMACS Running Buffer (Miltenyi Biotec/130-091-221) respectively 1:50 or at a final concentration of 1 µg/mL. Samples were acquired by using either a BD CytoflexS or a FACSymphony A5 Cell Analyzer (BD Biosciences). For fluorescence activated cell sorting a BD FACSAria Fusion was used.

Target	Clone	Conjugation	Producer	Working dilution
CD11b	M1/70	Pacific Blue	BioLegend	1/200
CD11b	M1/70	BV710	BioLegend	1/100
CD11c	N418	BV785	Biolegend	1/100
CD11c	N418	PE-Cy7	BioLegend	1/200
CD206 (MRC1)	C068C2	BV711	BioLegend	1/100
CD279 (PD1)	29F.1A12	PE-Cy7	BioLegend	1/100
CD31	MEC13.3	PE	BD Pharmigen	1/100
CD4	RM4-5	BUV737	BD Horizon	1/100
CD44	IM7	BV605	BD Horizon	1/100
CD45	30-F11	BV510	BioLegend	1/200
CD45R (B220)	RA3-6B2	APC/Cy7	BioLegend	1/200
CD62L	MEL-14	BV786	eBioscience	1/100
CD8	53-6.7	PE/Cy7	Biolegend	1/100
CD8	53-6.7	BV711	BioLegend	1/100
CD8	53-6.7	FITC	BD Pharmagen	1/200
CD86	GL-1	APC-Cy7	BioLegend	1/100
F4/80	BM8	FITC	BioLegend	1/100
F4/80	BM8	PE	BioLegend	1/100
F4/80	BM8	APC/Cy7	BioLegend	1/100
Ly6c	HK1.4	eFluor450	eBioscience	1/100
LY6G	1A8	BV605	Biosciences	1/100
Ly6G	1A8	BUV737	Biosciences	1/100
MHCII	M5/114.15.2	BV786	BioLegend	1/100
MRC1	C068C2	AF647	BioLegend	1/100
TIM3	B.2C12	APC	eBioscience	1/100
TotalSeq™-B0301 anti-mouse Hashtag 1 Antibody	M1/42 ; 30-F11	ACCCACCAGTAAGAC	BioLegend	1/100
TotalSeq™-B0302 anti-mouse Hashtag 1 Antibody	M1/42 ; 30-F11	GGTCGAGAGCATTCA	BioLegend	1/100
TotalSeq™-B0303 anti-mouse Hashtag 1 Antibody	M1/42 ; 30-F11	CTTGCCGCATGTCAT	BioLegend	1/100

Table 3. List of antibodies employed for FC

5.5 Immunofluoresce (IF)

5.5.1 Sample preparation

For IF, tissues collected during necropsy were immediately incubated in a paraformaldehyde solution 4 % in PBS (ChemCruz/ 30525-89-4) at 4°C for 4-12 hours according to tissue size. Afterwards, the PFA was replaced with a solution of 10% sucrose (Sigma-Aldrich) and 0.02% NaN3 in H_2O. After 8-15 h incubation at 4°C, sucrose solution was increased to 20%, and to 30% after additional 8-15 h. The organ was then embedded into Killik, O.C.T. Compound embedding medium for cryostat (Bio-Optica/ 05-9801). Sections of 20 nm thickness were prepared and placed on glass slides (Epredia/916155) using a cryostat. And stored at -20°C

5.5.2 Sample staining

Before staining, sections were air dried for 5 minutes at room temperature. For antigen retrieval, slides were incubated for 10 minutes at 95°C in a preheated water bath in the following solutions: (1) low pH antigen retrieval: 10 mM citric acid in H2O, pH adjusted to pH 6; (2) high pH antigen retrieval: 10 mM Tris base and 1mM EDTA plus 0.05 % tween in H2O, pH adjusted to pH 9. Slides were then cooled down for 15 minutes at room temperature and then washed with PBS 0.1% Triton X-100 (Sigma/9036-19-5) 5 min x 3 times. Blocking was performed using a blocking buffer composed of 5 % normal donkey serum, 1 % BSA (Sigma-Aldrich/A3912) and 0.1% Triton X-100 (Sigma/9036-19-5) in PBS. After 1h of blocking at RT, the blocking buffer was replaced by blocking buffer containing primary antibodies at indicated concentrations (see Table 4) and incubated overnight at 4°C. Sections were then washed with washing buffer (PBS containing 0.1 % TritonT X-100) for 5 min x 3 times. Sections were stained with the secondary antibodies in blocking buffer at the indicated concentrations (see Table 4). An incubation for 1h at room temperature in the dark was performed followed by 3x 5min washing steps with washing buffer. For staining of the nuclei, sections were covered with a 1/2000 dilution of Hoechst 33342 solution (Thermo Scientific/62249) in PBS for 2 min. Slides were washed additional 3 times per 5 min each with washing solution and mounted using Fluoromount-G (SouthernBiotech/0100-01). Images were acquired using an SP8 lightning confocal microscope (Leica Microsystems).

Table 4. List of antibodies employed for IF

Target	Conj	Host	Reactivity	Supplier	Cat number	Dilution
aChicken-AF488	AF488	Donkey	Chicken	Jackson Immuno Research	703-545-155	1/400
aChicken-AF568	AF568	Donkey	aChicken	Invitrogen	A78950	1/500
aRabbit-AF546	AF546	Goat	aRabbit	Invitrogen	A11010	1/500
aRabbit-AF647	AF647	Donkey	Rabbit	Invitrogen	A31573	1/500
aRat-AF488	AF6488	Goat	Rat	Invitrogen	A11006	1/500
aRat-AF555	AF555	Donkey	Rat	Abcam	ab150154	1/500
aRat-AF647	AF647	Goat	Rat	Invitrogen	A21247	1/500
CD11c	-	Rabbit	Mouse	Cell Signaling	97585S	1/200 (Ag retr pH9 or 6)
CD169	PE/Cy7	Rat	Mouse	BioLegend	142412	1/160
CD19	-	Rabbit	Mouse	Abcam	ab245235	1/100 (Ag retr pH9)
CD31	-	Rabbit	Mouse, Human, Pig	Invitrogen	PA5-16301	1/50 (Ag retr pH6)
F4/80	-	Rat	Mouse	Abcam	ab6640	1/200
GFP	-	Rat	-	BioLegend	338002	1/100
GFP	-	Chicken	-	Abcam	ab13970	1/500
MadCAM-1	-	Rat	Mouse	BioLegend	120702	1/200
MARCO	AF647	Rabbit	Mouse	R&D Systems	FAB29561R	1/200
mCherry	-	Rabbit	-	Abcam	ab167453	1/200
mCherry	-	Chicken	-	Abcam	ab205402	1/1000

5.6 Transcriptomic analysis

5.6.1 Bulk poly-A enriched RNA-seq

RNA was extracted from pelleted cells using the miRNeasy Micro Kit (Qiagen/217084). 10 ng of total RNA was employed as template for library preparation. Poly-A enriched RNAseq library preparation was performed using QIAseq UPX 3’ Transcriptome Kits (QIAgen/333088) according to manufacturer’s instructions.

We sequenced 10-20 mln 150 bp paired-end reads per sample in a NovaSeq 6000 Illumina apparatus. Base call files obtained from the Illumina sequencing were converted into FASTQ files and processed with QIAseq Ultraplex RNA Read Analysis (QIAgen) software using default setting. Resulting data was imported into R, and differential gene expression analysis performed with packages edgeR based on CPM UMI count. Following GSEA analysis was performed on R using both packages fgsea and enrichplot.

5.6.2 Bulk small RNA-seq

RNA was extracted from pelleted cells using the miRNeasy Micro Kit (Qiagen/217084). 100 ng of total RNA was employed as template for library preparation. small RNAseq library preparation was performed using QIAseq miRNA Library Kit (QIAgen/331502) according to manufacturer's instructions.

We sequenced 30 mln 75 bp single-end reads per sample in a NovaSeq 6000 Illumina apparatus. Base call files obtained as result from the Illumina sequencing were converted into FASTQ files and processed with online tool available at geneglobe.qiagen.com/analyze. Resulting data was imported into R, and secondary analysis was performed considering level of expressiom, FC between populations and miRNA family, as described in section 3.1.3.

5.6.3 Single cell RNA-seq

Immediately after sacrificing the mouse, spleens were collected and dissociated into single cells as described in section 5.4.1. Single cells were stained with anti-CD3, anti-B220 and Hashtag antibodies as described in section 5.4.2, then resuspended in MACS buffer containing Dapi. GFP+ cells, and CD3+, B220+ or double pos/neg cells were sorted with gating strategy displayed in Figure 7a.

Sorted cells were further processed for scRNA sequencing. ScRNA sequencing was performed using the Next GEM Single Cell 3' GEM Kit v3.1 from Chromium 10X according to manufacturer's recommendation (User Guide Chromium Next GEM Single Cell 3′ Reagent Kits v3.1). We loaded 24,000 cells belonging to the same sample per reaction. We sequenced 3 samples, 150 bp paired-end reads in a NovaSeq 6000 Illumina apparatus, $8*10^8$ reads total. Base call files obtained as result from the Illumina sequencing were converted into FASTQ files and processed with the Cell Ranger Single-Cell Software Suite (10X Chromium v3.1.0) using default setting.

Resulting data was imported into R and processed with the Seurat package (http://satijalab.org/seurat v4.0.3). All samples were merged into a single Seurat dataset and processed to remove cells with a low sequencing quality, those with a feature count below 1,000 and above 6,000, as well as cells with a fraction of mitochondrial genes higher than 10 %. Afterwards, we employed package DoubletFinder (v3) to annotate doublets of cells, which were excluded from the following analysis. RNA UMI-counts were normalized using a global-scaling normalization method and the Variance Stabilizing Transformations (SCTransform) was performed to scale based on the percentage of mitochondrial genes, the absolute count of RNAs in each cell, and the difference between S and G2/M cell cycle scores computed for each cell. A principal component analysis with 30 principal components (PCs) was performed for dimensional reduction, and a UMAP-representation as well as clusters (with a resolution of 1) were computed on those reductions. Marker genes for each cluster were obtained using the FindAllMarkers Seurat function, and consequently clusters were annotated and manually curated.

6 References

Afik R, Zigmond E, Vugman M, Klepfish M, Shimshoni E, Pasmanik-Chor M, Shenoy A, Bassat E, Halpern Z, Geiger T, *et al* (2016) Tumor macrophages are pivotal constructors of tumor collagenous matrix. *J Exp Med* 213: 2315–2331

Akgül Ö, Çetinkaya E, Ersöz Ş & Tez M (2014) Role of surgery in colorectal cancer liver metastases. *World J Gastroenterol* 20: 6113–6122

Alba R, Bosch A & Chillon M (2005) Gutless adenovirus: last-generation adenovirus for gene therapy. *Gene Therapy 2005 12:1* 12: S18–S27

Alló M, Agirreb E, Bessonovc S, Bertucci P, Acuña LG, Buggiano V, Bellorab N, Singhb B, Petrillo E, Blaustein M, *et al* (2014) Argonaute-1 binds transcriptional enhancers and controls constitutive and alternative splicing in human cells. *Proc Natl Acad Sci U S A* 111: 15622–15629

Amendola M, Passerini L, Pucci F, Gentner B, Bacchetta R & Naldini L (2009) Regulated and Multiple miRNA and siRNA Delivery Into Primary Cells by a Lentiviral Platform. *Molecular Therapy* 17: 1039–1052

Amendola M, Venneri MA, Biffi A, Vigna E & Naldini L (2005) Coordinate dual-gene transgenesis by lentiviral vectors carrying synthetic bidirectional promoters. *Nat Biotechnol* 23: 108–16

Anderson CF & Mosser DM (2002) A novel phenotype for an activated macrophage: the type 2 activated macrophage. *J Leukoc Biol* 72: 101–6

Androulidaki A, Iliopoulos D, Arranz A, Doxaki C, Schworer S, Zacharioudaki V, Margioris AN, Tsichlis PN & Tsatsanis C (2009a) The kinase Akt1 controls macrophage response to lipopolysaccharide by regulating microRNAs. *Immunity* 31: 220–231

Androulidaki A, Iliopoulos D, Arranz A, Doxaki C, Schworer S, Zacharioudaki V, Margioris AN, Tsichlis PN & Tsatsanis C (2009b) The kinase Akt1 controls macrophage response to lipopolysaccharide by regulating microRNAs. *Immunity* 31: 220–231

Annoni A, Brown BD, Cantore A, Sergi LS, Naldini L & Roncarolo M-G (2009) In vivo delivery of a microRNA-regulated transgene induces antigen-specific regulatory T cells and promotes immunologic tolerance. *Blood* 114: 5152–61

Auyeung VC, Ulitsky I, McGeary SE & Bartel DP (2013) Beyond secondary structure: primary-sequence determinants license pri-miRNA hairpins for processing. *Cell* 152: 844–58

Babiarz JE, Ruby JG, Wang Y, Bartel DP & Blelloch R (2008) Mouse ES cells express endogenous shRNAs, siRNAs, and other Microprocessor-independent, Dicer-dependent small RNAs. *Genes Dev* 22: 2773–2785

Baer C, Squadrito ML, Laoui D, Thompson D, Hansen SK, Kiialainen A, Hoves S, Ries CH, Ooi C-H & De Palma M (2016) Suppression of microRNA activity amplifies IFN-γ-induced macrophage activation and promotes anti-tumour immunity. *Nat Cell Biol* 18: 790–802

Bamboat ZM, Stableford JA, Plitas G, Burt BM, Nguyen HM, Welles AP, Gonen M, Young JW & DeMatteo RP (2009) Human liver dendritic cells promote T cell hyporesponsiveness. *J Immunol* 182: 1901–1911

Barouch DH, Kik S V., Weverling GJ, Dilan R, King SL, Maxfield LF, Clark S, Ng'ang'a D, Brandariz KL, Abbink P, *et al* (2011) International seroepidemiology of adenovirus serotypes 5, 26, 35, and 48 in pediatric and adult populations. *Vaccine* 29: 5203–5209

Barsig J, Flesch IE & Kaufmann SH (1998) Macrophages and hepatocytic cells as chemokine producers in murine listeriosis. *Immunobiology* 199: 87–104

Bartel DP (2004) MicroRNAs: Genomics, Biogenesis, Mechanism, and Function. *Cell* 116: 281–297

Bartel DP (2009) MicroRNAs: Target Recognition and Regulatory Functions. *Cell* 136: 215–233

Batool A, Wang YQ, Hao XX, Chen SR & Liu YX (2018) A miR-125b/CSF1-CX3CL1/tumor-associated macrophage recruitment axis controls testicular germ cell tumor growth. *Cell Death & Disease 2018 9:10* 9: 1–14

Bayón LG, Izquierdo MA, Sirovich I, van Rooijen N, Beelen RH & Meijer S (1996) Role of Kupffer cells in arresting circulating tumor cells and controlling metastatic growth in the liver. *Hepatology* 23: 1224–31

Beattie L, Sawtell A, Mann J, Frame TCM, Teal B, de Labastida Rivera F, Brown N, Walwyn-Brown K, Moore JWJ, MacDonald S, *et al* (2016) Bone marrow-derived and resident liver macrophages display unique transcriptomic signatures but similar biological functions. *J Hepatol* 65: 758–768

Behm-Ansmant I, Rehwinkel J, Doerks T, Stark A, Bork P & Izaurralde E (2006) mRNA degradation by miRNAs and GW182 requires both CCR4:NOT deadenylase and DCP1:DCP2 decapping complexes. *Genes Dev* 20: 1885–1898

Beljaars L, Schippers M, Reker-Smit C, Martinez FO, Helming L, Poelstra K & Melgert BN (2014) Hepatic Localization of Macrophage Phenotypes during Fibrogenesis and Resolution of Fibrosis in Mice and Humans. *Front Immunol* 5: 430

Berezikov E, Chung W-J, Willis J, Cuppen E & Lai EC (2007) Mammalian mirtron genes. *Mol Cell* 28: 328–36

Biffi A, Bartholomae CC, Cesana D, Cartier N, Aubourg P, Ranzani M, Cesani M, Benedicenti F, Plati T, Rubagotti E, *et al* (2011) Lentiviral vector common integration sites in preclinical models and a clinical trial reflect a benign integration bias and not oncogenic selection. *Blood* 117: 5332–5339

Biller LH & Schrag D (2021) Diagnosis and Treatment of Metastatic Colorectal Cancer: A Review. *JAMA* 325: 669–685

Bilzer M, Roggel F & Gerbes AL (2006) Role of Kupffer cells in host defense and liver disease. *Liver Int* 26: 1175–1186

Binenbaum Y, Fridman E, Yaari Z, Milman N, Schroeder A, David G Ben, Shlomi T & Gil Z (2018) Transfer of miRNA in macrophage-derived exosomes induces drug resistance in pancreatic adenocarcinoma. *Cancer Res* 78: 5287–5299

Birocchi F, Cusimano M, Rossari F, Beretta S, Rancoita PM V, Ranghetti A, Colombo S, Costa B, Angel P, Sanvito F, *et al* (2022) Targeted inducible delivery of immunoactivating cytokines reprograms glioblastoma microenvironment and inhibits growth in mouse models. *Sci Transl Med* 14: eabl4106

Blériot C, Barreby E, Dunsmore G, Ballaire R, Chakarov S, Ficht X, De Simone G, Andreata F, Fumagalli V, Guo W, *et al* (2021) A subset of Kupffer cells regulates metabolism through the expression of CD36. *Immunity* 54: 2101-2116.e6

Blériot C, Chakarov S & Ginhoux F (2020) Determinants of Resident Tissue Macrophage Identity and Function. *Immunity* 52: 957–970

Bohnsack MT, Czaplinski K & Görlich D (2004) Exportin 5 is a RanGTP-dependent dsRNA-binding protein that mediates nuclear export of pre-miRNAs. *RNA* 10: 185–191

Bottini S, Hamouda-Tekaya N, Mategot R, Zaragosi LE, Audebert S, Pisano S, Grandjean V, Mauduit C, Benahmed M, Barbry P, *et al* (2017) Post-transcriptional gene silencing mediated by microRNAs is controlled by nucleoplasmic Sfpq. *Nature Communications 2017 8:1* 8: 1–16

Bouwens L, Knook DL & Wisse E (1986) Local proliferation and extrahepatic recruitment of liver macrophages (Kupffer cells) in partial-body irradiated rats. *J Leukoc Biol* 39: 687–697

Braet F & Wisse E (2002) Structural and functional aspects of liver sinusoidal endothelial cell fenestrae: a review. *Comp Hepatol* 1: 1

Brennecke J, Stark A, Russell RB & Cohen SM (2005) Principles of microRNA-target recognition. *PLoS Biol* 3: 0404–0418

Broughton JP, Lovci MT, Huang JL, Yeo GW & Pasquinelli AE (2016) Pairing beyond the Seed Supports MicroRNA Targeting Specificity. *Mol Cell* 64: 320–333

Bulcha JT, Wang Y, Ma H, Tai PWL & Gao G (2021) Viral vector platforms within the gene therapy landscape. *Signal Transduction and Targeted Therapy 2021 6:1* 6: 1–24

Cai X, Yin Y, Li N, Zhu D, Zhang J, Zhang C-Y & Zen K (2012) Re-polarization of tumor-associated macrophages to pro-inflammatory M1 macrophages by microRNA-155. *J Mol Cell Biol* 4: 341–3

Callery MP, Mangino MJ & Flye MW (1991) Kupffer cell prostaglandin-E2 production is amplified during hepatic regeneration. *Hepatology* 14: 368–72

Cantore A, Fraldi A, Meneghini V & Gritti A (2022) In vivo Gene Therapy to the Liver and Nervous System: Promises and Challenges. *Front Med (Lausanne)* 8: 774618

Cantore A & Naldini L (2021) WFH State-of-the-art paper 2020: In vivo lentiviral vector gene therapy for haemophilia. *Haemophilia* 27: 122–125

Cantore A, Ranzani M, Bartholomae CC, Volpin M, Valle P Della, Sanvito F, Sergi LS, Gallina P, Benedicenti F, Bellinger D, *et al* (2015) Liver-directed lentiviral gene therapy in a dog model of hemophilia B. *Sci Transl Med* 7: 277ra28

Capece D, Fischietti M, Verzella D, Gaggiano A, Cicciarelli G, Tessitore A, Zazzeroni F & Alesse E (2013) The inflammatory microenvironment in hepatocellular carcinoma: a pivotal role for tumor-associated macrophages. *Biomed Res Int* 2013: 187204

Cappell KM, Sherry RM, Yang JC, Goff SL, Vanasse DA, McIntyre L, Rosenberg SA & Kochenderfer JN (2020) Long-Term Follow-Up of Anti-CD19 Chimeric Antigen Receptor T-Cell Therapy. *J Clin Oncol* 38: 3805–3815

Catarinella M, Monestiroli A, Escobar G, Fiocchi A, Tran NL, Aiolfi R, Marra P, Esposito A, Cipriani F, Aldrighetti L, *et al* (2016) IFNα gene/cell therapy curbs colorectal cancer colonization of the liver by acting on the hepatic microenvironment. *EMBO Mol Med* 8: 155–70

Cazalla D, Xie M & Steitz JA (2011) A primate herpesvirus uses the integrator complex to generate viral microRNAs. *Mol Cell* 43: 982–992

Chai ZT, Zhu XD, Ao JY, Wang WQ, Gao DM, Kong J, Zhang N, Zhang YY, Ye BG, Ma DN, *et al* (2015) MicroRNA-26a suppresses recruitment of macrophages by down-regulating macrophage colony-stimulating factor expression through the PI3K/Akt pathway in hepatocellular carcinoma. *J Hematol Oncol* 8: 1–11

Chaudhuri AA, So AY-L, Sinha N, Gibson WSJ, Taganov KD, O'Connell RM & Baltimore D (2011) MicroRNA-125b potentiates macrophage activation. *J Immunol* 187: 5062–5068

Chekulaeva M, Mathys H, Zipprich JT, Attig J, Colic M, Parker R & Filipowicz W (2011) miRNA repression involves GW182-mediated recruitment of CCR4-NOT through conserved W-containing motifs. *Nat Struct Mol Biol* 18: 1218–1226

Cheloufi S, Dos Santos CO, Chong MMW & Hannon GJ (2010) A dicer-independent miRNA biogenesis pathway that requires Ago catalysis. *Nature* 465: 584–589

Chen X, Ying X, Wang X, Wu X, Zhu Q & Wang X (2017) Exosomes derived from hypoxic epithelial ovarian cancer deliver microRNA-940 to induce macrophage M2 polarization. *Oncol Rep* 38: 522–528

Chen Z, Ying J, Shang W, Ding D, Guo M & Wang H (2021) miR-342-3p Regulates the Proliferation and Apoptosis of NSCLC Cells by Targeting BCL-2. *Technol Cancer Res Treat* 20: 15330338211041192

Cheng S, Cui Y, Fan L, Mu X & Hua Y (2018) T2DM inhibition of endothelial miR-342-3p facilitates angiogenic dysfunction via repression of FGF11 signaling. *Biochem Biophys Res Commun* 503: 71–78

Chiang HR, Schoenfeld LW, Ruby JG, Auyeung VC, Spies N, Baek D, Johnston WK, Russ C, Luo S, Babiarz JE, *et al* (2010) Mammalian microRNAs: experimental evaluation of novel and previously annotated genes. *Genes Dev* 24: 992–1009

Cilenti F, Barbiera G, Caronni N, Iodice D, Montaldo E, Barresi S, Lusito E, Cuzzola V, Vittoria FM, Mezzanzanica L, *et al* (2021) A PGE2-MEF2A axis enables context-dependent control of inflammatory gene expression. *Immunity* 54: 1665-1682.e14

Comi M, Amodio G, Passeri L, Fortunato M, Santoni de Sio FR, Andolfi G, Kajaste-Rudnitski A, Russo F, Cesana L & Gregori S (2020) Generation of Powerful Human Tolerogenic Dendritic Cells by Lentiviral-Mediated IL-10 Gene Transfer. *Front Immunol* 11

Cooks T, Pateras IS, Jenkins LM, Patel KM, Robles AI, Morris J, Forshew T, Appella E, Gorgoulis VG & Harris CC (2018) Mutant p53 cancers reprogram macrophages to tumor supporting macrophages via exosomal miR-1246. *Nat Commun* 9

De Creus A, Abe M, Lau AH, Hackstein H, Raimondi G & Thomson AW (2005) Low TLR4 expression by liver dendritic cells correlates with reduced capacity to activate allogeneic T cells in response to endotoxin. *J Immunol* 174: 2037–2045

Curtale G, Mirolo M, Renzi TA, Rossato M, Bazzoni F & Locati M (2013) Negative regulation of Toll-like receptor 4 signaling by IL-10-dependent microRNA-146b. *Proc Natl Acad Sci U S A* 110: 11499–504

Czimmerer Z, Varga T, Kiss M, Vázquez CO, Doan-Xuan QM, Rückerl D, Tattikota SG, Yan X, Nagy ZS, Daniel B, *et al* (2016) The IL-4/STAT6 signaling axis establishes a conserved microRNA signature in human and mouse macrophages regulating cell survival via miR-342-3p. *Genome Med* 8: 63

Daley D, Mani VR, Mohan N, Akkad N, Ochi A, Heindel DW, Lee KB, Zambirinis CP, Pandian GSB, Savadkar S, *et al* (2017) Dectin 1 activation on macrophages by galectin

9 promotes pancreatic carcinoma and peritumoral immune tolerance. *Nat Med* 23: 556–567

Dalwadi DA, Calabria A, Tiyaboonchai A, Posey J, Naugler WE, Montini E & Grompe M (2021) AAV integration in human hepatocytes. *Molecular Therapy* 29: 2898

Das A, Ganesh K, Khanna S, … CS-TJ of & 2014 undefined Engulfment of apoptotic cells by macrophages: a role of microRNA-21 in the resolution of wound inflammation. *journals.aai.orgA Das, K Ganesh, S Khanna, CK Sen, S RoyThe Journal of Immunology, 2014•journals.aai.org*

Das SK, Menezes ME, Bhatia S, Wang X-Y, Emdad L, Sarkar D & Fisher PB (2015) Gene Therapies for Cancer: Strategies, Challenges and Successes. *J Cell Physiol* 230: 259–71

David BA, Rezende RM, Antunes MM, Santos MM, Freitas Lopes MA, Diniz AB, Sousa Pereira RV, Marchesi SC, Alvarenga DM, Nakagaki BN, *et al* (2016a) Combination of Mass Cytometry and Imaging Analysis Reveals Origin, Location, and Functional Repopulation of Liver Myeloid Cells in Mice. *Gastroenterology* 151: 1176–1191

David BA, Rezende RM, Antunes MM, Santos MM, Freitas Lopes MA, Diniz AB, Sousa Pereira RV, Marchesi SC, Alvarenga DM, Nakagaki BN, *et al* (2016b) Combination of Mass Cytometry and Imaging Analysis Reveals Origin, Location, and Functional Repopulation of Liver Myeloid Cells in Mice. *Gastroenterology* 151: 1176–1191

Diehl KL, Vorac J, Hofmann K, Meiser P, Unterweger I, Kuerschner L, Weighardt H, Förster I & Thiele C (2020) Kupffer Cells Sense Free Fatty Acids and Regulate Hepatic Lipid Metabolism in High-Fat Diet and Inflammation. *Cells* 9

Doench JG & Sharp PA (2004) Specificity of microRNA target selection in translational repression. *Genes Dev* 18: 504–511

Doria-Rose NA, Klein RM, Daniels MG, O'Dell S, Nason M, Lapedes A, Bhattacharya T, Migueles SA, Wyatt RT, Korber BT, *et al* (2010) Breadth of Human Immunodeficiency Virus-Specific Neutralizing Activity in Sera: Clustering Analysis and Association with Clinical Variables. *J Virol* 84: 1631

Edwards JP, Zhang X, Frauwirth KA & Mosser DM (2006) Biochemical and functional characterization of three activated macrophage populations. *J Leukoc Biol* 80: 1298–307

Eggert T, Wolter K, Ji J, Ma C, Yevsa T, Klotz S, Medina-Echeverz J, Longerich T, Forgues M, Reisinger F, *et al* (2016) Distinct Functions of Senescence-Associated Immune Responses in Liver Tumor Surveillance and Tumor Progression. *Cancer Cell* 30: 533–547

van Egmond M, van Garderen E, van Spriel AB, Damen CA, van Amersfoort ES, van Zandbergen G, van Hattum J, Kuiper J & van de Winkel JG (2000) FcalphaRI-positive liver Kupffer cells: reappraisal of the function of immunoglobulin A in immunity. *Nat Med* 6: 680–5

Eiring AM, Harb JG, Neviani P, Garton C, Oaks JJ, Spizzo R, Liu S, Schwind S, Santhanam R, Hickey CJ, *et al* (2010) miR-328 functions as an RNA decoy to modulate hnRNP E2 regulation of mRNA translation in leukemic blasts. *Cell* 140: 652–65

Eisengart CA, Mestre JR, Naama HA, Mackrell PJ, Rivadeneira DE, Murphy EM, Stapleton PP & Daly JM (2000) Prostaglandins Regulate Melanoma-Induced Cytokine Production in Macrophages. *Cell Immunol* 204: 143–149

Elverum K & Whitman M (2020) Delivering cellular and gene therapies to patients: solutions for realizing the potential of the next generation of medicine. *Gene Ther* 27: 537–544

Ender C, Krek A, Friedländer MR, Beitzinger M, Weinmann L, Chen W, Pfeffer S, Rajewsky N & Meister G (2008) A human snoRNA with microRNA-like functions. *Mol Cell* 32: 519–528

Escobar G, Barbarossa L, Barbiera G, Norelli M, Genua M, Ranghetti A, Plati T, Camisa B, Brombin C, Cittaro D, *et al* (2018) Interferon gene therapy reprograms the leukemia microenvironment inducing protective immunity to multiple tumor antigens. *Nat Commun* 9: 2896

Escobar G, Gentner B, Naldini L & Mazzieri R (2014a) Engineered tumor-infiltrating macrophages as gene delivery vehicles for interferon-α activates immunity and inhibits breast cancer progression. *Oncoimmunology* 3: e28696

Escobar G, Moi D, Ranghetti A, Ozkal-Baydin P, Squadrito ML, Kajaste-Rudnitski A, Bondanza A, Gentner B, De Palma M, Mazzieri R, *et al* (2014b) Genetic engineering of hematopoiesis for targeted IFN-α delivery inhibits breast cancer progression. *Sci Transl Med* 6: 217ra3

Fontana L, Pelosi E, Greco P, Racanicchi S, Testa U, Liuzzi F, Croce CM, Brunetti E, Grignani F & Peschle C (2007) MicroRNAs 17-5p-20a-106a control monocytopoiesis through AML1 targeting and M-CSF receptor upregulation. *Nat Cell Biol* 9: 775–87

Fortunato M, Amodio G & Gregori S (2023) IL-10-Engineered Dendritic Cells Modulate Allogeneic CD8+ T Cell Responses. *Int J Mol Sci* 24: 9128

Frank AC, Ebersberger S, Fink AF, Lampe S, Weigert A, Schmid T, Ebersberger I, Syed SN & Brüne B (2019) Apoptotic tumor cell-derived microRNA-375 uses CD36 to alter the tumor-associated macrophage phenotype. *Nature Communications 2019 10:1* 10: 1–18

Frank AM & Buchholz CJ (2019) Surface-Engineered Lentiviral Vectors for Selective Gene Transfer into Subtypes of Lymphocytes. *Mol Ther Methods Clin Dev* 12: 19–31

Fu L-Q, Du W-L, Cai M-H, Yao J-Y, Zhao Y-Y & Mou X-Z (2020) The roles of tumor-associated macrophages in tumor angiogenesis and metastasis. *Cell Immunol* 353: 104119

Gabrilovich DI & Nagaraj S (2009) Myeloid-derived suppressor cells as regulators of the immune system. *Nat Rev Immunol* 9: 162–174

Gammella E, Buratti P, Cairo G & Recalcati S (2014) Macrophages: central regulators of iron balance. *Metallomics* 6: 1336–45

Gao G, Alvira MR, Somanathan S, Lu Y, Vandenberghe LH, Rux JJ, Calcedo R, Sanmiguel J, Abbas Z & Wilson JM (2003) Adeno-associated viruses undergo substantial evolution in primates during natural infections. *Proc Natl Acad Sci U S A* 100: 6081–6086

Gao G, Vandenberghe LH, Alvira MR, Lu Y, Calcedo R, Zhou X & Wilson JM (2004) Clades of Adeno-Associated Viruses Are Widely Disseminated in Human Tissues. *J Virol* 78: 6381–6388

Gao GP, Alvira MR, Wang L, Calcedo R, Johnston J & Wilson JM (2002) Novel adeno-associated viruses from rhesus monkeys as vectors for human gene therapy. *Proc Natl Acad Sci U S A* 99: 11854–11859

Gao Q & Wang Y (2021) LncRNA FTX Regulates Angiogenesis Through miR-342-3p/SPI1 Axis in Stroke. *Neuropsychiatr Dis Treat* Volume 17: 3617–3625

Gardner CR, Wasserman AJ & Laskin DL (1991) Liver macrophage-mediated cytotoxicity toward mastocytoma cells involves phagocytosis of tumor targets. *Hepatology* 14: 318–24

Gebert LFR & MacRae IJ (2019) Regulation of microRNA function in animals. *Nat Rev Mol Cell Biol* 20: 21–37

Geisler A & Fechner H (2016) MicroRNA-regulated viral vectors for gene therapy. *World J Exp Med* 6: 37–54

Genovese P, Schiroli G, Escobar G, Tomaso T Di, Firrito C, Calabria A, Moi D, Mazzieri R, Bonini C, Holmes MC, *et al* (2014) Targeted genome editing in human repopulating haematopoietic stem cells. *Nature* 510: 235–240

Gentner B, Visigalli I, Hiramatsu H, Lechman E, Ungari S, Giustacchini A, Schira G, Amendola M, Quattrini A, Martino S, *et al* (2010) Identification of hematopoietic stem cell-specific miRNAs enables gene therapy of globoid cell leukodystrophy. *Sci Transl Med* 2: 58ra84

Ghani S, Riemke P, Schönheit J, Lenze D, Stumm J, Hoogenkamp M, Lagendijk A, Heinz S, Bonifer C, Bakkers J, *et al* (2011) Macrophage development from HSCs requires PU.1-coordinated microRNA expression. *Blood* 118: 2275–2284

Graff JW, Dickson AM, Clay G, McCaffrey AP & Wilson ME (2012) Identifying functional microRNAs in macrophages with polarized phenotypes. *Journal of Biological Chemistry* 287: 21816–21825

Griffith TS, Stokes B, Kucaba TA, Earel JK, VanOosten RL, Brincks EL & Norian LA (2009) TRAIL gene therapy: from preclinical development to clinical application. *Curr Gene Ther* 9: 9–19

Groux H, Bigler M, De Vries JE & Roncarolo MG (1996) Interleukin-10 induces a long-term antigen-specific anergic state in human CD4+ T cells. *J Exp Med* 184: 19–29

Guilliams M, Bonnardel J, Haest B, Vanderborght B, Wagner C, Remmerie A, Bujko A, Martens L, Thoné T, Browaeys R, *et al* (2022) Spatial proteogenomics reveals distinct and evolutionarily conserved hepatic macrophage niches. *Cell* 185: 379-396.e38

Guillot A & Tacke F (2019) Liver Macrophages: Old Dogmas and New Insights. *Hepatol Commun* 3: 730–743

Guo S, Lu J, Schlanger R, Zhang H, Wang JY, Fox MC, Purton LE, Fleming HH, Cobb B, Merkenschlager M, *et al* (2010) MicroRNA miR-125a controls hematopoietic stem cell number. *Proc Natl Acad Sci U S A* 107: 14229–14234

Gutierrez-Guerrero A, Cosset FL & Verhoeyen E (2020) Lentiviral Vector Pseudotypes: Precious Tools to Improve Gene Modification of Hematopoietic Cells for Research and Gene Therapy. *Viruses* 12

van Haasteren J, Hyde SC & Gill DR (2018) Lessons learned from lung and liver in-vivo gene therapy: implications for the future. *Expert Opin Biol Ther* 18: 959–972

Hammond SM, Boettcher S, Caudy AA, Kobayashi R & Hannon GJ (2001) Argonaute2, a link between genetic and biochemical analyses of RNAi. *Science* 293: 1146–1150

Han J, Lee Y, Yeom K-H, Nam J-W, Heo I, Rhee J-K, Sohn SY, Cho Y, Zhang B-T & Kim VN (2006) Molecular basis for the recognition of primary microRNAs by the Drosha-DGCR8 complex. *Cell* 125: 887–901

Hastie E, Cataldi M, Marriott I & Grdzelishvili VZ (2013) Understanding and altering cell tropism of vesicular stomatitis virus. *Virus Res* 176: 16–32

Havens MA, Reich AA & Hastings ML (2014) Drosha Promotes Splicing of a Pre-microRNA-like Alternative Exon. *PLoS Genet* 10: e1004312

He M, Xu Z, Ding T, Kuang D-M & Zheng L (2009) MicroRNA-155 regulates inflammatory cytokine production in tumor-associated macrophages via targeting C/EBPbeta. *Cell Mol Immunol* 6: 343–52

He P, Xu Y-Q, Wang Z-J & Sheng B (2020) LncRNA LINC00210 regulated radiosensitivity of osteosarcoma cells via miR-342-3p/GFRA1 axis. *J Clin Lab Anal* 34: e23540

Heesters BA, Myers RC & Carroll MC (2014) Follicular dendritic cells: dynamic antigen libraries. *Nat Rev Immunol* 14: 495–504

Helmy KY, Katschke KJ, Gorgani NN, Kljavin NM, Elliott JM, Diehl L, Scales SJ, Ghilardi N & Van Lookeren Campagne M (2006) CRIg: a macrophage complement receptor required for phagocytosis of circulating pathogens. *Cell* 124: 915–927

Heo I, Joo C, Cho J, Ha M, Han J & Kim VN (2008) Lin28 mediates the terminal uridylation of let-7 precursor MicroRNA. *Mol Cell* 32: 276–284

Herbst F, Lang TJL, Eckert ESP, Wünsche P, Wurm AA, Kindinger T, Laaber K, Hemmati S, Hotz-Wagenblatt A, Zavidij O, *et al* (2021) The balance between the intronic miR-342 and its host gene Evl determines hematopoietic cell fate decision. *Leukemia* 35: 2948–2963

Heymann F, Peusquens J, Ludwig-Portugall I, Kohlhepp M, Ergen C, Niemietz P, Martin C, van Rooijen N, Ochando JC, Randolph GJ, *et al* (2015) Liver inflammation abrogates immunological tolerance induced by Kupffer cells. *Hepatology* 62: 279–291

Hinglais N, Kazatchkine MD, Mandet C, Appay MD & Bariety J (1989) Human liver Kupffer cells express CR1, CR3, and CR4 complement receptor antigens. An immunohistochemical study. *Lab Invest* 61: 509–14

Hou J, Wang P, Lin L, Liu X, Ma F, An H, Wang Z & Cao X (2009) MicroRNA-146a feedback inhibits RIG-I-dependent Type I IFN production in macrophages by targeting TRAF6, IRAK1, and IRAK2. *J Immunol* 183: 2150–8

Hsu YL, Hung JY, Chang WA, Jian SF, Lin YS, Pan YC, Wu CY & Kuo PL (2018) Hypoxic Lung-Cancer-Derived Extracellular Vesicle MicroRNA-103a Increases the Oncogenic Effects of Macrophages by Targeting PTEN. *Molecular Therapy* 26: 568–581

Hu X & Ivashkiv LB (2009) Cross-regulation of signaling pathways by interferon-gamma: implications for immune responses and autoimmune diseases. *Immunity* 31: 539–50

Huang C, Liu X-J, QunZhou, Xie J, Ma T-T, Meng X-M & Li J (2016) MiR-146a modulates macrophage polarization by inhibiting Notch1 pathway in RAW264.7 macrophages. *Int Immunopharmacol* 32: 46–54

Huang V, Place RF, Portnoy V, Wang J, Qi Z, Jia Z, Yu A, Shuman M, Yu J & Li L-C (2012) Upregulation of Cyclin B1 by miRNA and its implications in cancer. *Nucleic Acids Res* 40: 1695–707

Huang Y & Chi C (2019) Glioma cell proliferation is inhibited by miR-342-3p, miR-377 / E2F1 signaling pathway. *Neoplasma* 66: 524–531

Hume DA, Offermanns S & Bonnavion R (2022) Contamination of isolated mouse Kupffer cells with liver sinusoidal endothelial cells. *Immunity* 55: 1139–1140

Huntzinger E & Izaurralde E (2011) Gene silencing by microRNAs: contributions of translational repression and mRNA decay. *Nat Rev Genet* 12: 99–110

Hutchins PM & Heinecke JW (2015) Cholesterol efflux capacity, macrophage reverse cholesterol transport and cardioprotective HDL. *Curr Opin Lipidol* 26: 388–393

Iannacone M, Blériot C, Andreata F, Ficht X, Laura C, Garcia-Manteiga JM, Uderhardt S & Ginhoux F (2022) Response to contamination of isolated mouse Kupffer cells with liver sinusoidal endothelial cells. *Immunity* 55: 1141–1142

Ilkovitch D & Lopez DM (2009) The liver is a site for tumor-induced myeloid-derived suppressor cell accumulation and immunosuppression. *Cancer Res* 69: 5514–5521

Ishii T, Mimura I, Nagaoka K, Naito A, Sugasawa T, Kuroda R, Yamada D, Kanki Y, Kume H, Ushiku T, *et al* (2022) Effect of M2-like macrophages of the injured-kidney cortex on kidney cancer progression. *Cell Death Discov* 8: 480

Jablonski KA, Gaudet AD, Amici SA, Popovich PG & Guerau-de-Arellano M (2016) Control of the Inflammatory Macrophage Transcriptional Signature by miR-155. *PLoS One* 11: e0159724

Jayarajan V, Kounatidou E, Qasim W & Di W-L (2021) Ex vivo gene modification therapy for genetic skin diseases-recent advances in gene modification technologies and delivery. *Exp Dermatol* 30: 887–896

Jia L-T, Chen S-Y & Yang A-G (2012) Cancer gene therapy targeting cellular apoptosis machinery. *Cancer Treat Rev* 38: 868–76

Jiang K, Chen H, Fang Y, Chen L, Zhong C, Bu T, Dai S, Pan X, Fu D, Qian Y, *et al* (2021) Exosomal ANGPTL1 attenuates colorectal cancer liver metastasis by regulating Kupffer cell secretion pattern and impeding MMP9 induced vascular leakiness. *J Exp Clin Cancer Res* 40: 21

Jiang K, Guo S, Zhang T, Yang Y, Zhao G, Shaukat A, Wu H & Deng G (2018) Downregulation of TLR4 by miR-181a Provides Negative Feedback Regulation to Lipopolysaccharide-Induced Inflammation. *Front Pharmacol* 9

Jiang Y, Zhou J, Zhao J, Zhang H, Li L, Li H, Chen L, Hu J, Zheng W & Jing Z (2020) The U2AF2 /circRNA ARF1/miR-342–3p/ISL2 feedback loop regulates angiogenesis in glioma stem cells. *Journal of Experimental & Clinical Cancer Research* 39: 182

Ju C & Tacke F (2016) Hepatic macrophages in homeostasis and liver diseases: from pathogenesis to novel therapeutic strategies. *Cell Mol Immunol* 13: 316–27

Ke M, Zhang Z, Cong L, Zhao S, Li Y, Wang X, Lv Y, Zhu Y & Dong J (2019) MicroRNA-148b-colony-stimulating factor-1 signaling-induced tumor-associated macrophage infiltration promotes hepatocellular carcinoma metastasis. *Biomedicine & Pharmacotherapy* 120: 109523

Kerzel T, Giacca G, Beretta S, Bresesti C, Notaro M, Scotti GM, Balestrieri C, Canu T, Redegalli M, Pedica F, *et al* (2023) In vivo macrophage engineering reshapes the tumor microenvironment leading to eradication of liver metastases. *Cancer Cell*

Khvorova A, Reynolds A & Jayasena SD (2003) Functional siRNAs and miRNAs exhibit strand bias. *Cell* 115: 209–216

Kim SW, Ramasamy K, Bouamar H, Lin AP, Jiang D & Aguiar RCT (2012) MicroRNAs miR-125a and miR-125b constitutively activate the NF-κB pathway by targeting the tumor necrosis factor alpha-induced protein 3 (TNFAIP3, A20). *Proc Natl Acad Sci U S A* 109: 7865–7870

Kim YK & Kim VN (2007) Processing of intronic microRNAs. *EMBO J* 26: 775–783

Kimura Y, Inoue A, Hangai S, Saijo S, Negishi H, Nishio J, Yamasaki S, Iwakura Y, Yanai H & Taniguchi T (2016) The innate immune receptor Dectin-2 mediates the phagocytosis of cancer cells by Kupffer cells for the suppression of liver metastasis. *Proc Natl Acad Sci U S A* 113: 14097–14102

Knoll P, Schlaak J, Uhrig A, Kempf P, zum Büschenfelde KHM & Gerken G (1995) Human Kupffer cells secrete IL-10 in response to lipopolysaccharide (LPS) challenge. *J Hepatol* 22: 226–229

Knolle PA, Uhrig A, Hegenbarth S, Löser E, Schmitt E, Gerken G & Lohse AW (1998) IL-10 down-regulates T cell activation by antigen-presenting liver sinusoidal endothelial cells through decreased antigen uptake via the mannose receptor and lowered surface expression of accessory molecules. *Clin Exp Immunol* 114: 427–433

Koch M, Mollenkopf HJ, Klemm U & Meyer TF (2012) Induction of microRNA-155 is TLR- and type IV secretion system-dependent in macrophages and inhibits DNA-damage induced apoptosis. *Proc Natl Acad Sci U S A* 109

Kozomara A, Birgaoanu M & Griffiths-Jones S (2019) miRBase: from microRNA sequences to function. *Nucleic Acids Res* 47: D155–D162

Krenkel O & Tacke F (2017) Liver macrophages in tissue homeostasis and disease. *Nat Rev Immunol* 17: 306–321

Kristiansen M, Graversen JH, Jacobsen C, Sonne O, Hoffman HJ, Law SKA & Moestrup SK (2001) Identification of the haemoglobin scavenger receptor. *Nature* 409: 198–201

Lai X, Gupta SK, Schmitz U, Marquardt S, Knoll S, Spitschak A, Wolkenhauer O, Pützer BM & Vera J (2018) MiR-205-5p and miR-342-3p cooperate in the repression of the E2F1 transcription factor in the context of anticancer chemotherapy resistance. *Theranostics* 8: 1106–1120

Lan J, Sun L, Xu F, Liu L, Hu F, Song D, Hou Z, Wu W, Luo X, Wang J, *et al* (2019) M2 macrophage-derived exosomes promote cell migration and invasion in colon cancer. *Cancer Res* 79: 146–158

Latvala S, Jacobsen B, Otteneder MB, Herrmann A & Kronenberg S (2017) Distribution of FcRn Across Species and Tissues. *J Histochem Cytochem* 65: 321–333

Lavin Y, Winter D, Blecher-Gonen R, David E, Keren-Shaul H, Merad M, Jung S & Amit I (2014) Tissue-resident macrophage enhancer landscapes are shaped by the local microenvironment. *Cell* 159: 1312–26

Lechman ER, Gentner B, Van Galen P, Giustacchini A, Saini M, Boccalatte FE, Hiramatsu H, Restuccia U, Bachi A, Voisin V, *et al* (2012) Attenuation of miR-126 activity expands HSC in vivo without exhaustion. *Cell Stem Cell* 11: 799–811

Lee HY, Zhou K, Smith AM, Noland CL & Doudna JA (2013) Differential roles of human Dicer-binding proteins TRBP and PACT in small RNA processing. *Nucleic Acids Res* 41: 6568–6576

Lee JC, Mehdizadeh S, Smith J, Young A, Mufazalov IA, Mowery CT, Daud A & Bluestone JA (2020) Regulatory T cell control of systemic immunity and immunotherapy response in liver metastasis. *Sci Immunol* 5

Leebeek FWG & Miesbach W (2021) Gene therapy for hemophilia: a review on clinical benefit, limitations, and remaining issues. *Blood* 138: 923–931

Leucci E, Patella F, Waage J, Holmstrøm K, Lindow M, Porse B, Kauppinen S & Lund AH (2013) microRNA-9 targets the long non-coding RNA MALAT1 for degradation in the nucleus. *Sci Rep* 3

Li D, Duan M, Feng Y, Geng L, Li X & Zhang W (2016) MiR-146a modulates macrophage polarization in systemic juvenile idiopathic arthritis by targeting INHBA. *Mol Immunol* 77: 205–12

Li F, Deng Y, Zhang S, Zhu B, Wang J, Wang J, Wang X, Zhao Z, Deng W, Mao R, *et al* (2022) Human hepatocyte-enriched miRNA-192-3p promotes HBV replication through inhibiting Akt/mTOR signalling by targeting ZNF143 in hepatic cell lines. *Emerg Microbes Infect* 11: 616–628

Li H, Wu K, Tao K, Chen L, Zheng Q, Lu X, Liu J, Shi L, Liu C, Wang G, *et al* (2012) Tim-3/galectin-9 signaling pathway mediates T-cell dysfunction and predicts poor prognosis in patients with hepatitis B virus-associated hepatocellular carcinoma. *Hepatology* 56: 1342–1351

Li X-R, Chu H-J, Lv T, Wang L, Kong S-F & Dai S-Z (2014a) miR-342-3p suppresses proliferation, migration and invasion by targeting FOXM1 in human cervical cancer. *FEBS Lett* 588: 3298–307

Li X-R, Chu H-J, Lv T, Wang L, Kong S-F & Dai S-Z (2014b) miR-342-3p suppresses proliferation, migration and invasion by targeting FOXM1 in human cervical cancer. *FEBS Lett* 588: 3298–307

Li Y, Zhao L, Shi B, Ma S, Xu Z, Ge Y, Liu Y, Zheng D & Shi J (2015) Functions of miR-146a and miR-222 in Tumor-associated Macrophages in Breast Cancer. *Sci Rep* 5: 18648

Li Z, Lan X, Han R, Wang J, Huang Y, Sun J, Guo W & Chen H (2017) miR-2478 inhibits TGFβ1 expression by targeting the transcriptional activation region downstream of the TGFβ1 promoter in dairy goats. *Sci Rep* 7: 42627

Liu J, Carmell MA, Rivas F V., Marsden CG, Thomson JM, Song JJ, Hammond SM, Joshua-Tor L & Hannon GJ (2004) Argonaute2 is the catalytic engine of mammalian RNAi. *Science* 305: 1437–1441

Liu W, Kang L, Han J, Wang Y, Shen C, Yan Z, Tai Y & Zhao C (2018) miR-342-3p suppresses hepatocellular carcinoma proliferation through inhibition of IGF-1R-mediated Warburg effect. *Onco Targets Ther* 11: 1643–1653

Londoño M-C, Rimola A, O'Grady J & Sanchez-Fueyo A (2013) Immunosuppression minimization vs. complete drug withdrawal in liver transplantation. *J Hepatol* 59: 872–9

Lund E, Güttinger S, Calado A, Dahlberg JE & Kutay U (2004) Nuclear export of microRNA precursors. *Science* 303: 95–98

Lv S, Li J, Qiu X, Li W, Zhang C, Zhang Z-N & Luan B (2017) A negative feedback loop of ICER and NF-κB regulates TLR signaling in innate immune responses. *Cell Death Differ* 24: 492–499

Ma C, Kesarwala AH, Eggert T, Medina-Echeverz J, Kleiner DE, Jin P, Stroncek DF, Terabe M, Kapoor V, ElGindi M, *et al* (2016) NAFLD causes selective CD4(+) T lymphocyte loss and promotes hepatocarcinogenesis. *Nature* 531: 253–257

Ma F, Liu X, Li D, Wang P, Li N, Lu L & Cao X (2010) MicroRNA-466l upregulates IL-10 expression in TLR-triggered macrophages by antagonizing RNA-binding protein tristetraprolin-mediated IL-10 mRNA degradation. *J Immunol* 184: 6053–9

Ma H, Wu Y, Choi J-G & Wu H (2013) Lower and upper stem-single-stranded RNA junctions together determine the Drosha cleavage site. *Proc Natl Acad Sci U S A* 110: 20687–92

MacRae IJ, Zhou K & Doudna JA (2007) Structural determinants of RNA recognition and cleavage by Dicer. *Nature Structural & Molecular Biology 2007 14:10* 14: 934–940

MacRae IJ, Zhou K, Li F, Repic A, Brooks AN, Cande WZ, Adams PD & Doudna JA (2006) Structural basis for double-stranded RNA processing by Dicer. *Science* 311: 195–198

Makarova JA, Shkurnikov MU, Wicklein D, Lange T, Samatov TR, Turchinovich AA & Tonevitsky AG (2016) Intracellular and extracellular microRNA: An update on localization and biological role. *Prog Histochem Cytochem* 51: 33–49

Makarova-Rusher O V., Medina-Echeverz J, Duffy AG & Greten TF (2015) The yin and yang of evasion and immune activation in HCC. *J Hepatol* 62: 1420–1429

Mantovani A, Sica A, Allavena P, Garlanda C & Locati M (2009) Tumor-associated macrophages and the related myeloid-derived suppressor cells as a paradigm of the diversity of macrophage activation. *Hum Immunol* 70: 325–30

Mantovani A, Sica A, Sozzani S, Allavena P, Vecchi A & Locati M (2004) The chemokine system in diverse forms of macrophage activation and polarization. *Trends Immunol* 25: 677–86

Marofi F, Achmad H, Bokov D, Abdelbasset WK, Alsadoon Z, Chupradit S, Suksatan W, Shariatzadeh S, Hasanpoor Z, Yazdanifar M, *et al* (2022) Hurdles to breakthrough in CAR T cell therapy of solid tumors. *Stem Cell Res Ther* 13: 140

Martin J, Petrillo A, Smyth EC, Shaida N, Khwaja S, Cheow HK, Duckworth A, Heister P, Praseedom R, Jah A, *et al* (2020) Colorectal liver metastases: Current management and future perspectives. *World J Clin Oncol* 11: 761–808

Martinez FO, Helming L, Milde R, Varin A, Melgert BN, Draijer C, Thomas B, Fabbri M, Crawshaw A, Ho LP, *et al* (2013) Genetic programs expressed in resting and IL-4 alternatively activated mouse and human macrophages: similarities and differences. *Blood* 121: e57-69

Martinez-Nunez RT, Louafi F & Sanchez-Elsner T (2011) The interleukin 13 (IL-13) pathway in human macrophages is modulated by microRNA-155 via direct targeting of interleukin 13 receptor alpha1 (IL13Ralpha1). *J Biol Chem* 286: 1786–1794

Mass E, Ballesteros I, Farlik M, Halbritter F, Günther P, Crozet L, Jacome-Galarza CE, Händler K, Klughammer J, Kobayashi Y, *et al* (2016) Specification of tissue-resident macrophages during organogenesis. *Science* 353

Mast TC, Kierstead L, Gupta SB, Nikas AA, Kallas EG, Novitsky V, Mbewe B, Pitisuttithum P, Schechter M, Vardas E, *et al* (2010) International epidemiology of human pre-existing adenovirus (Ad) type-5, type-6, type-26 and type-36 neutralizing antibodies: Correlates of high Ad5 titers and implications for potential HIV vaccine trials. *Vaccine* 28: 950–957

Matsui M, Chu Y, Zhang H, Gagnon KT, Shaikh S, Kuchimanchi S, Manoharan M, Corey DR & Janowski BA (2013) Promoter RNA links transcriptional regulation of inflammatory pathway genes. *Nucleic Acids Res* 41: 10086–109

Matsumura H, Kondo T, Ogawa K, Tamura T, Fukunaga K, Murata S & Ohkohchi N (2014) Kupffer cells decrease metastasis of colon cancer cells to the liver in the early stage. *Int J Oncol* 45: 2303–10

McCoy CE, Sheedy FJ, Qualls JE, Doyle SL, Quinn SR, Murray PJ & O'Neill LAJ (2010) IL-10 inhibits miR-155 induction by toll-like receptors. *J Biol Chem* 285: 20492–20498

McGrath MM (2018) Diverse roles of TIM4 in immune activation: implications for alloimmunity. *Curr Opin Organ Transplant* 23: 44–50

Meister G, Landthaler M, Patkaniowska A, Dorsett Y, Teng G & Tuschl T (2004) Human Argonaute2 mediates RNA cleavage targeted by miRNAs and siRNAs. *Mol Cell* 15: 185–197

Meng X, Jiang Q, Chang N, Wang X, Liu C, Xiong J, Cao H & Liang Z (2016) Small activating RNA binds to the genomic target site in a seed-region-dependent manner. *Nucleic Acids Res* 44: 2274–82

Mielgo A & Schmid MC (2020) Liver Tropism in Cancer: The Hepatic Metastatic Niche. *Cold Spring Harb Perspect Med* 10

Milani M, Annoni A, Moalli F, Liu T, Cesana D, Calabria A, Bartolaccini S, Biffi M, Russo F, Visigalli I, *et al* (2019) Phagocytosis-shielded lentiviral vectors improve liver gene therapy in nonhuman primates. *Sci Transl Med* 11

Miller KD, Nogueira L, Devasia T, Mariotto AB, Yabroff KR, Jemal A, Kramer J & Siegel RL (2022) Cancer treatment and survivorship statistics, 2022. *CA Cancer J Clin* 72: 409–436

Mills CD, Kincaid K, Alt JM, Heilman MJ & Hill AM (2000) M-1/M-2 macrophages and the Th1/Th2 paradigm. *J Immunol* 164: 6166–73

Morris K V, Santoso S, Turner A-M, Pastori C & Hawkins PG (2008) Bidirectional transcription directs both transcriptional gene activation and suppression in human cells. *PLoS Genet* 4: e1000258

Mourelatos Z, Dostie J, Paushkin S, Sharma A, Charroux B, Abel L, Rappsilber J, Mann M & Dreyfuss G (2002) miRNPs: a novel class of ribonucleoproteins containing numerous microRNAs. *Genes Dev* 16: 720–728

Movita D, Kreefft K, Biesta P, van Oudenaren A, Leenen PJM, Janssen HLA & Boonstra A (2012) Kupffer cells express a unique combination of phenotypic and functional characteristics compared with splenic and peritoneal macrophages. *J Leukoc Biol* 92: 723–33

Murphy AJ, Guyre PM & Pioli PA (2010) Estradiol suppresses NF-kappa B activation through coordinated regulation of let-7a and miR-125b in primary human macrophages. *J Immunol* 184: 5029–37

Naito M & Takahashi K (1991) The role of Kupffer cells in glucan-induced granuloma formation in the liver of mice depleted of blood monocytes by administration of strontium-89. *Lab Invest* 64: 664–74

Naldini L (2011) Ex vivo gene transfer and correction for cell-based therapies. *Nat Rev Genet* 12: 301–15

Naldini L (2015) Gene therapy returns to centre stage. *Nature* 526: 351–60

Nathwani AC, Reiss UM, Tuddenham EGD, Rosales C, Chowdary P, McIntosh J, Della Peruta M, Lheriteau E, Patel N, Raj D, *et al* (2014) Long-term safety and efficacy of factor IX gene therapy in hemophilia B. *N Engl J Med* 371: 1994–2004

Nault J-C, Datta S, Imbeaud S, Franconi A, Mallet M, Couchy G, Letouzé E, Pilati C, Verret B, Blanc J-F, *et al* (2015) Recurrent AAV2-related insertional mutagenesis in human hepatocellular carcinomas. *Nat Genet* 47: 1187–93

Nault J-C, Mami I, La Bella T, Datta S, Imbeaud S, Franconi A, Mallet M, Couchy G, Letouzé E, Pilati C, *et al* (2016) Wild-type AAV Insertions in Hepatocellular Carcinoma Do Not Inform Debate Over Genotoxicity Risk of Vectorized AAV. *Mol Ther* 24: 660–1

Nguyen-Lefebvre AT & Horuzsko A (2015) Kupffer Cell Metabolism and Function. *J Enzymol Metab* 1

Nielsen SR, Quaranta V, Linford A, Emeagi P, Rainer C, Santos A, Ireland L, Sakai T, Sakai K, Kim Y-S, *et al* (2016) Macrophage-secreted granulin supports pancreatic cancer metastasis by inducing liver fibrosis. *Nat Cell Biol* 18: 549–60

Nishi K, Nishi A, Nagasawa T & Ui-Tei K (2013) Human TNRC6A is an Argonaute-navigator protein for microRNA-mediated gene silencing in the nucleus. *RNA* 19: 17–35

Nishihara T, Zekri L, Braun JE & Izaurralde E (2013) miRISC recruits decapping factors to miRNA targets to enhance their degradation. *Nucleic Acids Res* 41: 8692–8705

Novakowski KE, Huynh A, Han SJ, Dorrington MG, Yin C, Tu Z, Pelka P, Whyte P, Guarné A, Sakamoto K, *et al* (2016) A naturally occurring transcript variant of MARCO reveals the SRCR domain is critical for function. *Immunol Cell Biol* 94: 646–655

O'Connell RM, Chaudhuri AA, Rao DS & Baltimore D (2009) Inositol phosphatase SHIP1 is a primary target of miR-155. *Proc Natl Acad Sci U S A* 106: 7113–7118

O'Connell RM, Taganov KD, Boldin MP, Cheng G & Baltimore D (2007) MicroRNA-155 is induced during the macrophage inflammatory response. *Proc Natl Acad Sci U S A* 104: 1604–1609

Odegaard JI, Ricardo-Gonzalez RR, Red Eagle A, Vats D, Morel CR, Goforth MH, Subramanian V, Mukundan L, Ferrante AW & Chawla A (2008) Alternative M2 activation of Kupffer cells by PPARdelta ameliorates obesity-induced insulin resistance. *Cell Metab* 7: 496–507

De Palma M, Mazzieri R, Politi LS, Pucci F, Zonari E, Sitia G, Mazzoleni S, Moi D, Venneri MA, Indraccolo S, *et al* (2008) Tumor-targeted interferon-alpha delivery by Tie2-expressing monocytes inhibits tumor growth and metastasis. *Cancer Cell* 14: 299–311

De Palma M, Venneri MA, Roca C & Naldini L (2003) Targeting exogenous genes to tumor angiogenesis by transplantation of genetically modified hematopoietic stem cells. *Nat Med* 9: 789–95

Pan G, Liu Y, Shang L, Zhou F & Yang S (2021) EMT-associated microRNAs and their roles in cancer stemness and drug resistance. *Cancer Commun (Lond)* 41: 199–217

Pan K, Farrukh H, Chittepu VCSR, Xu H, Pan C-X & Zhu Z (2022) CAR race to cancer immunotherapy: from CAR T, CAR NK to CAR macrophage therapy. *J Exp Clin Cancer Res* 41: 119

Park JE, Dutta B, Tse SW, Gupta N, Tan CF, Low JK, Yeoh KW, Kon OL, Tam JP & Sze SK (2019) Hypoxia-induced tumor exosomes promote M2-like macrophage polarization of infiltrating myeloid cells and microRNA-mediated metabolic shift. *Oncogene* 38: 5158–5173

Park JE, Heo I, Tian Y, Simanshu DK, Chang H, Jee D, Patel DJ & Kim VN (2011) Dicer recognizes the 5' end of RNA for efficient and accurate processing. *Nature* 475: 201–205

Passeri L, Andolfi G, Bassi V, Russo F, Giacomini G, Laudisa C, Marrocco I, Cesana L, Di Stefano M, Fanti L, *et al* (2023) Tolerogenic IL-10-engineered dendritic cell-based therapy to restore antigen-specific tolerance in T cell mediated diseases. *J Autoimmun* 138

Patel A, Bah MA & Weiner DB (2020) In Vivo Delivery of Nucleic Acid-Encoded Monoclonal Antibodies. *BioDrugs* 34: 273–293

Patil S, Gao YG, Lin X, Li Y, Dang K, Tian Y, Zhang WJ, Jiang SF, Qadir A & Qian AR (2019) The Development of Functional Non-Viral Vectors for Gene Delivery. *Int J Mol Sci* 20

Peng KW, Pham L, Ye H, Zufferey R, Trono D, Cosset FL & Russell SJ (2001) Organ distribution of gene expression after intravenous infusion of targeted and untargeted lentiviral vectors. *Gene Ther* 8: 1456–63

Peng Y & Croce CM (2016) The role of MicroRNAs in human cancer. *Signal Transduct Target Ther* 1

Perrin GQ, Herzog RW & Markusic DM (2019) Update on clinical gene therapy for hemophilia. *Blood* 133: 407–414

Pisignano G, Napoli S, Magistri M, Mapelli SN, Pastori C, Di Marco S, Civenni G, Albino D, Enriquez C, Allegrini S, *et al* (2017) A promoter-proximal transcript targeted by genetic polymorphism controls E-cadherin silencing in human cancers. *Nat Commun* 8: 15622

Pitchiaya S, Heinicke LA, Park JI, Cameron EL & Walter NG (2017) Resolving Subcellular miRNA Trafficking and Turnover at Single-Molecule Resolution. *Cell Rep* 19: 630–642

Poletti V & Mavilio F (2021) Designing Lentiviral Vectors for Gene Therapy of Genetic Diseases. *Viruses* 13

Quintanal-Villalonga Á, Chan JM, Yu HA, Pe'er D, Sawyers CL, Sen T & Rudin CM (2020) Lineage plasticity in cancer: a shared pathway of therapeutic resistance. *Nat Rev Clin Oncol* 17: 360–371

Raichlin E, Daly RC, Rosen CB, McGregor CG, Charlton MR, Frantz RP, Clavell AL, Rodeheffer RJ, Pereira NL, Kremers WK, *et al* (2009) Combined heart and liver transplantation: a single-center experience. *Transplantation* 88: 219–25

Recchiuti A, Krishnamoorthy S, Fredman G, Chiang N & Serhan CN (2011) MicroRNAs in resolution of acute inflammation: identification of novel resolvin D1-miRNA circuits. *FASEB J* 25: 544–560

Rehwinkel J, Behm-Ansmant I, Gatfield D & Izaurralde E (2005) A crucial role for GW182 and the DCP1:DCP2 decapping complex in miRNA-mediated gene silencing. *RNA* 11: 1640–1647

Remmerie A, Martens L, Thoné T, Castoldi A, Seurinck R, Pavie B, Roels J, Vanneste B, De Prijck S, Vanhockerhout M, *et al* (2020) Osteopontin Expression Identifies a Subset of Recruited Macrophages Distinct from Kupffer Cells in the Fatty Liver. *Immunity* 53: 641-657.e14

Remmerie A & Scott CL (2018) Macrophages and lipid metabolism. *Cell Immunol* 330: 27–42

Rhu J, Heo JS, Choi SH, Choi DW, Kim JM, Joh JW & Kwon CHD (2017) Streamline flow of the portal vein affects the lobar distribution of colorectal liver metastases and has a clinical impact on survival. *Ann Surg Treat Res* 92: 348–354

De Rie D, Abugessaisa I, Alam T, Arner E, Arner P, Ashoor H, Åström G, Babina M, Bertin N, Burroughs AM, *et al* (2017) An integrated expression atlas of miRNAs and their promoters in human and mouse. *Nat Biotechnol* 35: 872–878

Riihimäki M, Hemminki A, Sundquist J & Hemminki K (2016) Patterns of metastasis in colon and rectal cancer. *Sci Rep* 6: 29765

Roberts RA, Ganey PE, Ju C, Kamendulis LM, Rusyn I & Klaunig JE (2007) Role of the Kupffer cell in mediating hepatic toxicity and carcinogenesis. *Toxicol Sci* 96: 2–15

Robinson MW, Harmon C & O'Farrelly C (2016) Liver immunology and its role in inflammation and homeostasis. *Cell Mol Immunol* 13: 267–76

Roden C, Gaillard J, Kanoria S, Rennie W, Barish S, Cheng J, Pan W, Liu J, Cotsapas C, Ding Y, *et al* (2017) Novel determinants of mammalian primary microRNA processing revealed by systematic evaluation of hairpin-containing transcripts and human genetic variation. *Genome Res* 27: 374–384

Romani B, Kavyanifard A & Allahbakhshi E (2017) Antibody production by in vivo RNA transfection. *Sci Rep* 7: 10863

Romani B, Kavyanifard A & Allahbakhshi E Antibody production by in vivo RNA transfection OPEN.

Romero-Cordoba SL, Rodriguez-Cuevas S, Bautista-Pina V, Maffuz-Aziz A, D'Ippolito E, Cosentino G, Baroni S, Iorio M V & Hidalgo-Miranda A (2018) Loss of function of miR-342-3p results in MCT1 over-expression and contributes to oncogenic metabolic reprogramming in triple negative breast cancer. *Sci Rep* 8: 12252

Rosa A, Ballarino M, Sorrentino A, Sthandier O, De Angelis FG, Marchioni M, Masella B, Guarini A, Fatica A, Peschle C, *et al* (2007) The interplay between the master transcription factor PU.1 and miR-424 regulates human monocyte/macrophage differentiation. *Proc Natl Acad Sci U S A* 104: 19849–54

Roy S (2016) miRNA in Macrophage Development and Function. *Antioxid Redox Signal* 25: 795–804

Ruby JG, Jan CH & Bartel DP (2007) Intronic microRNA precursors that bypass Drosha processing. *Nature* 448: 83–6

Rückerl D, Jenkins SJ, Laqtom NN, Gallagher IJ, Sutherland TE, Duncan S, Buck AH & Allen JE (2012) Induction of IL-4Rα-dependent microRNAs identifies PI3K/Akt signaling as essential for IL-4-driven murine macrophage proliferation in vivo. *Blood* 120: 2307–16

Schwartz JC, Younger ST, Nguyen N-B, Hardy DB, Monia BP, Corey DR & Janowski BA (2008) Antisense transcripts are targets for activating small RNAs. *Nat Struct Mol Biol* 15: 842–8

Schwarz DS, Hutvágner G, Du T, Xu Z, Aronin N & Zamore PD (2003) Asymmetry in the assembly of the RNAi enzyme complex. *Cell* 115: 199–208

Scott CL, Zheng F, De Baetselier P, Martens L, Saeys Y, De Prijck S, Lippens S, Abels C, Schoonooghe S, Raes G, *et al* (2016) Bone marrow-derived monocytes give rise to self-renewing and fully differentiated Kupffer cells. *Nat Commun* 7

Seki E & Brenner DA (2008) Toll-like receptors and adaptor molecules in liver disease: update. *Hepatology* 48: 322–35

Seki S, Nakashima H, Nakashima M & Kinoshita M (2011) Antitumor immunity produced by the liver Kupffer cells, NK cells, NKT cells, and CD8 CD122 T cells. *Clin Dev Immunol* 2011: 868345

Shimizu Y, Amano H, Ito Y, Betto T, Yamane S, Inoue T, Nishizawa N, Matsui Y, Kamata M, Nakamura M, *et al* (2017) Angiotensin II subtype 1a receptor signaling in resident hepatic macrophages induces liver metastasis formation. *Cancer Sci* 108: 1757–1768

Si W, Shen J, Zheng H & Fan W (2019) The role and mechanisms of action of microRNAs in cancer drug resistance. *Clinical Epigenetics 2019 11:1* 11: 1–24

Siegel RL, Wagle NS, Cercek A, Smith RA & Jemal A (2023) Colorectal cancer statistics, 2023. *CA Cancer J Clin* 73: 233–254

De Simone G, Andreata F, Bleriot C, Fumagalli V, Laura C, Garcia-Manteiga JM, Di Lucia P, Gilotto S, Ficht X, De Ponti FF, *et al* (2021) Identification of a Kupffer cell subset capable of reverting the T cell dysfunction induced by hepatocellular priming. *Immunity* 54: 2089-2100.e8

Soldi M, Sergi Sergi L, Unali G, Kerzel T, Cuccovillo I, Capasso P, Annoni A, Biffi M, Rancoita PMV, Cantore A, *et al* (2020) Laboratory-Scale Lentiviral Vector Production and Purification for Enhanced Ex Vivo and In Vivo Genetic Engineering. *Mol Ther Methods Clin Dev* 19: 411–425

Solomon LA, Podder S, He J, Jackson-Chornenki NL, Gibson K, Ziliotto RG, Rhee J & DeKoter RP (2017) Coordination of Myeloid Differentiation with Reduced Cell Cycle Progression by PU.1 Induction of MicroRNAs Targeting Cell Cycle Regulators and Lipid Anabolism. *Mol Cell Biol* 37

Soucie EL, Weng Z, Geirsdóttir L, Molawi K, Maurizio J, Fenouil R, Mossadegh-Keller N, Gimenez G, Vanhille L, Beniazza M, *et al* (2016) Lineage-specific enhancers activate self-renewal genes in macrophages and embryonic stem cells. *Science* 351

Squadrito ML, Etzrodt M, De Palma M & Pittet MJ (2013a) MicroRNA-mediated control of macrophages and its implications for cancer. *Trends Immunol* 34: 350–9

Squadrito ML, Etzrodt M, De Palma M & Pittet MJ (2013b) MicroRNA-mediated control of macrophages and its implications for cancer. *Trends Immunol* 34: 350–9

Squadrito ML, Pucci F, Magri L, Moi D, Gilfillan GD, Ranghetti A, Casazza A, Mazzone M, Lyle R, Naldini L, *et al* (2012) miR-511-3p modulates genetic programs of tumor-associated macrophages. *Cell Rep* 1: 141–54

Su GL, Klein RD, Aminlari A, Zhang HY, Steinstraesser L, Alarcon WH, Remick DG & Wang SC (2000) Kupffer cell activation by lipopolysaccharide in rats: role for lipopolysaccharide binding protein and toll-like receptor 4. *Hepatology* 31: 932–6

Sung H, Ferlay J, Siegel RL, Laversanne M, Soerjomataram I, Jemal A & Bray F (2021) Global Cancer Statistics 2020: GLOBOCAN Estimates of Incidence and Mortality Worldwide for 36 Cancers in 185 Countries. *CA Cancer J Clin* 71: 209–249

Tabara H, Sarkissian M, Kelly WG, Fleenor J, Grishok A, Timmons L, Fire A & Mello CC (1999) The rde-1 gene, RNA interference, and transposon silencing in C. elegans. *Cell* 99: 123–132

Tabas I, Bornfeldt KE, Libby P & Tall AR (2016) Macrophage Phenotype and Function in Different Stages of Atherosclerosis. *Circ Res* 118: 653–667

Taganov KD, Boldin MP, Chang KJ & Baltimore D (2006) NF-κB-dependent induction of microRNA miR-146, an inhibitor targeted to signaling proteins of innate immune responses. *Proc Natl Acad Sci U S A* 103: 12481–12486

Tai MC, Kajino T, Nakatochi M, Arima C, Shimada Y, Suzuki M, Miyoshi H, Yatabe Y, Yanagisawa K & Takahashi T (2015) miR-342-3p regulates MYC transcriptional activity via direct repression of E2F1 in human lung cancer. *Carcinogenesis* 36: 1464–73

Takahashi K (1989) Sequential analysis of macrophage tissue differentiation and Kupffer cell exchange after human liver transplantation. *Cells of the Hepatic Sinusoid* 2: 406–409

Tang B, Zhu J, Wang Y, Chen W, Fang S, Mao W, Xu Z, Yang Y, Weng Q, Zhao Z, *et al* (2023a) Targeted xCT-mediated Ferroptosis and Protumoral Polarization of Macrophages Is Effective against HCC and Enhances the Efficacy of the Anti-PD-1/L1 Response. *Adv Sci (Weinh)* 10: e2203973

Tang C, Sun H, Kadoki M, Han W, Ye X, Makusheva Y, Deng J, Feng B, Qiu D, Tan Y, *et al* (2023b) Blocking Dectin-1 prevents colorectal tumorigenesis by suppressing prostaglandin E2 production in myeloid-derived suppressor cells and enhancing IL-22 binding protein expression. *Nat Commun* 14: 1493

Tang R, Li L, Zhu D, Hou D, Cao T, Gu H, Zhang J, Chen J, Zhang CY & Zen K (2012) Mouse miRNA-709 directly regulates miRNA-15a/16-1 biogenesis at the posttranscriptional level in the nucleus: evidence for a microRNA hierarchy system. *Cell Res* 22: 504–515

Tanzer A & Stadler PF (2004) Molecular evolution of a microRNA cluster. *J Mol Biol* 339: 327–35

Tao N, Gao GP, Parr M, Johnston J, Baradet T, Wilson JM, Barsoum J & Fawell SE (2001) Sequestration of adenoviral vector by Kupffer cells leads to a nonlinear dose response of transduction in liver. *Mol Ther* 3: 28–35

Theurl M, Theurl I, Hochegger K, Obrist P, Subramaniam N, van Rooijen N, Schuemann K & Weiss G (2008) Kupffer cells modulate iron homeostasis in mice via regulation of hepcidin expression. *J Mol Med (Berl)* 86: 825–35

Tili E, Michaille J-J, Cimino A, Costinean S, Dumitru CD, Adair B, Fabbri M, Alder H, Liu CG, Calin GA, *et al* (2007) Modulation of miR-155 and miR-125b levels following lipopolysaccharide/TNF-alpha stimulation and their possible roles in regulating the response to endotoxin shock. *J Immunol* 179: 5082–5089

Timmers M, Vekemans K, Vermijlen D, Asosingh K, Kuppen P, Bouwens L, Wisse E & Braet F (2004) Interactions between rat colon carcinoma cells and Kupffer cells during the onset of hepatic metastasis. *Int J Cancer* 112: 793–802

Trabucchi M, Briata P, Garcia-Mayoral M, Haase AD, Filipowicz W, Ramos A, Gherzi R & Rosenfeld MG (2009) The RNA-binding protein KSRP promotes the biogenesis of a subset of microRNAs. *Nature* 459: 1010–1014

Vansaun MN, Mendonsa AM & Lee Gorden D (2013) Hepatocellular proliferation correlates with inflammatory cell and cytokine changes in a murine model of nonalchoholic fatty liver disease. *PLoS One* 8: e73054

Vasudevan S (2012) Posttranscriptional upregulation by microRNAs. *Wiley Interdiscip Rev RNA* 3: 311–330

Velu CS, Baktula AM & Grimes HL (2009) Gfi1 regulates miR-21 and miR-196b to control myelopoiesis. *Blood* 113: 4720–8

Vorsatz C, Friedrich N, Nimmerjahn F & Biburger M (2021) There Is Strength in Numbers: Quantitation of Fc Gamma Receptors on Murine Tissue-Resident Macrophages. *Int J Mol Sci* 22

Wan S, Kuo N, Kryczek I, Zou W & Welling TH (2015) Myeloid cells in hepatocellular carcinoma. *Hepatology* 62: 1304–12

Wang F, Liang S, Liu X, Han L, Wang J & Du Q (2018) LINC00460 modulates KDM2A to promote cell proliferation and migration by targeting miR-342-3p in gastric cancer. *Onco Targets Ther* 11: 6383–6394

Wang HH, McIntosh AR, Hasinoff BB, Rector ES, Ahmed N, Nance DM & Orr FW (2000) B16 melanoma cell arrest in the mouse liver induces nitric oxide release and sinusoidal cytotoxicity: a natural hepatic defense against metastasis. *Cancer Res* 60: 5862–9

Wang J, Li S, Liu Y, Zhang C, Li H & Lai B (2020) Metastatic patterns and survival outcomes in patients with stage IV colon cancer: A population-based analysis. *Cancer Med* 9: 361–373

Wang L, Xia JW, Ke ZP & Zhang BH (2019) Blockade of NEAT1 represses inflammation response and lipid uptake via modulating miR-342-3p in human macrophages THP-1 cells. *J Cell Physiol* 234: 5319–5326

Wang Y, Guo X, Wang L, Xing L, Zhang X & Ren J (2022) miR-342-3p Inhibits Acute Myeloid Leukemia Progression by Targeting SOX12. *Oxid Med Cell Longev* 2022: 1275141

Wang Y, van der Tuin S, Tjeerdema N, van Dam AD, Rensen SS, Hendrikx T, Berbée JFP, Atanasovska B, Fu J, Hoekstra M, *et al* (2015) Plasma cholesteryl ester transfer protein is predominantly derived from Kupffer cells. *Hepatology* 62: 1710–22

Wei J, Zhang J, Wang D, Cen B, Lang JD & DuBois RN (2022) The COX-2–PGE2 Pathway Promotes Tumor Evasion in Colorectal Adenomas. *Cancer Prevention Research* 15: 285–296

Wei Y, Li L, Wang D, Zhang CY & Zen K (2014) Importin 8 regulates the transport of mature microRNAs into the cell nucleus. *J Biol Chem* 289: 10270–10275

Wen SW, Ager EI & Christophi C (2013) Bimodal role of Kupffer cells during colorectal cancer liver metastasis. *Cancer Biol Ther* 14: 606–13

Willekens FLA, Werre JM, Kruijt JK, Roerdinkholder-Stoelwinder B, Groenen-Döpp YAM, van den Bos AG, Bosman GJCGM & van Berkel TJC (2005) Liver Kupffer cells rapidly remove red blood cell-derived vesicles from the circulation by scavenger receptors. *Blood* 105: 2141–5

Wu J, Li J, Salcedo R, Mivechi NF, Trinchieri G & Horuzsko A (2012) The proinflammatory myeloid cell receptor TREM-1 controls Kupffer cell activation and development of hepatocellular carcinoma. *Cancer Res* 72: 3977–86

Xi Y & Xu P (2021) Global colorectal cancer burden in 2020 and projections to 2040. *Transl Oncol* 14: 101174

Xiao M, Li J, Li W, Wang Y, Wu F, Xi Y, Zhang L, Ding C, Luo H, Li Y, *et al* (2017) MicroRNAs activate gene transcription epigenetically as an enhancer trigger. *RNA Biol* 14: 1326–1334

Xie X, Liu H, Wang M, Ding F, Xiao H, Hu F, Hu R & Mei J (2015) miR-342-3p targets RAP2B to suppress proliferation and invasion of non-small cell lung cancer cells. *Tumour Biol* 36: 5031–8

Xu Y, Huang X, Luo Q & Zhang X (2021) MicroRNAs Involved in Oxidative Stress Processes Regulating Physiological and Pathological Responses. *Microrna* 10: 164–180

Xue X, Fei X, Hou W, Zhang Y, Liu L & Hu R (2018) miR-342-3p suppresses cell proliferation and migration by targeting AGR2 in non-small cell lung cancer. *Cancer Lett* 412: 170–178

Yang C-Y, Chen J-B, Tsai T-F, Tsai Y-C, Tsai C-Y, Liang P-H, Hsu T-L, Wu C-Y, Netea MG, Wong C-H, *et al* (2013) CLEC4F is an inducible C-type lectin in F4/80-positive cells and is involved in alpha-galactosylceramide presentation in liver. *PLoS One* 8: e65070

Yang M, Chen J, Su F, Yu B, Su F, Lin L, Liu Y, Huang JD & Song E (2011) Microvesicles secreted by macrophages shuttle invasion-potentiating microRNAs into breast cancer cells. *Mol Cancer* 10: 1–13

Yao J, Dai Y, Liu Z, Hu W & Wan Y (2022) miR-342-3p Suppresses glioblastoma development via targeting CDK6. *Acta Biochim Pol* 69: 393–397

Yao R-R, Li J-H, Zhang R, Chen R-X & Wang Y-H (2018) M2-polarized tumor-associated macrophages facilitated migration and epithelial-mesenchymal transition of HCC cells via the TLR4/STAT3 signaling pathway. *World J Surg Oncol* 16: 9

Yi R, Qin Y, Macara IG & Cullen BR (2003) Exportin-5 mediates the nuclear export of pre-microRNAs and short hairpin RNAs. *Genes Dev* 17: 3011–3016

Ying X, Wu Q, Wu X, Zhu Q, Wang X, Jiang L, Chen X & Wang X (2016) Epithelial ovarian cancer-secreted exosomal miR-222-3p induces polarization of tumor-associated macrophages. *Oncotarget* 7: 43076–43087

You Q, Cheng L, Kedl RM & Ju C (2008) Mechanism of T cell tolerance induction by murine hepatic Kupffer cells. *Hepatology* 48: 978–90

Yu J, Green MD, Li S, Sun Y, Journey SN, Choi JE, Rizvi SM, Qin A, Waninger JJ, Lang X, *et al* (2021) Liver metastasis restrains immunotherapy efficacy via macrophage-mediated T cell elimination. *Nat Med* 27: 152–164

Zeng Y, Yi R & Cullen BR (2005) Recognition and cleavage of primary microRNA precursors by the nuclear processing enzyme Drosha. *EMBO J* 24: 138–148

Zhang MY, Calin GA, Yuen KS, Jin DY & Chim CS (2020) Epigenetic silencing of miR-342-3p in B cell lymphoma and its impact on autophagy. *Clin Epigenetics* 12: 150

Zhang X & Zeng Y (2010) The terminal loop region controls microRNA processing by Drosha and Dicer. *Nucleic Acids Res* 38: 7689–97

Zhang Y, Fan M, Zhang X, Huang F, Wu K, Zhang J, Liu J, Huang Z, Luo H, Tao L, *et al* (2014) Cellular microRNAs up-regulate transcription via interaction with promoter TATA-box motifs. *RNA* 20: 1878–89

Zhang Y & Zhang H (2017) RNAa Induced by TATA Box-Targeting MicroRNAs. *Adv Exp Med Biol* 983: 91–111

Zhang Y, Zhang M, Li X, Tang Z, Wang X, Zhong M, Suo Q, Zhang Y & Lv K (2016) Silencing MicroRNA-155 Attenuates Cardiac Injury and Dysfunction in Viral Myocarditis via Promotion of M2 Phenotype Polarization of Macrophages. *Sci Rep* 6

Zhang Y, Zhang M, Zhong M, Suo Q & Lv K (2013) Expression profiles of miRNAs in polarized macrophages. *Int J Mol Med* 31: 797–802

Zhao L & Zhang Y (2015) miR-342-3p affects hepatocellular carcinoma cell proliferation via regulating NF-κB pathway. *Biochem Biophys Res Commun* 457: 370–7

Zhao Q, Kuang D-M, Wu Y, Xiao X, Li X-F, Li T-J & Zheng L (2012) Activated CD69+ T cells foster immune privilege by regulating IDO expression in tumor-associated macrophages. *J Immunol* 188: 1117–1124

Zhao W, Dai S, Yue L, Xu F, Gu J, Dai X & Qian X (2022) Emerging mechanisms progress of colorectal cancer liver metastasis. *Front Endocrinol (Lausanne)* 13: 1081585

Zheng L, Chen Y, Ye L, Jiao W, Song H, Mei H, Li D, Yang F, Li H, Huang K, *et al* (2017a) miRNA-584-3p inhibits gastric cancer progression by repressing Yin Yang 1- facilitated MMP-14 expression. *Sci Rep* 7: 8967

Zheng P, Chen L, Yuan X, Luo Q, Liu Y, Xie G, Ma Y & Shen L (2017b) Exosomal transfer of tumor-associated macrophage-derived miR-21 confers cisplatin resistance in gastric cancer cells. *Journal of Experimental and Clinical Cancer Research* 36: 1–13

Zhou J, Li X, Wu X, Zhang T, Zhu Q, Wang X, Wang H, Wang K, Lin Y & Wang X (2018) Exosomes released from tumor-associated macrophages transfer miRNAs that induce a Treg/Th17 cell imbalance in epithelial ovarian cancer. *Cancer Immunol Res* 6: 1578–1592

Zhu X, Shen H, Yin X, Yang M, Wei H, Chen Q, Feng F, Liu Y, Xu W & Li Y (2019) Macrophages derived exosomes deliver miR-223 to epithelial ovarian cancer cells to elicit a chemoresistant phenotype. *Journal of Experimental and Clinical Cancer Research* 38: 1–14

Zigmond E, Samia-Grinberg S, Pasmanik-Chor M, Brazowski E, Shibolet O, Halpern Z & Varol C (2014) Infiltrating monocyte-derived macrophages and resident kupffer cells display different ontogeny and functions in acute liver injury. *J Immunol* 193: 344–53

Zimmermann HW, Bruns T, Weston CJ, Curbishley SM, Liaskou E, Li KK, Resheq YJ, Badenhorst PW & Adams DH (2016) Bidirectional transendothelial migration of monocytes across hepatic sinusoidal endothelium shapes monocyte differentiation and regulates the balance between immunity and tolerance in liver. *Hepatology* 63: 233–246

Zonari E, Pucci F, Saini M, Mazzieri R, Politi LS, Gentner B & Naldini L (2013a) A role for miR-155 in enabling tumor-infiltrating innate immune cells to mount effective antitumor responses in mice. *Blood* 122: 243–252

Zonari E, Pucci F, Saini M, Mazzieri R, Politi LS, Gentner B & Naldini L (2013b) A role for miR-155 in enabling tumor-infiltrating innate immune cells to mount effective antitumor responses in mice. *Blood* 122: 243–252

Chiara Brescia